Low molecular weight polysialic acid prevents lipopolysaccharide-induced inflammatory dopaminergic neurodegeneration in humanized *SIGLEC11* transgenic mice

Doctoral thesis

to obtain a doctorate (PhD)

from the Faculty of Medicine

of the University of Bonn

Huan Liao

from Hunan, China

2021

Written with authorization of

the Faculty of Medicine of the University of Bonn

First reviewer: Prof. Dr. Harald Neumann

Second reviewer: Prof. Dr. Thomas Langmann

Day of oral examination: 05.07.2021

For the institute of Reconstructive Neurobiology

Director: Prof. Dr. Oliver Brüstle

Table of Contents

List of abbreviation

6-OHDA	6-hydroxydopamine
α-syn	α-synuclein
BBB	Blood brain barrier
BDNF	Brain-derived neurotrophic factor
BSA	Bovine serum albumin
C1q	Complement component 1q
C3	Complement component 3
C4	Complement factor 4
CD68	Cluster of Differentiation 68
CFB	Complement factor B
CFH	Complement factor H
CFI	Complement factor I
CNS	Central nervous system
CR3	Complement receptor 3
CV	Column volume
CVO	Circumventricular organ
CXCL12	CXC-family chemokine ligand 12
CXCR4	CXC-family chemokine receptor 4
Cy3	Cyanine 3
Cyba	Cytochrome b-245 alpha chain
Cybb	Cytochrome b-245 heavy chain
DAMP	Danger-associated molecular pattern
DAPI	4',6-diamidino-2-phenylindole
DC	Dendritic cells
ddH2O	Double-distilled water

DMSO	Dimethyl sulfoxide
dNTP	Deoxynucleotide triphosphates
EDTA	Ethylendiamintetraacetate
ESdM	Embryonic stem cell-derived microglia
Fcer1g	Fc fragment of IgE, high affinity I, receptor for gamma polypeptide
FPLC	Fast protein liquid chromatography
GBS	Group B *Streptococcus*
GWAS	Genome-wide association studies
HSCT/DAP10	Hematopoietic cell signal transducer
IBA1	Ionized calcium binding adaptor molecule 1
IFNγ	Interferon γ
IGF-1	Insulin-like growth factor 1
IL	Interleukin
iNOS	Inducible nitric oxide synthase
ITAM	Immunoreceptor tyrosine-based activatory motif
Itgam	Integrin alpha M
ITIM	Immunoreceptor tyrosine-based inhibition motif
JNK	C-Jun NH2-terminal protein kinase
Kdn	Deaminoneuraminic acid
LB	Lewy body
LPS	Lipopolysaccharide
LRRK2	Leucine rich repeat kinase 2
MAC	Membrane attack complex
MPTP	1-methyl-4 phenyl-1, 2, 3, 6 tetrahydropyridine
NaCl	Sodium chloride
NADPH	Nicotinamide adenine dinucleotide phosphate

NCAM	Neural cell adhesion molecule
NEU1	N-acetyl-alpha-neuramindase 1
Neu5Ac	N-acetylneuraminic acid
Neu5Gc	N-glycolylneuraminic acid
NeuN	Neuronal nuclei
NGS	Normal goat serum
NLRP3	Nucleotide-binding oligomerization domain-leucine-rich repeats containing pyrin domain 3
NOS	Nitric oxide synthase
Nos2	Nitric oxide 2
P	Phosphate
PAMP	Pathogen-associated molecular pattern
PBS	Phosphate Buffer Saline
PCR	Polymerase chain reaction
PD	Parkinson’s disease
PET	Positron emission tomography
PFA	Paraformaldehyde
poly (I:C)	Polyinosinic polycytidylic acid
polySia	Polysialic acid
polySia avDP20	PolySia with an average degree of polymerization of 20
ROS	Reactive oxygen species
RT	Reverse transcription
SHP-1/PTPN6	SRC homology region 2 domain-containing phosphatase-1
SHP-2/PTPN11	SRC homology region 2 domain-containing phosphatase-2
Sia	Sialic acid
SIGLEC	Sialic acid binding immunoglobulin-like lectin
SIRP	Signal regulatory protein

SN	Substantia nigra
SN*pc*	Substantia nigra *pars compacta*
SN*pr*	Substantia nigra *pars reticulata*
SPF	Specific pathogen free
sqRT-PCR	Semi-quantitative real-time PCR
SYK	Spleen tyrosine kinase
SynCAM	Synaptic cell-adhesion molecule
TAE	Tris/Acetic acid/EDTA
TBA	Thiobarbituric acid
TGFβ	Transforming growth factor beta
TH	Tyrosine hydroxylase
TLR4	Toll-like receptor 4
TNFα	Tumor necrosis factor-α
TREM2	Triggering receptor expressed on myeloid cells-2
TWAS	Transcriptome-wide association study
TYROBP/DAP12	TYRO protein tyrosine kinase binding protein/DNAX-activating protein of 12 kDa
VEGF	Vascular endothelial growth factor

1. Introduction

1.1 Parkinson's disease

1.1.1 Epidemiology of PD

Parkinson's disease (PD) is a progressive neurodegenerative disease. Although it has a number of non-motor manifestations, it is mainly characterized by motor symptoms, including bradykinesia, resting tremor and rigidity, leading to severe disability at a later stage (Poewe *et al*, 2017). PD has a rapid increasing prevalence worldwide. It is estimated that approximately 6.1 million people were diagnosed as PD all over the world in 2016, with a substantial increase from 2.5 million in 1990 (Collaborators, 2018; Pringsheim *et al*, 2014). Furthermore, both of the prevalence and incidence of PD are projected to augment by over 30 % by 2030 due to the aging population (Dorsey *et al*, 2007), resulting in a heavy burden on the society as well as the economy as a whole.

1.1.2 Neuropathology of PD

PD mainly has two pathological characteristics (see Figure 1-1). One is the loss of dopaminergic neurons in the substantia nigra *pars compacta* (SN*pc*), causing the movement disorders. This pathological feature is limited to the region of the ventrolateral substantia nigra in the early stage of PD. As the disease progresses, it is widespread in more brain regions (Damier *et al*, 1999; Fearnley & Lees, 1991). The other pathological characteristic of PD is the Lewy body (LB), featured by α-synuclein protein aggregates inside neurons. The Lewy body pathology is observed in cholinergic and monoaminergic neurons in brainstem as well as in neurons in the olfactory system at an early stage of PD. At a later stage, it is found in more brain areas, including the limbic and neocortical regions. (Poewe *et al.*, 2017).

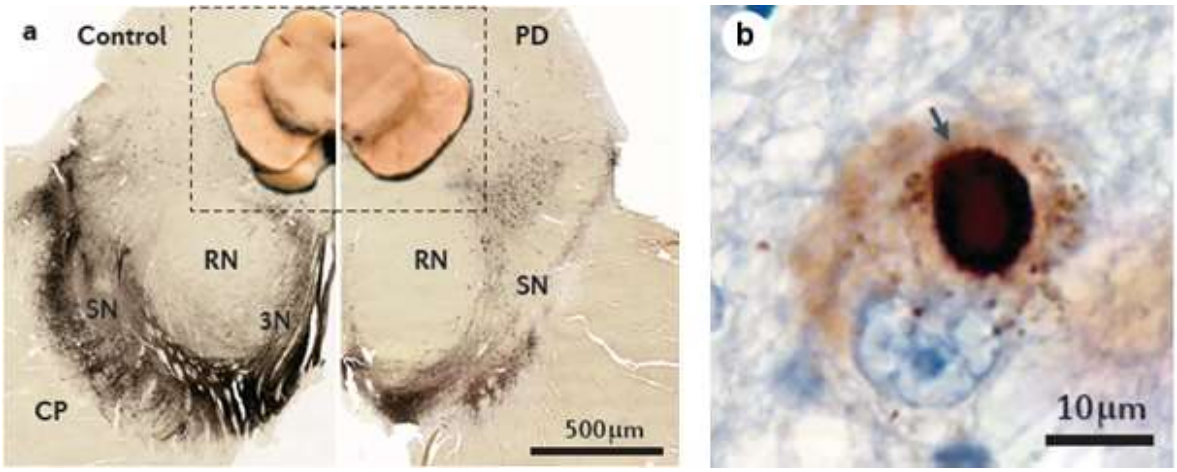

Figure 1 - 1 The main pathological characteristics of Parkinson disease. a, Parkinson disease (PD) is featured by the loss of pigmented dopaminergic neurons in the substantia nigra (SN) (right panel) compared with healthy control (left panel). b, Immunohistochemical staining of α-synuclein displays the round, intracytoplasmic Lewy bodies (arrow in part b) (Image is adapted from Poewe et al., 2017).

Braak staging has been proposed to explain the neuropathological progression of PD since 2003 (Braak *et al*, 2003). Braak et al. analyzed LB distribution at postmortem and revealed that LB pathology has a chronologically predictable sequence, in a rostro-caudally spreading fashion in the brain. At early stages of PD (stages 1 and 2), LB pathology are mainly observed in the medulla and the olfactory bulb. This early pathology is related to some early non-motor symptoms, mainly including autonomic disorders (e.g., constipation), decreased smell, and sleep-related dysfunctions. As the disease progresses (stages 3 and 4), SN*pc* is involved and the pathology extends to other midbrain and basal forebrain structures. During stages 3 and 4, patients start to present the classic motor symptoms of PD. In the final stages of PD (stages 5 and 6), the pathology involves the entire neocortex and high-order areas. Clinically, patients at these stages have significant gait problems and cognitive impairment (Braak *et al.*, 2003).

1.1.3 Microglia and the pathophysiology of PD

1.1.3.1 Microglia

Microglia are the most abundant resident immune cells in the central nervous system (CNS) (Waisman *et al*, 2015). They arise from yolk sac–derived progenitors that migrated into the CNS during early embryonic development and stay in the brain by self-maintenance, which makes them different from other tissue-resident macrophages, that are derived from bone marrow precursors in the adult (Ginhoux *et al*, 2010). Thus, microglia solely rely on their self-renewal ability to achieve maintenance and local expansion upon receiving an activation insult (Ajami *et al*, 2007). Functionally, microglia are multifaceted by obtaining different phenotypes. They play a critical role in normal brain development, maturation, homeostasis as well as injury repair. For instance, microglia mediate synaptic pruning and remodeling in normal brain development in a complement component 1q (C1q)- and complement component 3 (C3)-dependent manner, contributing to functional neuronal networks (Paolicelli *et al*, 2011; Stevens *et al*, 2007). As well, microglia play an important role in learning and memory by supporting learning-related synapse formation via releasing brain-derived neurotrophic factor (Parkhurst *et al*, 2013). In addition, microglia phagocytose the apoptotic cells generated during adult neurogenesis via the phagocytic receptors Axl and Mer (Fourgeaud *et al*, 2016). In pathological conditions, microglia migrate to the lesions to exacerbate or relieve disease progression.

Overall, microglia switch their states between resting and activation to exert their functions, depending on the microenvironment. In the healthy CNS, microglia have resting states. They keep scanning the brain environments and sensing pathology with their multi-branched, long processes (Nimmerjahn *et al*, 2005). After sensing a detrimental attack in the CNS, microglia transit to an activated state and become more rounded and “amoeboid” in shape with short processes. Activated microglia have enhanced phagocytic capacity, and possibly secrete pro-inflammatory factors to exacerbate injury or anti-inflammatory

factors to reduce lesions (Colonna & Butovsky, 2017). Transition from the resting to activated state requires a tight control, thus allowing an appropriate response of microglia (Joers *et al*, 2017). Intriguingly, activation of microglia is often related to neurodegeneration (Labzin *et al*, 2018). Thus, microglia attract more and more attention in the field of neurodegenerative diseases, including PD.

1.1.3.2 Microglia activation in PD

Accumulating evidence supports that microglia are involved in PD. Genome-wide association studies (GWAS) and transcriptome-wide association study (TWAS) suggested that genes expressed in microglia are involved in immune cell-mediated clearance and/or protein clearance and are major risk factors of developing PD (Chang *et al*, 2017; Li *et al*, 2019; Nalls *et al*, 2019; Nalls *et al*, 2014). For instance, the human leukocyte antigen gene (HLA-DRA) has a specific expression in microglia and has been identified as a genetic risk factor for late-onset PD in a GWAS study (Hamza *et al*, 2010). Furthermore, while microglial triggering receptor expressed on myeloid cells-2 (TREM2) has a key role in the effective phagocytosis of apoptotic neuronal cells, p.R47H variant of TREM2 is a risk factor for PD (Rayaprolu *et al*, 2013). These data indicate that microglia possess a specific role in regulating the progression of PD (Block *et al*, 2007; Kannarkat *et al*, 2013).

Moreover, positron emission tomography (PET) studies show that microgliosis occurred in the early stage of PD and sustained response during the progression of PD (Gerhard *et al*, 2006; Terada *et al*, 2016). For instance, PET with tracer ([11C] DPA-713) revealed high levels of tracer binding (indicating microglial activation) in the occipital, temporal and parietal cortex in PD patients at an early stage, and this binding became higher after 1 year (Terada *et al.*, 2016). These clinical findings indicate that microglial activation has a pathogenic rather than compensatory role in the PD.

Consistently, multiple mouse models of PD also showed reactive microglia and prominent microgliosis. These models include transgenic models of PD based on α-Syn and PD models induced by toxins, such as lipopolysaccharide (LPS), 6-hydroxydopamine (6-OHDA), or 1-methyl-4 phenyl-1, 2, 3, 6 tetrahydropyridine (MPTP), and rotenone (Bodea *et al*, 2014; Czlonkowska *et al*, 1996; Hoenen *et al*, 2016; Manocha *et al*, 2017; Marinova-Mutafchieva *et al*, 2009; Ojha *et al*, 2016; Smeyne *et al*, 2016; Wu *et al*, 2002). Of note, repeated intraperitoneal injection of mice over four consecutive days with Gram-negative bacterial endotoxin lipopolysaccharides (LPS) induced a microglial inflammatory phenotype and caused loss of dopaminergic neurons in the substantia nigra (Bodea *et al.*, 2014). Moreover, animal models also revealed that microgliosis precedes dopaminergic neuronal loss, indicating that cell death is not a prerequisite for microglial activation (Marinova-Mutafchieva *et al.*, 2009; Su *et al*, 2008). Taken together, these preclinical studies indicate a critical role of microglia activation in PD disease progression.

Activated microglia have double-sided effects in the progression of brain diseases, meaning that they are both neurotoxic and neuroprotective (see Figure 1-2). On the one hand, microglia can release pro-inflammatory cytokines, such as tumor necrosis factor-α (TNFα), interleukin 1β (IL-1β), inducible nitric oxide synthase (iNOS / NOS2) and interleukin-12 (IL-12), and remove apoptotic cell debris via phagocytose. These functions appear to be associated with the loss of dopaminergic neurons in PD. On the other hand, microglia can attenuate inflammation and promote injury repair via the secretion of anti-inflammatory cytokines, such as IL-4, IL-13, IL-10, transforming growth factor beta (TGFβ), and neurotrophic insulin-like growth factor 1(IGF-1) (Wyss-Coray & Mucke, 2002). Noteworthy, microglia present both pro- and anti-inflammatory cytokines in the early stage of PD. As well, the status of microglia is regulated dynamically during the progression of PD in a MPTP-induced PD mouse model (Pisanu *et al*, 2014).

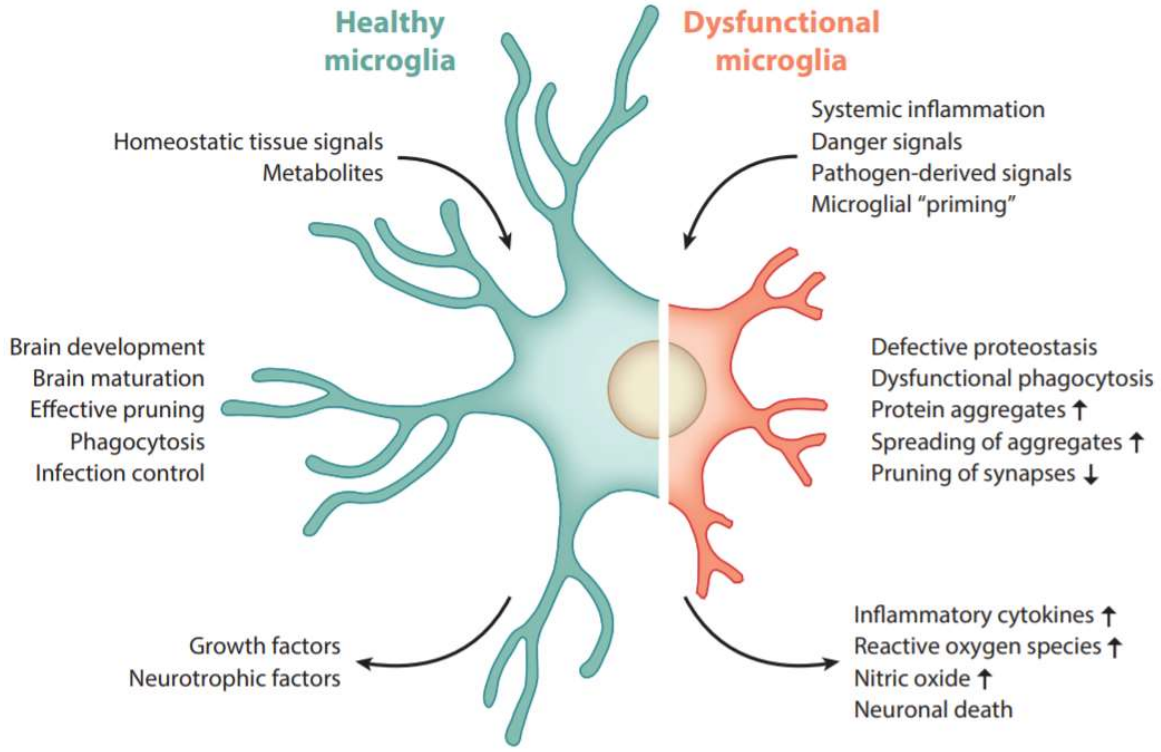

Figure 1 - 2 The double-sided effects of microglial function. In the healthy condition, microglia receive homeostatic tissue signals from surrounding cells in the microenvironment and make major contribution to brain development, maturation, synaptic pruning, phagocytosis, and infection control. Moreover, healthy microglia secret growth factors and neurotrophic factors to support neurons. In the pathological condition (such as systemic inflammation, age, pathogen-derived signals), microglia can recognize both pathogen-associated molecular patterns (PAMPs) and danger-associated molecular patterns (DAMPs), leading to a "primed" state. Dysfunctional microglia with defective proteostasis and dysfunctional phagocytosis, can increase pathogenic aggregates, as well as a hyperinflammatory state (more inflammatory cytokines, reactive oxygen species and nitric oxide), leading to neuronal death. (Image is adapted from Labzin et al., 2017)

1.1.3.3 Microglia-mediated neuroinflammation in PD

The involvement of neuroinflammation in PD has been documented over decades. In post-mortem pathological studies, a high level of inflammatory mediators has been identified in the brain tissue of PD patients. For instance, there are high levels of the CXC-family chemokine ligand 12 (CXCL12) and its receptor CXC-family chemokine receptor 4

(CXCR4), as well as TNFα, IL-1β, interferon γ (IFNγ), reactive oxygen species (ROS) and nitric oxide synthase (NOS) in the nigral tissue (Shimoji *et al*, 2009). In addition, higher concentrations of the IL-1β, IL-2, IL-6 and TNFα have also been identified in the striatum (Hunot *et al*, 1999; Mogi *et al*, 1994a; Mogi *et al*, 1996a; Mogi *et al*, 1994b). *In vivo* studies on biological samples further confirmed the presence of these microglial-related inflammatory mediators in PD. Similar panel of proinflammatory mediators (IL-1β, IL-6, IFNγ, and TNFα) have been observed both in cerebrospinal fluid and blood (serum and plasma) samples (Blum-Degen *et al*, 1995; Brodacki *et al*, 2008; Mogi *et al.*, 1994b; Mount *et al*, 2007; Pereira *et al*, 2016).

Midbrain dopaminergic neurons are sensitive to inflammatory cytokines, such as TNFα and IFNγ (McGuire *et al*, 2001; Mount *et al.*, 2007). Microglia are densely populated in the substantial nigra, thus enhancing the sensitivity of nigra dopaminergic neurons to inflammatory stimuli (Lawson *et al*, 1990). LPS can trigger an inflammatory response by directly activating Toll-like receptor 4 (TLR4) on microglia. It has been demonstrated that single intranigral injection of LPS in rats can lead to permanent damage to the dopaminergic neurons in the substantial nigra, as observed 1-year post-injection (Herrera *et al*, 2000). Chronic infusion of a low dose of LPS into the rat substantial nigra leads to a rapid activation of microglia that reached peak in 2 weeks, followed by delayed and gradual selective loss of nigral dopaminergic neurons (Gao *et al*, 2002). Further *in vitro* assays demonstrated that microglial activation and release of neurotoxic factors precede dopaminergic neurodegeneration in LPS-treated rat mesencephalic neuron-glia cultures (Gao *et al.*, 2002). The interaction between microglia-mediated neuroinflammation and neuronal dysfunction appears to be complicated. Inflammation can directly injury neurons or contribute to neuronal cell death through the release of neurotoxic cytokines. Conversely, neuronal cell death can trigger inflammation by releasing apoptotic and necrotic cellular factors that activate microglia, thus inducing further neuronal injury.

Dopaminergic neurons in substantial nigra are also quite vulnerable to metabolic and oxidative stress (Poewe *et al.*, 2017). First, this type of neurons needs plenty of energy to sustain their particularly long unmyelinated axons and great numbers of synapses (Bolam & Pissadaki, 2012; Pissadaki & Bolam, 2013). Second, lots of energy are required for them to maintain autonomous pacemaking activities (Surmeier *et al*, 2011; Surmeier *et al*, 2017). Third, higher levels of intracellular dopamine and its metabolites can induce toxic oxidative stress (Lotharius & Brundin, 2002; Mosharov *et al*, 2009). Consistently, accumulating preclinical and clinical evidence indicated that neuroinflammation involving a microglial oxidative burst contributes to disease progression (Gao *et al*, 2008; Halliday *et al*, 2011; Hirsch & Hunot, 2009; Ransohoff, 2016), although it remains unclear whether oxidative stress occurs early or late during the demise of neurons. Additionally, both complement C3 and its receptor complement receptor 3 (CR3) participated in microglial clearance mechanisms and can trigger a microglial oxidative burst (Linnartz *et al*, 2012; Ramaglia *et al*, 2012; Schafer *et al*, 2012). Moreover, the complement factor C3 has been shown to be causally involved in the loss of dopaminergic neurons in a LPS-triggered mouse model of PD (Bodea *et al.*, 2014). Furthermore, ITGAM, the integrin subunit of CR3, has also been implicated to play a role in dopaminergic neurodegeneration via a pathway involving LPS-induced reactive oxygen production by microglia (Pei *et al*, 2007). Additionally, knocking out the PD-risk gene DJ-1, encoding a putative antioxidant, was associated with increased cellular oxidative stress (Guzman *et al*, 2010) and reduced alpha-synuclein phagocytosis by microglia (Nash *et al*, 2017).

Overall, dopaminergic neurons in substantial nigra are particularly vulnerable to neuroinflammation. Importantly, microglia-mediated inflammation in animal models of PD often precedes detectable neuronal injury and neurodegeneration. Therefore, it is becoming obvious that microglia-mediated neuroinflammation plays a key role in the pathogenesis of PD.

Although highly efficacious symptomatic therapeutics are available, none of them is curative and PD remains a chronic progressive neurodegenerative disease that mostly leads to severe disability over time (Poewe *et al.*, 2017). Given the critical role of neuroinflammation in the pathogenesis of PD, the chronic neuroinflammation in the brains of PD patients could be potential targets to modify disease progression.

1.2 Polysialic acid

1.2.1 Polysialylation

Sialic acids (Sias) are monosaccharides with nine carbons. They attached to the glycocalyx of cell surfaces and secreted glycoproteins of vertebrates as terminal caps (Varki, 2017). Among the three major types of Sias in vertebrates, N-acetylneuraminic acid (Neu5Ac) is the most enriched Sia in human tissue, while N-glycolylneuraminic acid (Neu5Gc) and deaminoneuraminic acid (Kdn) have only trace amounts in human (Bardor *et al*, 2005; Hara *et al*, 1987; Inoue *et al*, 1996; Tangvoranuntakul *et al*, 2003). Sias can be modified by multiple ways, including methylation, sulfation, lactylation, acetylation and lactonization, leading to a diverse family with over 50 members with different structures (Angata & Varki, 2002). Additionally, Sia residual connects with acceptor sugar (Galactose, N-acetylgalactosamine, Neu5Ac) using a defined linkage (α2,3-, α2,6-, α2,8-) via sialyltransferases. Moreover, Sias can utilize intersialyl linkages to form homopolymers with different degrees of polymerization. Polysialic acid (polySia) is such a homopolymer generated from Neu5Ac monomers via α2,8-linkage (see Figure 1-3), with a degree of polymerization between 10 and around 200 (Schnaar *et al*, 2014). Thus, there exists a huge amount of glycoconjugates.

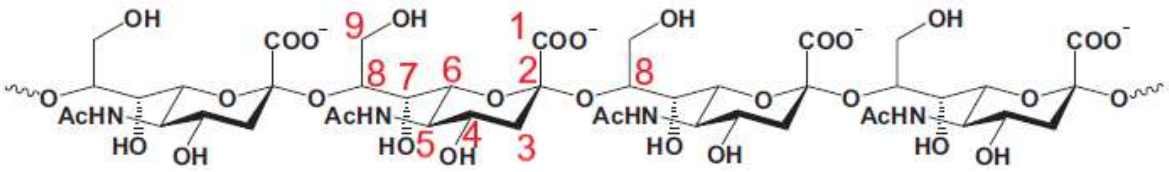

Figure 1 - 3 Schematic of α2,8-glycosidically linked N-acetylneuraminic acid with a nine-carbon backbone. (Design was adapted from Hildebrand H & Dityatev A., 2015).

The nervous tissue is highly polysialylated. The polysialylation of glycoconjugates attributes to two types of sialyltransferases, ST8Sia2 and ST8Sia4. It has been well documented that α2,8-linked polySia mainly attach to neural cell adhesion molecule (NCAM) (Cremer *et al*, 1994), although it can also attach to synaptic cell-adhesion molecule (SynCAM) (Galuska *et al*, 2010), neuropilin-2 (Curreli *et al*, 2007) and E-selectin ligand 1 (Thiesler *et al*, 2021; Werneburg *et al*, 2016). Some of these polysialylated glycoproteins have been observed on or in microglia (Thiesler *et al.*, 2021; Werneburg *et al.*, 2016). A recent study revealed that polysialylated NCAM is present on the mouse microglial cell Ra2. It also has been demonstrated that LPS triggered the rapid clearance of the polysialic acid (polySia) on the microglia cell surface by the exovesicular sialidase N-acetyl-alpha-neuramindase 1 (NEU1) (Sumida *et al*, 2015). Moreover, polysialylated neuropilin-2 and E-selectin ligand 1 have been observed in the Golgi compartment of murine microglia and human THP-1 macrophages (Thiesler *et al.*, 2021; Werneburg *et al.*, 2016). Interestingly, LPS promoted the translocation of polysialylated neuropilin-2 and E-selectin ligand 1 to the cell surface and enhanced their release in the extracellular space by ectodomain shedding (Thiesler *et al.*, 2021; Werneburg *et al.*, 2016). Compared with the embryonic brain, the adult brain has much lower levels of the α2,8-linked polySia. In particular, polySia-NCAM is mainly located in the areas of adult brain, which are associated with neurogenesis and neural plasticity (Angata *et al*, 2004; Sato & Kitajima, 2019).

Polysialylation modulates brain innate immune functions, and regulates synaptogenesis, neurogenesis, cell proliferation and migration, axon guidance, fasciculation, learning, memory, and cell adhesion (Hildebrandt & Dityatev, 2015; Monnier *et al*, 2001; Schnaar *et al.*, 2014; Varki & Gagneux, 2012). Moreover, it plays a critical part in capturing neurotrophic factors, growth factors, neurotransmitters and ions, cytokines, chemokines, and transcription factors (Colley *et al*, 2014; Sato & Kitajima, 2013, 2019). For instance, polySia binds to locally produced extracellular brain-derived neurotrophic factor (BDNF) under normal conditions. However, inflammation can trigger the removal of polySia on microglia by the sialidase NEU1 (Sumida *et al.*, 2015), thus releasing BDNF.

1.2.2 Sialic acid -related signaling

Sias can bind to sialic acid binding immunoglobulin-like lectins (SIGLEC) to exert their immunomodulatory function. SIGLECs are receptors expressed on immune cells, such as microglia, macrophages, dendritic cells (DC), monocytes, neutrophils. Most SIGLEC receptors own intracellular immunoreceptor tyrosine-based inhibition motifs (ITIMs) to mediate inhibitory signaling. Besides conserved SIGLEC-2, these SIGLEC receptors are SIGLEC-E, -F, and -G in mice and SIGLEC-3, -5, -6, -7, -8, -9, -10, -11, and -12 in humans (Duan & Paulson, 2020). When SIGLECs bind to Sias of glycoconjugates, their intracellular ITIMs inhibit the activatory signal coming from receptors containing immunoreceptor tyrosine-based activatory motifs (ITAMs) (Crocker, 2005; Crocker *et al*, 2007; Linnartz & Neumann, 2013).

ITAM-signaling bearing receptors of microglia, such as TREM2 and CR3, play a critical role in activation, phagocytosis and inflammation (Klaus *et al*, 2020). After ligand recognition, these receptors associate with the ITAM-bearing adaptor protein DNAX-activating protein of 12 kDa (TYROBP/DAP12). Then, the intracellular phosphorylated ITAMs activates a series of downstream signaling cascades, resulting in inflammation,

phagocytosis and superoxide production. This activatory effects of DAP12 is counter-regulated by the inhibitory ITIM signaling of SIGLECs, which upon ligand binding could inhibit downstream signaling by dephosphorylation of the ITAMs (Liao *et al*, 2020). In detail, the inhibition step starts from the phosphorylation of ITIMs via SRC family kinases. Then, the phosphorylated ITIM tyrosine recruits tyrosine phosphatases, such as SRC homology region 2 domain-containing phosphatase-1 (SHP-1/PTPN6) or SRC homology region 2 domain-containing phosphatase-2 (SHP-2/PTPN11) (Duan & Paulson, 2020). Afterwards, this recruitment dephosphorylates the signaling molecules in the ITAM-signaling cascade, thus suppressing the activation of immune cells. Finally, activated immune cell-mediated activities, including phagocytosis, oxidative burst or inflammation, are reduced (Linnartz *et al*, 2010) (Figure 1-4).

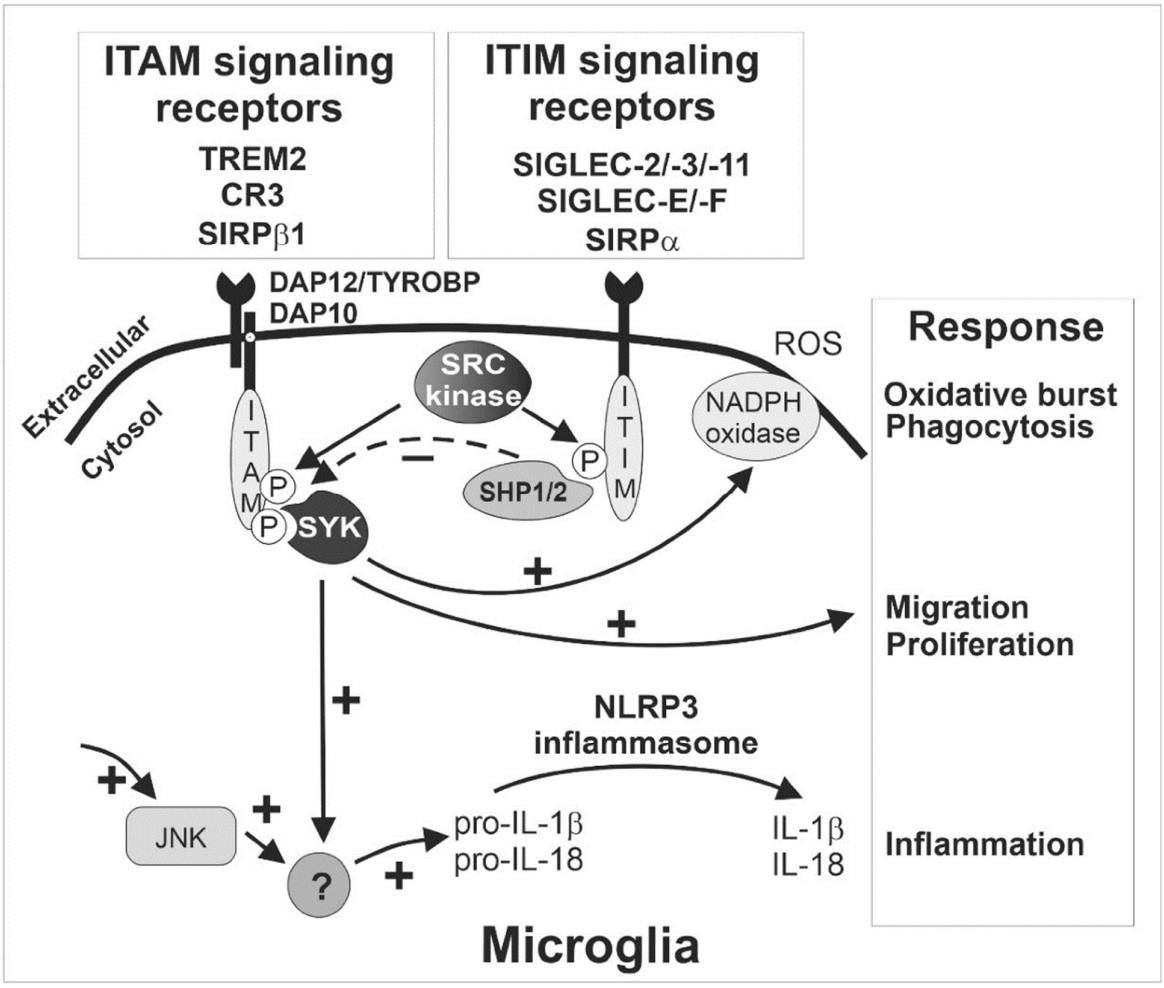

Figure 1 - 4 The double-sided effects of microglial function mediated by the ITAM- and ITIM-signaling receptors. Inhibitory SIGLEC receptors recruit and activate SHP1/2 after the phosphorylation of ITIMs via SRC family kinases, which can counter-regulate intracellular signals emanating from ITAM-signaling receptors by dephosphorylation of the ITAMs. The ITIM signaling pathway inactivates SYK (dotted '-' arrow) and thus inhibits several responses of microglia ('+' arrows) including phagocytosis, oxidative burst, migration, proliferation, and inflammation. Additionally, ITIM signaling via inhibition of SYK also prevents inflammasome activation, since both SYK- and JNK-dependent pathways are necessities for inflammasome activation. CR3, complement receptor 3 as heterodimer of CD11b/ITGAM and CD18/ITGB2; HSCT/DAP10, hematopoietic cell signal transducer; IL, interleukin; ITAM, immunoreceptor tyrosine-based activation motif; ITIM, immunoreceptor tyrosine-based inhibition motif; JNK, C-Jun NH2-terminal protein kinase; NADPH, nicotinamide adenine dinucleotide phosphate; NLRP3, nucleotide-binding oligomerization domain-leucine-rich repeats containing pyrin domain 3; P, phosphate; ROS, reactive oxygen species; SHP1/2, Src homology region 2 domain-containing phosphatase-1/2, also named PTPN6/PTPN11 gene; SIGLEC, sialic acid-binding immunoglobulin type lectin; SIRP, signal regulatory protein; SYK, spleen tyrosine kinase; TREM2, triggering receptor expressed on myeloid cells 2; TYROBP/DAP12, TYRO protein tyrosine kinase binding protein/DNAX-activating protein of 12 kDa. (Image is adapted from Liao et al, 2020)

For instance, SIGLEC-5 recognized sialylated oligosaccharide ligands, thus inhibiting phagocytosis of apoptotic bodies by macrophages (Rapoport *et al*, 2005). Similarly, SIGLEC-11 prevented microglia-mediated uptake of apoptotic neuronal material and decreased LPS-triggered inflammation (Wang & Neumann, 2010). Moreover, murine SIGLEC-E compromised the capacity of microglia to phagocyte neural debris and inhibited phagocytosis-associated oxidative burst (Claude *et al*, 2013). Furthermore, human SIGLEC-3 impaired microglial phagocytosis of aggregated amyloid-β 42 peptide (Griciuc *et al*, 2013). Most recently, it was revealed that SIGLEC-2 damaged the phagocytic ability of microglia during aging and the blockage of SIGLEC-2 enhanced the clearance of α-synuclein fibrils, amyloid-β oligomers, and myelin debris in mice (Pluvinage *et al*, 2019). Interestingly, SIGLECs bearing ITIMs also prevent inflammation via inhibiting the activation of inflammasome. It has been reported that SIGLEC-5 attenuated NLRP3 inflammasome activation induced by Group B *Streptococcus* (GBS) infection (Tsai *et al*, 2020). Likewise, SIGLEC-7 bound GBS β-protein and inhibited NLRP3 inflammasome

activation, thus preventing inflammation in natural killer cells (Fong *et al*, 2018). Thus, modulation of ITIM-containing SIGLECS might be a novel therapeutic strategy for treating inflammation-related neurodegeneration.

Sialic acid residues can also modulate immune activities via inhibition of the complement cascade. It is known that sialylation play a critical role in preventing maternal complement attack to protect fetal extraembryonic tissue (Abeln *et al*, 2019). As well, free Sia monosaccharides decreased the level of C3 and complement component 5, but not complement factor H (CFH) and complement factor I (CFI) in normal human serum. Moreover, free Sia can prevent LPS-induced cleavage of C3 and complement factor B (CFB) when it's added to human serum. Therefore, free Sia might be a negative regulator of the activation of C3 and its followed complement cascade (Fujita *et al*, 1999). However, relatively high concentrations of free Sia were required to observe these effects, questioning whether soluble Sia own the same capacity to inhibit complement activation as glycan-associated Sia has.

It has been reported that uncontrolled activation of CR3 signaling induced early synapse loss in an Alzheimer's disease mouse model (Hong *et al*, 2016). Interestingly, *in vitro* culture systems revealed that desialylation of neurites triggered their removal via CR3-mediated phagocytosis by co-cultured murine microglia (Linnartz *et al.*, 2012) or human macrophages (Linnartz-Gerlach *et al*, 2016). Thus, the sialylation of axons and dendrites seems to be required to avoid uncontrolled elimination by microglia via CR3. Moreover, it was shown that polySia with an average degree of polymerization of 20 (polySia avDP20) inhibited alternative complement activation, thus leading to less cell lysis and less complement-mediated membrane attack complex formation in normal human serum by using mouse hepatoma cells (Karlstetter *et al*, 2017). Recently, Blaum et al. reported that CFH preferred to bind to trisaccharide Neu5Acα2-3Galβ1-4Glc residues, but not to α2.8-linked disialic acid (Blaum *et al*, 2015). This preferential binding forms the complement

component 3b-CFH-Neu5Ac complex (Blaum *et al.*, 2015), which is critical for inhibiting complement amplification (Hyvarinen *et al*, 2016; Parente *et al*, 2017). Since disialic acid and polySia have different properties, it is still to be determined whether polySia avDP20 can also form a complement component 3b-CFH-Neu5Ac complex to prevent complement amplification.

1.2.3 Evidence for bioactivity of soluble polysia avDP20

Evidence for the bioactivity of soluble polySia avDP20 was mainly coming from two recent studies with, both, *in vitro* and *in vivo* data (Karlstetter *et al.*, 2017; Shahraz *et al*, 2015).

In vitro, polySia avDP20 interacted with the ITIM-bearing SIGLEC11 receptor, thus preventing inflammation, vascular endothelial growth factor (VEGF) expression, phagocytosis and oxidative burst of human macrophages as well as reducing loss of neurites in a macrophage-neuron co-culture system (Karlstetter *et al.*, 2017; Shahraz *et al.*, 2015). In detail, polySia avDP20 attenuated LPS triggered gene transcription and protein release of TNF-α and VEGF in human macrophages (Karlstetter *et al.*, 2017; Shahraz *et al.*, 2015). In addition, polySia avDP20 inhibited the LPS-induced increase in human THP1 macrophage phagocytosis, without affecting basal phagocytosis or endocytosis (Shahraz *et al.*, 2015). Moreover, polySia avDP20 reduced the oxidative burst of macrophages initiated by neural debris (Shahraz *et al.*, 2015) or fibrillary amyloid-β1-42 (Shahraz *et al.*, 2015) or debris derived from necrotic human ARPE-19 cells (Karlstetter *et al.*, 2017). Furthermore, in a human macrophage-neuron co-culture system, polySia avDP20 also prevented loss of neurites caused by fibrillary amyloid-β1-42 (Shahraz *et al.*, 2015). Similarly, polySia avDP20 interacted with SIGLEC-E to inhibit the LPS-induced increase of *Tnf- α* transcription in murine embryonic stem cell-derived microglia (ESdM) (Karlstetter *et al.*, 2017). Moreover, polySia avDP20 also inhibited phagocytosis and reactive oxygen species (ROS) production of the mouse microglia cells ESdM incubated

with debris derived from necrotic human ARPE-19 cells, dependent of SIGLEC-E (Karlstetter *et al.*, 2017). Noteworthy, polySia avDP20 also prevented complement-mediated lysis, formation of the membrane attack complex, and activation of the alternative complement pathway (Karlstetter *et al.*, 2017).

In vivo, low-dose intravitreal injection of polySia avDP20 in humanized transgenic mice expressing SIGLEC11 on mononuclear phagocytes blocked mononuclear phagocyte reactivity and prevented laser-induced vascular damage in the retina. Furthermore, polySia avDP20 reduced deposition of the membrane attack complex in both *SIGLEC11* transgenic and wild-type mice (Karlstetter *et al.*, 2017).

Thus, polySia avDP20 might be a disease-modifying therapeutic candidate that prevents PD-related inflammation and neurodegeneration.

1.3 Aim of the study

The aim of this study was to investigate whether polySia avDP20 can prevent inflammation and neurodegeneration in an LPS-induced PD model in wild type and *SIGLEC11* transgenic mice.

2. Materials and methods

2.1 Materials

2.1.1 Chemicals and Reagents

Name	Company
Purified α2.8-linked long chain polySia	provided by Prof. Thomas Scheper, Technical Chemistry, Hannover, Germany or produced in the institute
Citric acid	Carl Roth, Germany
Na_2HPO4	Carl Roth, Germany
NaOH	Carl Roth, Germany
Sodium chloride (NaCl)	Carl Roth, Germany
Ampuwa	Fresenius GmbH, Germany
Ammonium bicarbonate	Sigma, Germany
Ethanol (C2H6O)	Carl Roth, Germany
Tris	Carl Roth, Germany
Glycine	Carl Roth, Germany
Glycerol	Sigma, Germany
Bromphenol blue	Sigma, Germany
Stains-All	Sigma, Germany
Tris HCL	Carl Roth, Germany
Methanol	Carl Roth, Germany
N-acetylneuraminic acid	Carbosynth, UK
Phosphoric acid	Honeywell-Fluka, USA
Periodic acid	Honeywell-Fluka, USA
Sodium thiosulfate	Honeywell-Fluka, USA

Sodium sulfate	Honeywell-Fluka, USA
Sulfuric acid	Honeywell-Fluka, USA
2-thiobarbituric acid	Sigma, Germany
1-butanol	Sigma, Germany
12 N HCl (37 %)	Carl Roth, Germany
DMEM–F12 medium	Gibco/Thermo Fisher Scientific, Germany
N2 supplement	GE Healthcare, Germany
L-glutamine	Gibco/Thermo Fisher Scientific, Germany
Penicillin/streptomycin	Gibco/Thermo Fisher Scientific, Germany
Dimethyl sulfoxide (DMSO)	Roche, Germany
Trypan blue 0.4 %	Gibco/Thermo Fisher Scientific, Germany
Lipopolysaccharide from *E.coli* 0111:B4 strain, for *in vitro* assays	InvivoGen, Germany
Lipopolysaccharide from *Salmonella abortus equi* S-form, for *in vivo* assays	Enzo LifeSciences, Germany
KETANEST® S (Ketamin)	Pfizer Pharma, Germany
Rompun® 2 % (Xylazin)	Bayer, Germany
Phosphate Buffer Saline (PBS)	Gibco/Thermo Fisher Scientific, Germany
QIAzol Lysis Reagent	Qiagen, Germany
Trichloromethane/chloroform	Carl Roth, Germany
Ultra-Pure DEPC treated water	Invitrogen, USA
Deoxynucleotide triphosphates (dNTP) 10 mM	Paqlab Biotechnologies, UK
Primer random p(dN)6	Roche, Germany
SuperScript® III Reverse Transcriptase	Invitrogen, Germany
SYBR® Green ERTM qPCR Super Mix	Invitrogen by Life Technologies, USA
Paraformaldehyde (PFA)	Sigma, Germany

Sucrose	Carl Roth, Germany
Sodium azide	Sigma, Germany
O.C.T.TM Compound, Tissue Tek®	Sakura, USA
Bovine serum albumin (BSA)	Sigma, Germany
Triton X-100	Sigma, Germany
Normal goat serum (NGS)	Sigma, Germany
AquaPoly/Mount	Polysciences Europe, Germany
4',6-diamidino-2-phenylindole (DAPI)	Sigma, Germany
Agarose (PeqGOLD Universal)	PeqLab, Germany
Ethidium Bromide (10 g/l)	Carl Roth, Germany
Acetic acid	Carl Roth, Germany
Ethylendiamintetraacetate (EDTA)	Carl Roth, Germany
Double-distilled water (ddH2O)	autoclaved and filtered in the institute

2.1.2 Buffers and solutions

Name	**Ingredients**
Citric acid-Na2HPO4 buffer solution, pH 4.8	50.7 ml 0.1 M-citric acid 49.3 ml 0.2 M-Na2HPO4
25 mM Ammonium bicarbonate	1.98 g ammonium bicarbonate up to 1 litre deionized water
1 M Ammonium bicarbonate	79.056 g ammonium bicarbonate up to 1 litre deionized water
1 M NaOH	40 g NaOH in 1 litre deionized water
1 M NaCl in 25 mM phosphoric acid	58.44 g NaCl 1.7 ml 15 M phosphoric acid up to 1 litre deionized water

1 M NaCl in 0.1 M NaOH	58.44 g NaCl 100 ml 1M NaOH up to 1 litre deionized water
50 % ethanol	500 ml pure ethanol up to 1 litre deionized water
Tris-Glycin native running buffer (10 x)	Tris base 29g (25 mM) Glycine 144g (192 mM) up to 1 litre deionized water
2 x Tris-Glycine sample loading buffer	4 M Tris HCL 10 % Glycerol 0.1 % Bromphenol blue
Stains-All solution	a pipette tip of Stains-All powder 25 ml methanol 25 ml ddH2O
50 mM phosphoric acid	167 µl phosphoric acid (15 M) up to 50 ml Ampuwa
0.1 M NaOH	5 ml 1 M NaOH up to 50 ml Ampuwa
oxidizing solution (= 200 mM periodic acid, 50 mM phosphoric acid)	2.28 g periodic acid 167 µl phosphoric acid (15 M) up to 50 ml Ampuwa
reducing solution (= 316 mM sodium thiosulfate, 500 mM sodium sulfate, 200 mM sulfuric acid)	2.5 g sodium thiosulfate 3.55 g sodium sulfate up to 48 ml Ampuwa add 2 ml sulfuric acid (5 M)
3 % TBA solution (= 200 mM 2-thiobarbituric acid, 300 mM sodium hydroxide)	1.5 g 2-thiobarbituric acid up to 35 ml Ampuwa add 15 ml NaOH (1 M)

	− protect solution from light
acidic n-butanol (= 37 % hydrochloric acid, 1-butanol)	5 ml HCl (37 %) 45 ml 1-butanol
Anaesthesia solution (Ketamin/Xylazin)	2 ml Ketanest 0.5 ml Rompun 2.5 ml ddH2O
4 % paraformaldehyde (PFA), pH 7.3	20 g PFA 30 ml 1M NaOH 50 ml PBS (10 x) up to 1 litre ddH2O
30 % sucrose solution	30 g sucrose in 100 ml 1 x PBS 0.1 % sodium azide
10x BSA	10 g BSA in 100 ml 1 x PBS
1 % Agarose gel	0.7 g agarose 3.5 µl ethidium bromide 70 ml 1 x Tris/Acetic acid/EDTA buffer
10 x Tris/Acetic acid/EDTA (TAE) buffer	96.8 g Tris base 22.8 g acetic acid 7.4 g EDTA up to 2 litre ddH2O
Reverse transcription mix	1 µl Roche random primer mix (2.5 mg/ml) 1µl dNTPs (10 mM) 11 µl RNA 4 µl 5X RT 1st Strand Buffer 2 µl 0.1 M DTT 1 µl SuperScript III
semi-quantitative real-time PCR (sqRT-PCR) reaction mix (25 µl)	1 µl 200 ng/ µl cDNA 12.5 µl Syber Green Master Mix

	9.5 µl DEPC treated water 1µl forward/reverse primer each (10 pM primers added)

2.1.3 Cell culture media and reagents

N2 cell culture medium (for ESdM)

Component	Volume	Company
DMEM/F-12	500 ml	Gibco/Thermo Fisher Scientific, Germany
N2 medium	5 ml	Gibco/Thermo Fisher Scientific, Germany
L-glutamine	1.2 ml	Gibco/Thermo Fisher Scientific, Germany
Penicillin/Streptomycin (100 X)	5 ml	Gibco/Thermo Fisher Scientific, Germany

2.1.4 Mice

Mouse strain	Origin/Provider
C57BL/6J	Charles River, Sulzfeld, Germany
B6D2 F1/C57/Bl6/6J *SIGLEC11* transgenic mice	University of Bonn, Germany

2.1.5 Primers (all are mouse primers except human *SIGLEC11*)

Gene	Forward Sequence	Reverse Sequence
Gapdh	AACTTTGGCATTGTGGAAGG	GGATGCAGGGATGATGTTCT
Il1β	CTTCCTTGTGCAAGTGTCTG	CAGGTCATTCTCATCACTGTC
Tnfα	GGTGCCTATGTCTCAGCCTCTT	GCCATAGAACTGATGAGAGGGAG
Iba1	GAAGCG AATGCTGGAGAAAC	AAGATGGCAGATCTCTTGCC
Tmem119	GTGTCTAACAGGCCCCAGAA	AGCCACGTGGTATCAAGGAG

Cd68	CAGGGAGGTTGTGACGGTAC	GAAACATGGCCCGAAGTATC
Dap12	ACAGCGGAAGGGACCCGGAAA	TCAGGCCGCTGATGGGCATA
Fcer1g	CTGTCTACACGGGCCTGAAC	AAAGAATGCAGCCAAGCACG
C3	TAGTGCTACTGCTGCTGTTGGC	GCTGGAATCTTGATGGAGACGCTT
Itgam	AATTGGGGTGGGAAATGCCT	TGGTACTTCCTGTCTGCGTG
C4	TGGAGGACAAGGACGGCTA	GGCCCTAACCCTGAGCTGA
Nos-2	AAGCCCCGCTACTACTCCAT	GCTTCAGGTTCCTGATCCAA
Cyba	CCTCCACTTCCTGTTGTCGG	TCACTCGGCTTCCTTTCGGAC
Cybb	GGGAACTGGGCTGTGAATGA	CAGTGCTGACCCAAGGAGTT
Tlr4	AGATCTGAGCTTCAACCCCTTG	TCCACAGCCACCAGATTCTC
Cd14	TGTGGACACGGAAGCAGATC	CGTTGCGGAGGTTCAAGATG
Myd88	ACAAACGCCGGAACTTTTCG	GAAACAACCACCACCATGCG
Bad	ACATTCATCAGCAGGGACGG	ACTCATCGCTCATCCTTCGG
Casp8	TGGAGAAGAGGACCATGCTG	AGTCACACAGTTCCGCCATT
Fadd	GTGGCCTGGACCTGTTCAC	GGGCCAGTCTTTTCCAGTCT
Erk1	GTCTCTGCCCTCGAAAACCA	ATCAACTCCTTCAGCCGCTC
Pik3cd	GTCCACTCCTCCTCCATCCT	CAGCATTCACTTTTCGGCCC
Mlkl	CAAACAGTGAAGCCCCCTGA	AGCTGCTGATGTTTCTGTGGA
Ripk1	TGTACCCTTACCTCCGAGCA	GGCTGCGGTTTTGTCTGTTT
Ripk3	TTCCAGGACTGCGAACCAAA	TCTTTGGCTTGGCTCTCTGG
SIGLEC11	CACTGGAAGCTGGAGCATGG	ATTCATGCTGGTGACCCTGG

2.1.6 Antibodies

2.1.6.1 Primary antibodies

Antigen	Host	Reactivity	Company	Dilution
CD68	rat	mouse	Bio-Rad, MCA1957	1:500

Ionized calcium binding adaptor molecule 1 (IBA1)	rabbit	mouse	Synaptic system, #234003	1:500
Neuronal nuclei (NeuN)	mouse	mouse	Millipore, MAB377	1:500
Tyrosine hydroxylase (TH)	rabbit	mouse	Sigma, # T8700-1VL	1:500

2.1.6.2 Secondary antibodies

Fluorophore	Host	Reactivity	Company	Dilution
Alexa Fluor® 488	goat	rabbit	Invitrogen, #A11008	1:500 for TH 1:400 for IBA1
Cyanine 3(Cy3)-conjugated F(ab')2 fragment	goat	mouse	Dianova, #115-166-072	1:200
Cy3-conjugated F(ab')2 fragment	goat	rat	Dianova, #112-166-072	1:200

2.1.7 Kits and markers

Name	Company
10 kDa Dextrane Sulphate	TdB, Germany
5 kDa Dextrane Sulphate	TdB, Germany
O' RangeRuler 10 bp DNA ladder	Thermo Scientific, USA
100 base pair DNA ladder	Invitrogen, Germany
KAPA mouse genotyping Hot Start Kit	PeqLab, Germany
RED Extract-N-Amp Tissue PCR Kit	Sigma, Germany
RNase-Free DNase Set	Qiagen, Germany
RNeasy® Mini Kit	Qiagen, Germany
SuperScript III Reverse Transcriptase	Invitrogen, Germany

2.1.8 Consumables

Name	Company
Luer syringe, 20 ml	BD Biosciences, USA
1 ml syringe	Braun, Germany
Injection needles	Braun, Germany
Combifix adapter	Braun, Germany
10 µl, 100 µl, 1000 µl pipette tips	StarLab, Germany
5 ml, 10 ml, 25 ml plastic pipettes	Costar, Germany
15 ml, 50 ml plastic tubes	Sarstedt, Germany
Disposable vinyl specimen molds (Cryomold®, 25 x 20 x 5 mm)	Tissue-Tek® Sakura, USA
Erlenmeyer flask, 250 ml	Schott-Duran, Germany
Examination gloves (Micro-Touch)	Ansell Healthcare, Belgium
Glass cover slips (24 x 60 mm)	Thermo Scientific, USA
Polymerase chain reaction (PCR) tubes, 500 µl	Biozym Scientific GmbH, Germany
QPCR Seal optical clear film	PeqLab, Germany
QPCR Semi-skirted 96 well PCR plate	PeqLab, Germany
Stainless steel beads (7 mm)	Qiagen, Germany
SuperFrost® Plus microscope slides	Thermo Scientific, USA
Culture dish (35, 100, 150 mm)	Sarstedt, Germany
12-well plate	Greiner Bio One, Germany
Filter (0.22 µm)	Sarstedt, Germany
Filter (0.45 µm)	Corning, USA
Glass bottle (100, 500, 1000 ml)	Schott-Duran, Germany
Neubauer counting-chamber	Paul Marienfeld GmbH, Germany
Scalpel (Feather disposable scalpel)	Thermo Scientific, USA
Tubes (0.2 ml; 8-strip)	Biozym Scientific GmbH, Germany

Tubes (0.5, 1.5, 2 ml)	Biozym Scientific GmbH, Germany
Tubes (1.8 ml cryotubes)	Nalge Nunc, Denmark
Cell scraper	Sarstedt, Germany
pH test strives (Tritest L pH 1-11)	Macherey & Nagel, Germany

2.1.9 Technical equipment

Name	**Company**
ÄKTA-FPLC	Amersham Bioscience, UK
Sartobind Q Membrane Adsorber (3ml)	Sartorius, Germany
Thermo-block	Eppendorf GmbH, Germany
Mini-Protean Tetra Vertical Electrophoresis Cell	Bio-Rad, Germany
Electrophoresis Power Supply EPS-301	Amersham Bioscience, Germany
HI 9321 Microprocessor pH meter	Hanna Instruments, Germany
Power Pack P25	Biometra, Germany
4-20 % Mini-Protean TGX Stain-Free Protein Gel, 15 well	Bio-Rad, Germany
GelDoc	BioRad, Germany
Perfect BlueTM Horizontal Midi/Mini Gel Systems	PeqLab, Germany
NanoDrop 2000c spectrophotometer	Thermo Scientific, USA
Thermocycler T3 (PCR machine)	Biometra, Germany
Mastercycler realplex 4	Eppendorf, Germany
Freezer -20 °C ProfiLine	Liebherr, Germany
Freezer -80 °C Herafreeze	Heraeus, Germany
Fridge (4˚C)	Liebherr, Germany
Biofuge Fresco/ pico (centrifuges)	Heraeus, Germany

Megafuge, 1.0 R. (centrifuge)	Heraeus, Germany
Microm Cryo Star HM 560	Thermo Scientific, USA
Pumpdrive 5001 (perfusion pump)	Heidolph, Germany
Tissue Lyser LT	Qiagen, Germany
Vortex Genie2	Scientific Industries Inc., USA
Autoclave (Systec D150)	Systec GmbH, Germany
Incubator (Hera Cell 150)	Heraeus Holding GmbH, Germany
Scale (Acculab)	Sartorius, Germany
Vaccum controller (VaccuHandControl)	Vaccumbrand, USA
Vaccum pump (Vaccu-lan network for lab)	Vaccumbrand, USA
Waterbath (WB/OB7-45)	Memmert GmbH & CoKG, Germany
Infinite mplex	Tecan, Switzerland
AxioImager.Z1/ApoTome microscope	Zeiss, Germany
Fluoview1000 Confocal microscope	Olympus, Germany

2.1.10 Software

Name	**Company**
AxioVisio V4.8.2.0	Zeiss, Germany
Corel Draw® 2019	Corel GmbH, Germany
GraphPad Prism 9	GraphPad Software Inc., USA
ImageJ 1.43m	National Institute of Health, USA
EndNote X6	Thomson ISI ResearchSoft, USA
Master cycler ep realplex	Eppendorf, Germany
Microsoft Office 2010	Microsoft, USA
NanoDrop 2000/2000c	Thermo Fisher Scientific, USA

Olympus FluoView V3.1	Olympus, Germany
QuantityOne	Bio-Rad, Germany

2.2 Methods

2.2.1 Production and separation of polySia

The α2.8-linked long chain polySia (~50 -70 kDa) was either kindly provided by Prof. Thomas Scheper, Technical Chemistry, Hannover, Germany or produced in our laboratory as described previously (de Vries *et al*, 2017; Rode *et al*, 2008). PolySia avDP20 was obtained from long chain polySia by a controlled thermal hydrolysis followed a gradient isolation with a fast protein liquid chromatography (FPLC)-based anion exchange chromatography. For thermal hydrolysis, polySia was dissolved in citric acid-Na2HPO4 buffer solution with a final pH 4.8. Then sample was heated at 65 °C for 60 min for spontaneous hydrolysis of long chain polySia. For isolation of polySia avDP20, the pH of fragmented polySia was adjusted to 8 using 0.2 M Na2HPO4 or 1 M NaOH and diluted with Ampuwa water to achieve a Na+ concentration < 0.15 M. After sterile filtration, hydrolyzed polySia was loaded to a 3 x 3 ml Sartobind Q Membrane Adsorber (96IEXQ42EUC11--A, Sartorius) and separated via FPLC-system using 25 mM/1M ammonium bicarbonate buffer as running /elution buffer. After loading, a washing step with 4 column volume (CV) 25 mM ammonium bicarbonate was followed. Then, step gradient elution was performed over 18 CV with elution buffer using 3 segments (32%: 4 CV; 54%: 8 CV; 100%: 6 CV; gradient delay: 10 ml) with a flow-rate of 5 ml/minute. Collected fractions were tested via gel chromatography for appropriate molecular weights.

2.2.2 Size determination of polySia via gel chromatography

For gel chromatography, polySia collected during anion exchange chromatography during different fractions was mixed 1:2 (v/v) with 2 x Tris-Glycine sample loading buffer and loaded on a 4-20 % Mini-PROTEAN TGX Precast Gel and separated for 45-55 minutes by electrophoresis at 120 V. Sulphated dextrans of different sizes (10 kDa and 5 kDa, TdB Consultancy) and O' RangeRuler DNA ladder (10 bp, Thermo Scientific) were used as markers. To remove the blue band background, the gel was washed for about 45 minutes with distilled water. Subsequently, the gel was stained for half an hour at room temperature with 'stains-all' solution and washed with distilled water overnight to clear the background. Fractions with molecular weight around 6 kDa (polySia avDP20) were diafiltrated, lyophilized and then dissolved in Ampuwa water.

2.2.3 Determination of polySia concentration

Determination of the concentration of polySia was performed by an arsenite-free thiobarbituric acid (TBA)-assay. A standard solution with concentrations ranging from 0-4 mg/ml N-acetylneuraminic acid was used for establishing standard curve and all steps of adding reagent were performed on ice. Briefly, 50 µl of eight standards and polySia was heated at 70°C with 500 rpm for 18 hours with pretreated 200 µl 50 mM phosphoric acid to obtain single N-acetylneuraminic acid (sialic acid monomers). The heated samples and the standard solutions were then neutralized with 100 µl 100 mM NaOH followed by treatment with 100 µl oxidizing solution (200 mM periodic acid, 50 mM phosphoric acid) and incubated at 37°C for 0.5 hour with 500 rpm. Subsequently, standards and samples were treated with 500 µl reducing solution (316 mM sodium thiosulfate, 500 mM sodium sulfate, 200 mM sulfuric acid, prepared for every individual assay when the above hydrolysis step began and was kept at room temperature overnight before using) and incubated at room temperature for 10 min. Then, 500 µl of 3 % TBA solution (200 mM 2-

thiobarbituric acid, 300 mM sodium hydroxide) was added followed by a heating step (15 min at 95 °C) in order to form a red colored complex. Afterwards, 700 µl of the standards and samples above were mixed thoroughly with 855 µl acidic n-butanol (n-butanol plus 10% of 12 N HCl) by vortexing. Then, all tubes were centrifuged at 12000 rpm for 5 min to separate two phases. The absorbance of the colorful upper phase of all samples and standards was measured at 549 nm spectrophotometrically (Infinite® 200 Pro, Tecan). The concentration of polySia was then calculated based on standard curve.

2.2.4 Mouse microglia cell line culture

Embryonic stem cell-derived microglia (ESdM) (Beutner *et al*, 2013) were used as substitute for primary cultured microglia. After thawing in pre-warmed N2 culture medium (DMEM–F12 medium, supplemented with 1 % N2 supplement, 0.48 mM L-glutamine, and 1 % penicillin/streptomycin), the cell suspension was centrifuged to get rid of DMSO (1500 rpm, 5 minutes). Then, the cell pellet was resuspended in N2 culture medium and kept in 5 x 10 cm2 diameter culture dishes in an incubator at 37 ˚C with 5 % CO_2. The medium was changed after 24 hours. After another two days, cultured cells reached 80 % - 90 % confluency, cells were detached by a cell scraper, centrifuged (1500 rpm, 5 minutes), and resuspended in fresh N2 culture medium in a 50 ml falcon tube. Then the cells were seeded for bioactivity test.

2.2.5 Bioactivity test

The ESdM cells (1.6 x 10^5 cells/ well) was seeded in 1 ml of culture medium on a 12 well plate and allowed to rest at 37 ˚C with 5 % CO_2. Twenty-four hours later, medium was changed and cells were treated with lipopolysaccharide (LPS, 1 µg/ml, *E.coli* 0111:B4 strain, InvivoGen) or polySia avDP20 (5 µM / 15 µM) or 1 µg/ml LPS plus 5 µM / 15 µM polySia avDP20 or without LPS/polySia avDP20 for another 24 hours. Then, cells were

harvested for isolation of RNA. Semi-quantitative real-time PCR for gene transcription analysis was performed as described below (see 2.2.8).

2.2.6 Experimental animals and genotyping

All animal experiments have obtained the approval from the authors' institutional and governmental review boards and have been complied with the Helsinki Declaration. C57BL/6J mice were obtained from Charles River. *SIGLEC11* transgenic mice (*SIGLEC-11*$^{+/-}$) were generated by pro-nuclear injection as previously described (Karlstetter *et al.*, 2017) and were backcrossed for at least 10 generations with C57BL/6J mice before performing experiments. All mice were maintained in SPF (specific pathogen free) environment with free access to both water and food. The genotyping of the *SIGLEC11* mice was done as described below. RED Extract-N-Amp Tissue PCR Kit with forward primer (5'-CACTGGAAGCTGGAGCATGG-3') and reverse primer (5'-ATTCATGCTGGTGACCCTGG-3') were used to perform *SIGLEC11* genotyping PCR.

Tissue of either ear or tail was taken for the isolation of genomic DNA using the KAPA mouse genotyping Hot Start Kit by using the Master mix as described in Table 2.1 according to the manufacturer's protocol (75 °C for 10 minutes, then 95 °C for 5 minutes, then 4 °C for pause). Then, PCR Master mix with the genotype-specific primers was prepared using the RED Extract-N-Amp Tissue PCR Kit as described in Table 2.2. Afterwards, *SIGLEC11* genotyping of the transgenic mice via PCR with the prepared Master mix was performed over 35 cycles for step 2 to 4 (step 1: initial denaturation 95 °C for 3 minutes; step 2: denaturation 95 °C for 30 seconds; step 3: annealing 60 °C for 40 seconds; step 4: extension 72 °C for 50 seconds; step 5: final extension 72 °C for 10 minutes, then 4 °C for pause).

Table 2. 1 DNA extraction with KAPA kit

Master Mix	**1 x**
DEPC treated H2O	88 µl
10 x KAPA Express Buffer	10 µl
1 U/ µl KAPA Express Extract Enzyme	2 µl

Table 2. 2 PCR with REDExtract kit

Master Mix	**1 x**
DEPC treated H2O	3 µl
DNA	4 µl
REDExtract	10 µl
reverse primer (10 pmol/ µl)	1.5 µl
forward primer (10 pmol/ µl)	1.5 µl

After the PCR, PCR products were loaded onto 1 % agarose gel containing ethidium bromide (1:10000). A 100 base pair DNA ladder was applied as a reference marker. The samples were run at 120 V for 25 - 30 minutes. Afterwards, the gels were visualized using GelDoc with QuantityOne software to get genotyping results (see Figure 2-1).

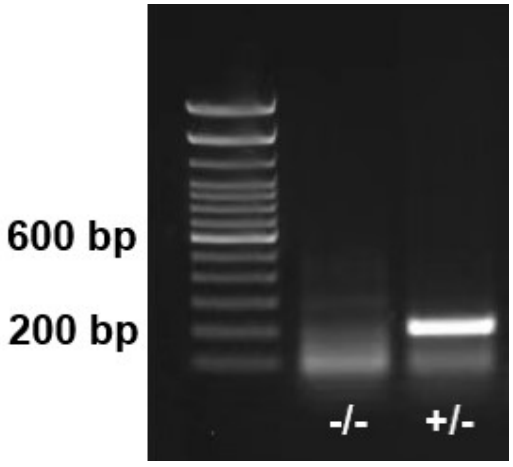

Figure 2 - 1 *SIGLEC11* genotyping example. A 1 % agarose gel with the representative PCR products of *SIGLEC11* genotype is shown. The genotypes were determined by the bands *SIGLEC11* +/- 200 bp.

2.2.7 Experimental animal models

For *in vivo* experiments, *SIGLEC11* transgenic and wild type male mice aged 3-month-old were injected intraperitoneally with four daily 100 µl injections with 1 µg / gram body weight (gbw) bacterial lipopolysaccharides (LPS, lipopolysaccharide from *Salmonella abortus equi* S-form, Enzo LifeSciences) or with 10 µg / gbw polySia avDP20 or with 1 µg / gbw LPS plus 10 µg / gbw polySia avDP20 or with PBS vehicle as control. On the 5th or 19th day after the first day of the treatment mentioned above, mice hearts were perfused with 1 × PBS under deep anesthesia. Then, left brains were immediately homogenized in 1 ml QIAzol with a stainless steel bead in a Tissue Lyser LT for 6 minutes at 50 Hz. for further RNA isolation, while right brains were kept in 4 % paraformaldehyde (PFA) for at least 24 hours at 4 °C for further immunohistochemistry experiments.

2.2.8 Semi-quantitative real-time PCR for gene transcription analysis

Total RNA was isolated from either mouse brains or ESdM via RNeasy RNA isolation kit according to the protocol described below (Table 2.3).

Table 2. 3 RNA isolation

Step	Quantity	Condition	Time
Tissues or cells with QIAzol	1 ml	Room temperature	5 min
Mixed and incubated with chloroform	200 µl	Room temperature	3 min
Centrifugation		12000 rpm, 4˚ C	15 min
Transfer the upper colorless phase into another 2 ml tube	500 µl		
Add 70% EtOH and mix	500 µl		

Transferred the mix into a RNeasy column	600 µl		
Centrifugation		10000 rpm, 4˚ C	1 min
Discard flow-through			
Transferred the rest of mix into a RNeasy column	400 µl		
Centrifugation		10000 rpm, 4˚ C	1 min
Discard flow-through			
Add RW1 buffer	350 µl		
Centrifugation		10000 rpm, 4˚ C	1 min
Discard flow-through			
Incubation with DNase I (10 µl DNase stock + 70 µl RDD buffer)	80 µl	Room temperature	15 min
Add RW1 buffer	350 µl		
Centrifugation		10000 rpm, 4˚ C	1 min
Discard flow-through			
Add RPE buffer	500 µl		
Centrifugation		10000 rpm, 4˚ C	1 min
Discard flow-through			
Add RPE buffer	500 µl		
Centrifugation		10000 rpm, 4˚ C	2 min
Transfer column into another 2 ml tube			
Centrifugation		17000 rpm, 4˚ C	1 min
Transfer column in a 1.5 ml tube			
Incubate with DEPC treated water	50 µl	Room temperature	1 min
Centrifugation		10000 rpm, 4˚ C	1 min
Collect the flow-through			

Continue with reverse transcription or store at -80°C			

After RNA isolation, the synthesis of cDNA by reverse transcription was performed using Random Primer mix and SuperScript III RT set according to the protocol described below (Table 2.4).

Table 2. 4 Reverse transcription (RT)

Prepare RT mixture (I)	**Components**	**Quantity**
	dNTPS	1 µl
	2.5 mg/ml Primer random p(dN)6	1 µl
	RNA	11 µl
Initiate RT program	**Temperature**	**Time**
	65 ˚C	5 min
	4 ˚C	1 min
	4 ˚C	pause
Add RT mixture (II)	**Components**	**Quantity**
	5 x first-strand buffer	4 µl
	0.1 M DTT	2 µl
	Superscript® III	1 µl
Continue RT program	**Temperature**	**Time**
	25 ˚C	5 min
	55 ˚C	60 min
	70 ˚C	20 min
	4 ˚C	pause

After reverse transcription, the ABI 5700 Sequence Detection System was used for semi-quantitative real-time PCR (sqRT-PCR) running for 40 cycles with a Tm of 60 °C (Table

2.5), performed with specific oligonucleotides and SYBR® GreenER™ qPCR SuperMix Universal (see 2.1.2 for the preparation of sqRT-PCR reaction mix). For sqRT-PCR quantification, the ΔΔCT method was performed with GAPDH as internal standard.

Table 2. 5 sqRT-PCR program

Step		**Temperature**	**Time**	**Cycle**
1. Initial denaturation		95 ˚C	8 minutes 30 seconds	
2. Amplification	Denaturation	95 ˚C	15 seconds	40
	Annealing	60 ˚C	30 seconds	
	Elongation	72 ˚C	30 seconds	
3. Inactivation		95 ˚C	1 minutes	
4. Melting curve		55 ˚C – 95 ˚C	20 minutes	
5. Final denaturation		95 ˚C	15 seconds	
6. Pause		4 ˚C	pause	

2.2.9 Immunohistochemistry

The right hemispheres were collected and stored as described above. Afterwards, brains were transferred from 4 % paraformaldehyde (PFA) into 30 % sucrose supplemented with 0.1 % sodium azide and stored at 4 °C until processed into frozen cryosections. Then, fixed brains were sectioned in the rostral-caudal coronal plane with a thickness of 20 µm and mounted onto superfrost slides. For neuronal quantifications, slides containing SN*pc* matched levels (e.g. bregma −3.20, −3.40 and −3.80 mm) per animal were blocked with blocking solution (PBS containing 10 % bovine serum albumin, 0.2 % triton X-100 and 5 % normal goat serum for 1 hour followed by 2-hour incubation with primary

antibodies against dopaminergic neurons marker tyrosine hydroxylase (TH) (1:500, rabbit-anti) and against neuronal nuclei marker NeuN (1:500, mouse-anti-human/mouse) in blocking solution. After 3 times washing with 1 × PBS, the slices were incubated with corresponding secondary antibodies in blocking solution for 2 hours at room temperature (Alexa-488-conjugated goat-anti-rabbit antibody, 1:500 and Cy3-conjugated goat anti-mouse IgG F(ab´)2 antibody, 1:200). After 2 times washing with 1 × PBS, slides were stained by 4′,6-diamidino-2-phenylindole (DAPI, 1:10000) followed by washing with 1 × PBS once. Then, slides were mounted with Aqua-poly/mount and were stored at 4 °C until images were taken. Images was acquired as described before (Bodea *et al.*, 2014; Shahraz *et al*, 2021) with an AxioObserver Z1 inverted microscope with Apotome (Carl Zeiss) via AxioCam Rm (AxioVision software).

For microglia evaluation, sections at bregma level −3.18 mm were blocked with blocking solution (PBS containing 10 % bovine serum albumin, 0.25 % triton X-100) for 2 hour at room temperature followed by overnight incubation (about 18 hours) at 4 °C with primary antibodies against microglial marker ionized calcium binding adaptor molecule1 (IBA1, 1:500, rabbit-anti) and against lysosomal marker CD68 (1:500, rat-anti-mouse) in incubation solution (PBS containing 5 % bovine serum albumin, 0.05 % triton X-100). After 5 times washing with 1 × PBS, the slices were incubated with corresponding secondary antibodies in blocking solution for 2 hours at room temperature (Alexa-488-conjugated goat-anti-rabbit antibody, 1:400 and Cy3-conjugated goat-anti-rat IgG F(ab´)2 antibody, 1:200). After 3 times washing with 1 × PBS, slides were stained by 4′,6-diamidino-2-phenylindole (DAPI, 1:10000) followed by washing with 1 × PBS once. Then, slides were mounted with Aqua-poly/mount and were stored at 4 °C until images were taken. Four confocal z-stacks were taken in the substantia nigra *pars reticulata* (SN*pr*) for each mouse with an SP8 confocal microscope using a 40 x objective lense and the LAS-X software (both Leica, Germany). IBA1-positive cells were counted in the SN*pr* in the section levels mentioned above. Additionally, the area occupied by IBA1-positive and CD68-positive

staining was analyzed. Respective isotype control and secondary antibodies were utilized in all immunostainings in parallel to the antigen-specific staining. All images were analyzed by using ImageJ software (National Institutes of Health).

2.2.10 Statistical analysis

At least three independent experiments were performed. Data are presented as mean ± SEM. Data normality and the equality of variances were examined by Shapiro-Wilk test and Brown-Forsythe test, respectively. Data were analyzed by Welch's ANOVA followed by Dunnett's T3 post hoc test for unequal variances and one-way ANOVA followed by Bonferroni post hoc test for equal variances using GraphPad Prism 9.0.0 (GraphPad Software, Inc.). Results are considered statistically significant as $*p < 0.05$, $**p < 0.01$, or $***p < 0.001$.

3. Results

3.1 Production of polySia avDP20

To isolate polysialic acid with a molecular weight of ~ 6 kDa (polySia avDP20), the biotechnologically produced long chain polySia was hydrolysed by mild heating and then separated by anion exchange chromatography. The gel electrophoresis confirmed the low molecular weight of around 6 kDa of polySia avDP20 (Figure 3-1A). Then, polySia avDP20 was diafiltrated, lyophilized and dissolved in Ampuwa water. Subsequently, the concentration of polySia avDP20 was determined by the TBA assay.

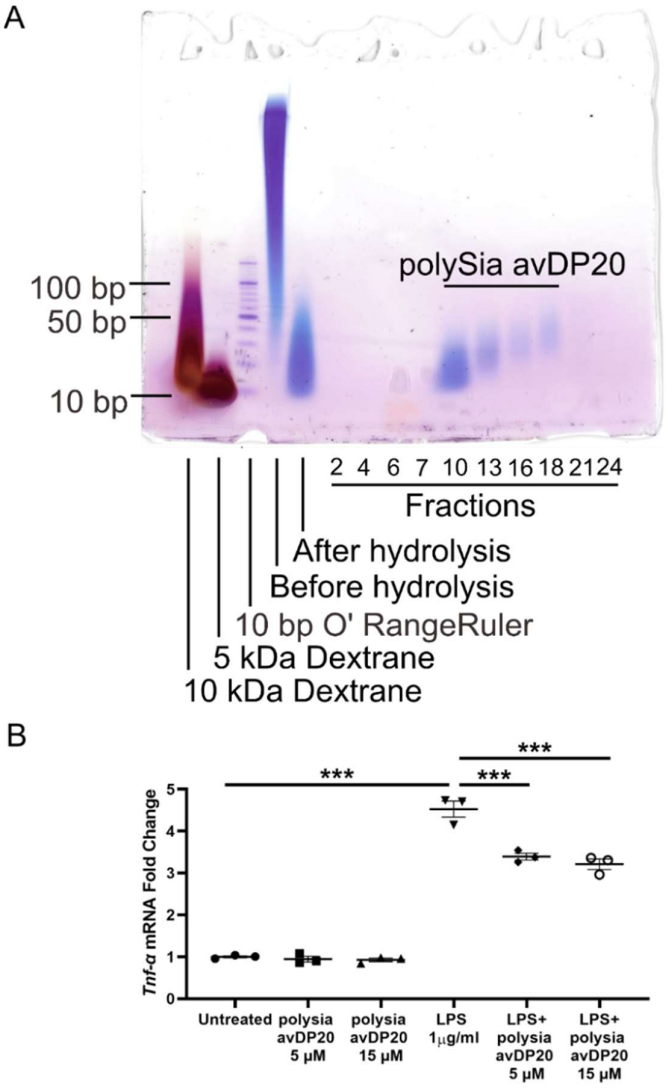

Figure 3 - 1 PolySia avDP20 was produced and inhibited inflammation in LPS challenged embryonic stem cell-derived microglia (ESdM). (A). Fragmented polySia was obtained after heat-mediated hydrolysis and polySia avDP20 was isolated via anion exchange chromatography. PolySia avDP20 showed a molecular weight of ~6 kDa. Thus, fractions 10 to 18 are aimed polySia avDP20. Dextran sulfate with molecular weights of ~5 kDa and ~10 kDa as well as O' RangeRuler 10bp DNA ladder served as molecular weight controls. (B). The levels of *Tnf-α* mRNA expression were reduced after 24 hours of co-treatment with LPS (1 µg/ml) and polySia avDP20 (5 and 15 µM) in ESdM. Data are presented as mean ± SEM. n = 3, ns = not significant, ***P < 0.001, ANOVA followed by Bonferroni correction.

3.2 PolySia avDP20 inhibited Tnf-α mRNA expression in LPS activated mouse microglial lines (ESdM)

As shown previously (Karlstetter *et al.*, 2017; Shahraz *et al.*, 2015), polySia avDP20 inhibited expression of tumor necrosis factor-α (*Tnf-α*) in both human THP1 macrophages with SIGLEC11 receptor and murine embryonic stem cell-derived microglia (ESdM) without SIGLEC11 receptor upon LPS treatment. To confirm the anti-inflammatory effect of polySia avDP20 *in vitro* before the application of polySia avDP20 for *in vivo* experiments, we analyzed the effect of polySia avDP20 on ESdM which has the nearest functionally related SIGLEC receptor of SIGLEC11, namely SIGLEC-E. Thus, we performed semi-quantitative real-time PCR (sqRT-PCR) for gene transcripts of *Tnf-α*. After 24 hours of co-treatment with LPS and polySia avDP20, a reduction in *Tnf-α* gene transcripts was observed at both 5 µM polySia avDP20 (mean ± SEM; *Tnf-α* reduced from 4.53 ± 0.19 to 3.39 ± 0.08, P < 0.001; Figure 3-1B) and 15 µM polySia avDP20 (mean ± SEM; *Tnf-α* reduced from 4.53 ± 0.19 to 3.21 ± 0.12, P < 0.001; Figure 1B) in 1 µg/ml LPS-stimulated ESdM.

3.3 PolySia avDP20 inhibited activation of inflammation-, TLR4 signaling- and phagocytosis-related pathways in *SIGLEC11* transgenic mice brain upon LPS application

To investigate the effect of polySia avDP20 on immune-related features of PD *in vivo*, four consecutive daily intraperitoneal injections of 1 µg / gbw LPS or 1 µg / gbw LPS plus 10 µg / gbw polySia avDP20 were performed in both wild type and humanized *SIGLEC11* transgenic mice or littermate controls. Then, mice brains were analyzed via sqRT-PCR on day 5 and day 19. As shown previously (Shahraz *et al.*, 2021), repeated systemic challenge with LPS induced dopaminergic neurodegeneration that was associated with activation of phagocytosis-related gene transcription and microglia. Therefore, we first explored the effect of polySia avDP20 in this animal model in relation to inflammation associated gene transcription.

PolySia avDP20 inhibited the LPS-induced gene transcription of *Il-1β* in *SIGLEC11* transgenic mice on day 19, but not on day 5. In detail, transcription levels of *Il-1β* decreased from 3.63 ± 0.41 in LPS-injected *SIGLEC11* transgenic mice to 2.13 ± 0.18 (mean ± SEM; $p = 0.0282$; Figure 3-2A) after treatment with polySia avDP20. Unexpectedly, polySia avDP20 elevated the gene transcription of *Il-1β* in wild type mice without LPS challenge on day 5 (mean ± SEM; increased from 1.04 ± 0.11 to 1.70 ± 0.17, $p = 0.0499$; Figure S1A).

Additionally, polySia avDP20 inhibited the LPS-induced gene transcription of *Cd14* and *Myd88* of the TLR4 signaling pathway in *SIGLEC11* transgenic mice on day 19, but not on day 5. In detail, a reduction in *Cd14* gene transcripts was observed in LPS-challenged *SIGLEC11* transgenic mice after treatment with polySia avDP20 (mean ± SEM; reduced from 2.46 ± 0.19 to 1.76 ± 0.10, $p = 0.0034$; Figure 3-2B). Similarly, *Myd88* mRNA levels were attenuated from 1.21 ± 0.08 to 0.92 ± 0.05 in *SIGLEC11* transgenic mice by treatment with polySia avDP20 (mean ± SEM; $p = 0.0158$; Figure 3-2B). Additionally, polySia avDP20 elevated the gene transcription of *Cd14* in wild type mice without LPS

challenge on day 5 (mean ± SEM; increased from 1.01 ± 0.05 to 1.59 ± 0.14, p = 0.0387; Figure S1B).

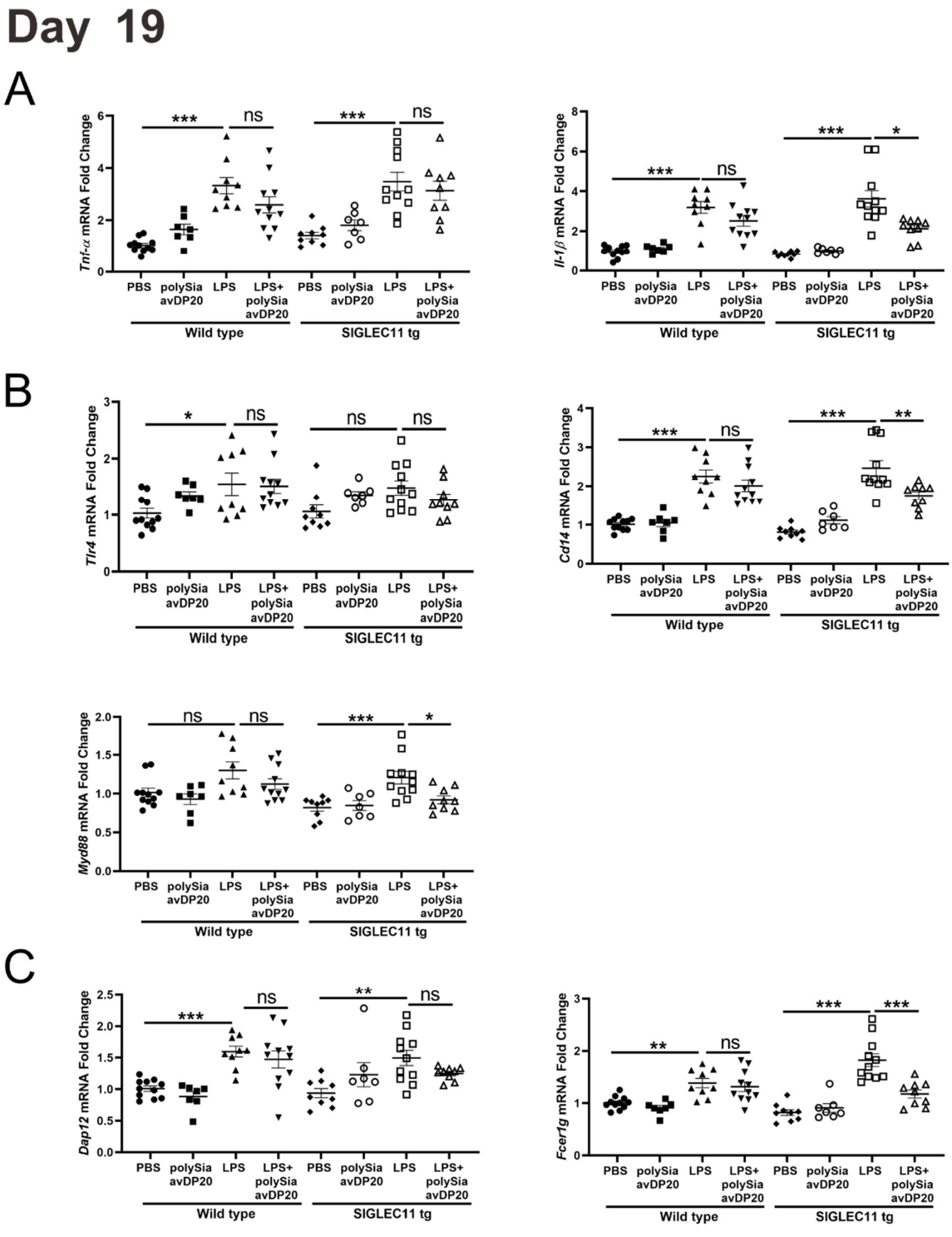

Figure 3 - 2 PolySia avDP20 attenuated the elevated transcription levels of inflammatory pathway-, TLR4 signaling pathway- and phagocytosis pathway-related genes in *SIGLEC11* transgenic mice brain upon repeated systemic challenge with LPS. (A). For inflammatory pathway, *Tnf-α* and *Il-1β* transcription were selected to study the effects of polySia avDP20 in both wild type mice and *SIGLEC11* transgenic mice on day 19. PolySia avDP20 inhibited the LPS-induced gene transcription of *Il-1β* in *SIGLEC11* transgenic mice on day 19. (B). For TLR4 signaling pathway pathway, *Tlr4*, *Cd14*, and *Myd88* transcription were selected to study the effects of polySia avDP20 in both wild type mice and *SIGLEC11* transgenic mice on day 19. PolySia avDP20 inhibited the LPS-induced gene transcription of *Cd14* and *Myd88* in *SIGLEC11* transgenic mice on day 19. (C). For phagocytosis pathway, *Dap12* and *Fcer1g* transcription were selected to study the effects of polySia avDP20 in both wild type mice and *SIGLEC11* transgenic mice on day 19. PolySia avDP20 inhibited the LPS-induced gene transcription of *Fcer1g* in *SIGLEC11* transgenic mice on day 19. Data are presented as mean ± SEM. n = 7-11, ns = not significant, *P < 0.05, **P < 0.01, ***P < 0.001, Welch's ANOVA followed by Dunnett's T3 post hoc test for unequal variances and one-way ANOVA followed by Bonferroni post hoc test for equal variances.

To explore the effect of polySia avDP20 on phagocytosis-related pathway, we analyzed the genes of the two main transmembrane-signaling molecules, namely TYRO protein tyrosine kinase-binding protein (*Tyrobp/Dap12*) and Fc fragment of IgE, high affinity I, receptor for gamma polypeptide (*Fcer1g*). PolySia avDP20 attenuated LPS-induced gene transcription of *Fcer1g* in *SIGLEC11* transgenic mice on day 19, but not on day 5. In detail, *Fcer1g* mRNA levels were reduced from 1.82 ± 0.12 in LPS-injected *SIGLEC11* transgenic mice to 1.18 ± 0.08 (mean ± SEM; $p < 0.0001$; Figure 3-2C) after treatment with polySia avDP20. Interestingly, the *Fcer1g* mRNA levels upon polySia avDP20 treatment alone was significantly higher than those observed in PBS control group in wild type mice on day 5 (mean ± SEM; 1.01 ± 0.05 vs 1.32 ± 0.04; $p = 0.0024$; Figure S1C).

Taken together, application of polySia avDP20 attenuated the increased mRNA levels of the inflammatory cytokine *Il-1β*, the TLR4 signaling pathway related genes *Cd14* and *Myd88* and the phagocytosis signaling pathway related gene *Fcer1g* after LPS challenge in *SIGLEC11* transgenic mice on day 19.

3.4 PolySia avDP20 prevented activation of complement and oxidative burst-related pathways in *SIGLEC11* transgenic mice brain upon LPS application

To examine the effect of polySia avDP20 on complement-related pathways, we analyzed the complement factor 3 (*C3*), integrin alpha M (*Itgam*)-one subunit of the complement factor C3 receptor and complement factor 4 (*C4*) for investigation. PolySia avDP20 decreased LPS-induced gene transcription of *Itgam* and *C4* in *SIGLEC11* transgenic mice on day 19 but not on day 5. In detail, *Itgam* mRNA expression were reduced from 1.48 ± 0.13 in LPS-injected *SIGLEC11* transgenic mice to 1.04 ± 0.06 (mean ± SEM; p =0.0419; Figure 3-3A) after treatment with polySia avDP20. Similarly, *C4* mRNA expression were attenuated from 2.21 ± 0.31 to 1.16 ± 0.13 in SIGLEC11 transgenic mice (mean ± SEM; p =0.0453; Figure 3-3A). Interestingly, polySia avDP20 treatment alone elevated the mRNA levels of both *Itgam* and *C4* in wild type mice on day 5 (mean ± SEM; *Itgam*: 1.02 ± 0.07 vs 1.84 ± 0.10; p = 0.0002; *C4:* 1.02 ± 0.08 vs 2.10 ± 0.24; p = 0.0258; Figure S2A). Oppositely, polySia avDP20 treatment alone decreased the mRNA levels of both *Itgam* and *C4* in *SIGLEC11* transgenic mice on day 5 (mean ± SEM; *Itgam*: 1.41 ± 0.12 vs 0.91 ± 0.07; p = 0.0332; *C4:* 1.62 ± 0.21 vs 0.80 ± 0.12; p = 0.0364; Figure S2A).

To study the effect of polySia avDP20 on oxidative burst-related pathways, we analyzed nitric oxide 2 (*Nos2*) and the two subunits of NADPH oxidase complex, namely cytochrome b-245 alpha chain (*Cyba*) as well as cytochrome b-245 heavy chain (*Cybb*). PolySia avDP20 reduced the LPS-induced gene transcription of *Cybb* in *SIGLEC11* transgenic mice on day 19, but not on day 5. In detail, *Cybb* mRNA expression were decreased from 4.02 ± 0.27 in LPS-treated *SIGLEC11* transgenic mice to 2.80 ± 0.31 (mean ± SEM; p =0.003; Figure 3-3B) after treatment with polySia avDP20. Interestingly, polySia avDP20 treatment alone elevated the mRNA levels of *Cybb* in wild type mice on day 5 (mean ± SEM; 0.97 ± 0.09 vs 1.60 ± 0.13; p = 0.0144; Figure S2B).

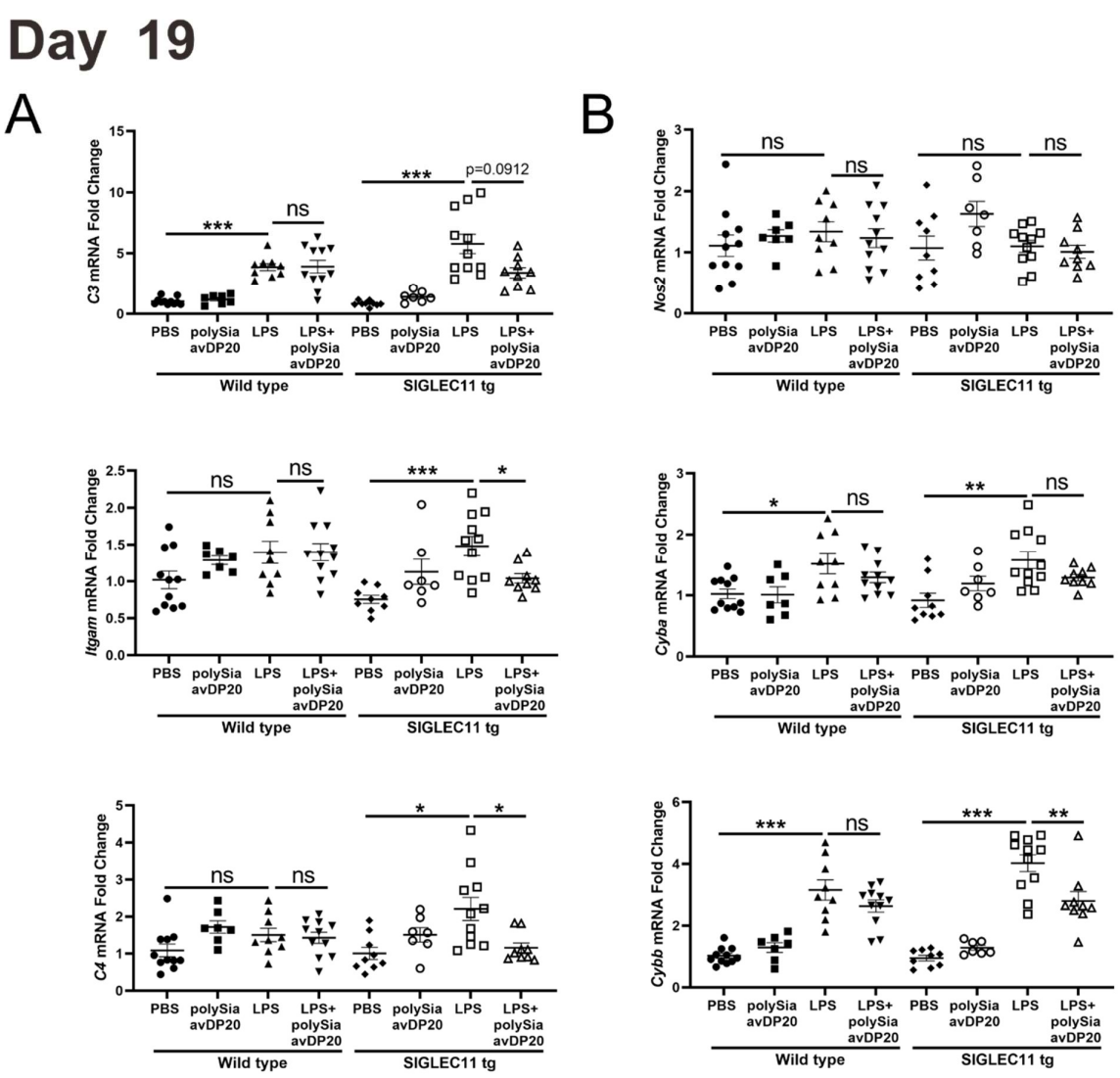

Figure 3 - 3 PolySia avDP20 attenuated the increased transcription levels of complement pathway- and radical production pathway-related genes in *SIGLEC11* transgenic mice brain upon repeated systemic challenge with LPS. (A). For complement pathway, *C3*, *Itgam*, and *C4* transcription were analyzed to evaluate the effects of polySia avDP20 in both wild type mice and *SIGLEC11* transgenic mice on day 19. PolySia avDP20 inhibited the LPS-induced gene transcription of *Itgam* and *C4* in *SIGLEC11* transgenic mice on day 19. (B). For radical production pathway, *Nos2*, *Cyba*, and *Cybb* transcription were selected to study the effects of polySia avDP20 in both wild type mice and *SIGLEC11* transgenic mice on day 19. PolySia avDP20 inhibited the LPS-induced gene transcription of *Cybb* in *SIGLEC11* transgenic mice on day 19. Data are presented as mean ± SEM. n = 7-11, ns = not significant, *P < 0.05, **P < 0.01, ***P < 0.001, Welch's ANOVA followed by Dunnett's T3 post hoc test for unequal variances and one-way ANOVA followed by Bonferroni post hoc test for equal variances.

In summary, treatment of polySia avDP20 reduced the elevated transcription levels of complement pathway related genes (*Itgam and C4*) and the oxidative burst pathway-related gene *Cybb* after LPS challenge in *SIGLEC11* transgenic mice on day 19.

3.5 PolySia avDP20 prevented activation of apoptosis and necroptosis-related pathways in *SIGLEC11* transgenic mice brain upon LPS application

Furthermore, we analyzed genes related to the apoptosis (*Bad, Casp8, Fadd, Erk1, and Pik3cd*) and necroptosis (*Mlkl, Ripk1, and Ripk3*) pathways to study the effect of polySia avDP20 on cell death.

PolySia avDP20 prevented the elevated transcription levels of the apoptosis pathway-related gene *Casp8* upon LPS challenge in *SIGLEC11* transgenic mice on day 19, but not on day 5. In detail, *Casp8* mRNA levels were decreased from 1.37 ± 0.07 in LPS-injected *SIGLEC11* transgenic mice to 1.11 ± 0.06 (mean ± SEM; p =0.0187; Figure 3-4A) after treatment with polySia avDP20. Unexpectedly, higher expression of *Bad* and *Pik3cd* mRNA were observed in the group treated with polySia avDP20 alone compared to PBS controls in *SIGLEC11* transgenic mice on day 19 (mean ± SEM; *Bad*: 0.98 ± 0.10 vs 1.42 ± 0.13; p = 0.0143; *Pik3cd*: 0.83 ± 0.09 vs 1.46 ± 0.16; p = 0.0123; Figure 3-4A). Similarly, *Pik3cd* mRNA levels were higher in the group treated with polySia avDP20 alone than those observed in PBS controls in wild type mice on day 5 (mean ± SEM; 1.04 ± 0.12 vs 2.12 ± 0.19; p < 0.0001; Figure S3A).

PolySia avDP20 also prevented the elevated transcription levels of the necroptosis pathway-related genes *Ripk1* and *Ripk3* upon LPS challenge in *SIGLEC11* transgenic mice on day 19, but not on day 5. In detail, *Ripk1* mRNA levles were decreased from 1.27 ± 0.12 in LPS-injected *SIGLEC11* transgenic mice to 0.89 ± 0.04 (mean ± SEM; p =0.0099; Figure 3-4B) after treatment with polySia avDP20. Similarly, *Ripk3* transcript

levels were reduced from 1.42 ± 0.15 to 0.92 ± 0.09 in *SIGLEC11* transgenic mice (mean ± SEM; p =0.0255; Figure 3-4B). Additionally, *Ripk1* mRNA level were elevated in the group treated with polySia avDP20 alone compared to PBS controls in wild type mice on day 5 (mean ± SEM; 1.02 ± 0.08 vs 1.73 ± 0.18; p = 0.0059; Figure S3B).

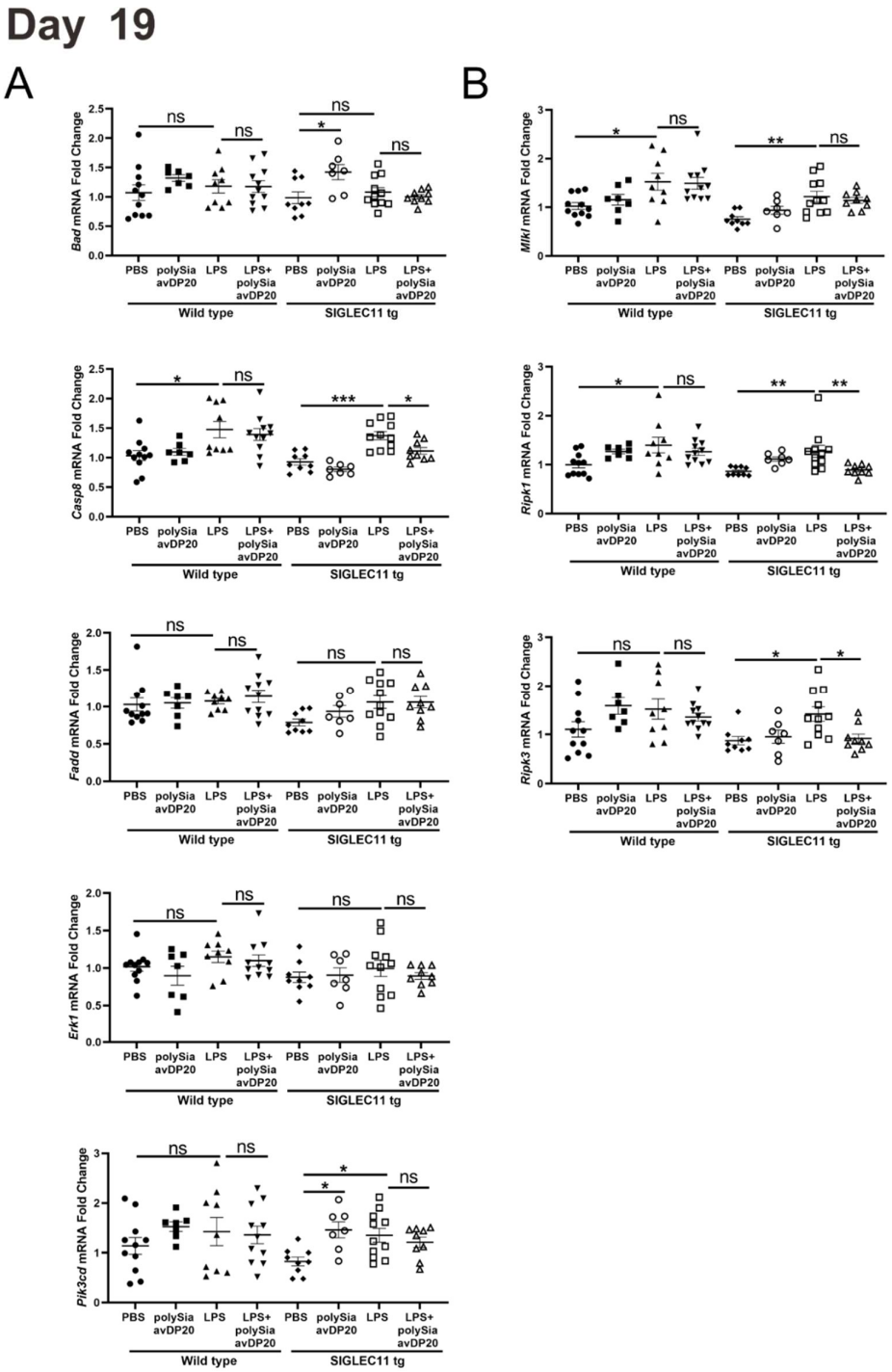

Figure 3 - 4 PolySia avDP20 attenuated the increased transcription levels of apoptosis pathway- and necroptosis pathway-related genes in *SIGLEC11* transgenic mice brain upon repeated systemic challenge with LPS. (A). *Bad*, *Casp8*, *Fadd*, *Erk1*, and *Pik3cd* transcription levels were analyzed to determine the effects of polySia avDP20 in both wild type mice and *SIGLEC11* transgenic mice on day 19. PolySia avDP20 inhibited the LPS-induced gene transcription of *Casp8* in *SIGLEC11* transgenic mice on day 19. Unexpectedly, higher transcript levels of *Bad* and *Pik3cd* were observed in the group treated with polySia avDP20 alone compared to PBS controls in *SIGLEC11* transgenic mice on day 19. (B). For necroptosis pathway, *Mlkl*, *Ripk1*, and *Ripk3* transcription were selected to study the effects of polySia avDP20 in both wild type mice and *SIGLEC11* transgenic mice on day 19. PolySia avDP20 inhibited the LPS-induced gene transcription of both *Ripk1* and *Ripk3* in *SIGLEC11* transgenic mice on day 19. Data are presented as mean ± SEM. n = 7-11, ns = not significant, *P < 0.05, **P < 0.01, ***P < 0.001, Welch's ANOVA followed by Dunnett's T3 post hoc test for unequal variances and one-way ANOVA followed by Bonferroni post hoc test for equal variances.

Taken together, treatment of polySia avDP20 reduced the elevated transcription levels of the apoptosis pathway-related genes (*Casp8*) and necroptosis pathway-related genes (*Ripk1* and *Ripk3*) after LPS challenge in *SIGLEC11* transgenic mice on day 19. Furthermore, *Pik3cd* and *Ripk1* mRNA levels were higher in the group treated with polySia avDP20 alone, than those observed in PBS controls in wild type mice on day 5. Similarly, *Bad* and *Pik3cd* mRNA levels were higher in the group treated with polySia avDP20 alone than those observed in PBS controls in *SIGLEC11* transgenic mice on day 19.

3.6 PolySia avDP20 attenuated the microglia activation in *SIGLEC11* transgenic mice brain upon LPS application at both transcription and protein levels

To check the effect of polySia avDP20 on the microglia response, we analyzed widely used microglia markers Ionized calcium binding adaptor molecule 1 (IBA1), TMEM119, and Cluster of Differentiation 68 (CD68).

First, we performed a transcription analysis by sqRT-PCR for the microglial markers *Iba1*, *Tmem119* and *Cd68*. We observed a reduction of the LPS-induced gene transcription of *Iba1* after treatment of polySia avDP20 in *SIGLEC11* transgenic mice on day 19, but not

on day 5. In detail, *Iba1* mRNA expression were reduced from 2.08 ± 0.18 in LPS-treated *SIGLEC11* transgenic mice to 1.42 ± 0.07 (mean ± SEM; p =0.0253; Figure 3-5) after polySia avDP20-injection. Similarly, the increased levels of *Cd68* upon LPS challenge was reduced in *SIGLEC11* transgenic mice after the treatment of polySia avDP20 (mean ± SEM; 1.42 ± 0.13 vs 1.04 ± 0.07; p = 0.0453; Figure 3-5). Furthermore, *Iba1* mRNA levels were higher in the group treated with polySia avDP20 alone than those observed in PBS controls in wild type mice on day 5 (mean ± SEM; 1.02 ± 0.07 vs 1.38 ± 0.09; p = 0.0560; Figure S4). However, *Cd68* mRNA levels were lower in the group treated with polySia avDP20 alone than those observed in PBS controls in *SIGLEC11* transgenic mice on day 5 (mean ± SEM; 1.06 ± 0.10 vs 0.65 ± 0.03; p = 0.0297; Figure S4).

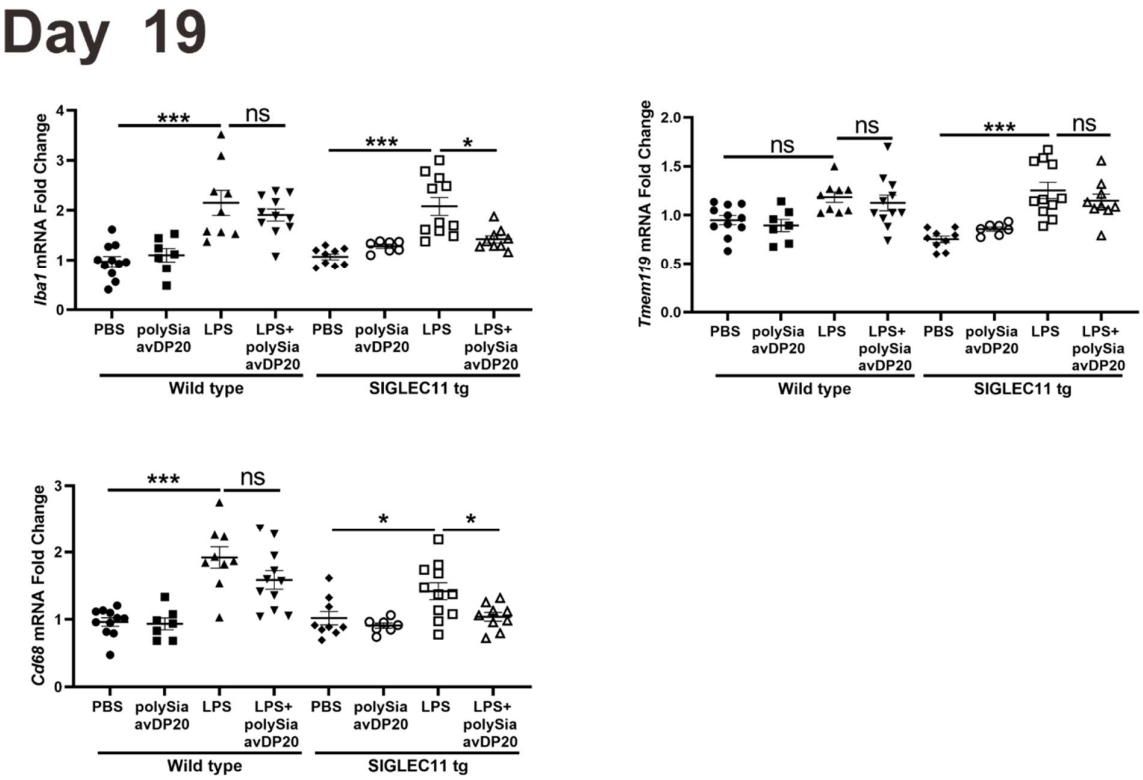

Figure 3 - 5 PolySia avDP20 attenuated the increased transcription levels of the microglial marker genes *Cd68 and Iba1* in *SIGLEC11* transgenic mice brain upon repeated systemic challenge with LPS. *Cd68*, *Iba1*, and *Tmem119* gene transcription levels were analyzed to determine the effects of polySia avDP20 on the microglia status in both wild type mice and *SIGLEC11* transgenic mice on day 19. PolySia avDP20 inhibited the LPS-induced gene transcription of *Iba1* and *Cd68* in *SIGLEC11* transgenic mice on day 19. Data are presented as mean ± SEM. n = 6-11, ns = not significant, *P <

0.05, **P < 0.01, ***P < 0.001, Welch's ANOVA followed by Dunnett's T3 post hoc test for unequal variances and one-way ANOVA followed by Bonferroni post hoc test for equal variances.

Furthermore, we studied matched bregma levels of brain sections for the protein expression of the microglial activation marker IBA1 and CD68 in the substantia nigra *pars reticulata* (SN*pr*) via immunohistochemistry. For quantification of the IBA1 intensity of the immunohistochemistry, polySia avDP20 displayed a good trend to decrease the relative IBA1 intensity induced by LPS challenge in *SIGLEC11* transgenic mice on day 5 (mean ± SEM; 291.0 ± 20.86 % vs 226.1 ± 21.05 %; p = 0.0996; Figure S5B), and significantly reduced that in *SIGLEC11* transgenic mice on day 19 (mean ± SEM; 154.4 ± 12.77 % vs 107.5 ± 5.73 %; p = 0.021; Figure 3-6B). Likewise, polySia avDP20 showed a trend to prevent the LPS-caused increase of relative IBA1 positive cell density in *SIGLEC11* transgenic mice on day 5 (mean ± SEM; 316.5 ± 26.27 % vs 226.6 ± 10.34 %; p = 0.0572; Figure S5B), and significantly reduced that in both wild type mice and *SIGLEC11* transgenic mice on day 19 (mean ± SEM; wild type mice: 140.7 ± 11.56 % vs 109.2 ± 4.86 %; p = 0.022; *SIGLEC11* transgenic mice: 125.0 ± 6.00 % vs 99.95 ± 5.20 %; p = 0.0111; Figure 3-6B). In addition, quantification of the CD68 immunohistochemistry data showed that the elevated relative CD68 intensity upon LPS challenge was diminished in both wild type mice (mean ± SEM; 235.1 ± 30.24 % vs 126.0 ± 15.04 %; p = 0.0016; Figure 3-6B) and *SIGLEC11* transgenic mice (mean ± SEM; 224.6 ± 25.43 % vs 80.86 ± 5.12 %; p = 0.001; Figure 3-6B) after the treatment of polySia avDP20 on day 19 but not on day 5.

Day 19

A

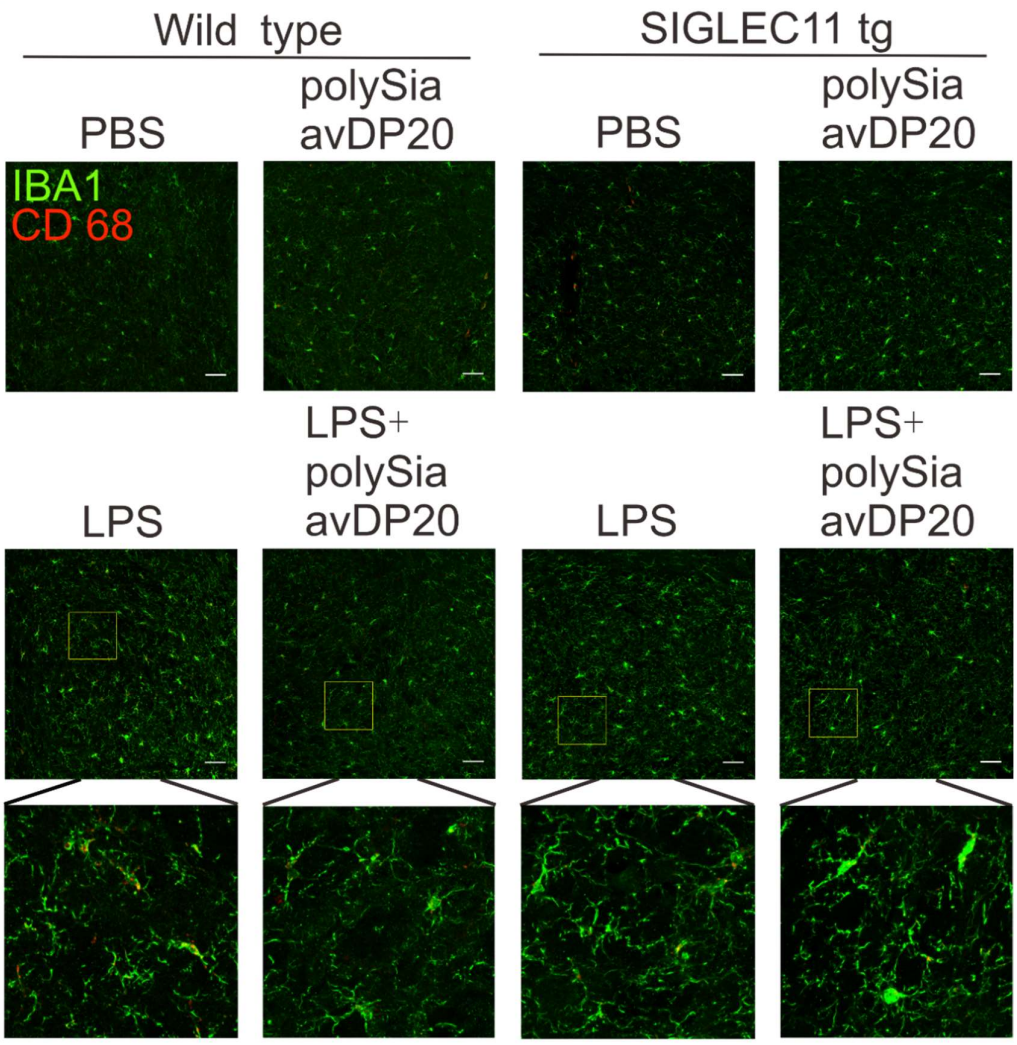
Wild type
SIGLEC11 tg
PBS
polySia avDP20
PBS
polySia avDP20
IBA1
CD 68
LPS
LPS+ polySia avDP20
LPS
LPS+ polySia avDP20
Magnification

B

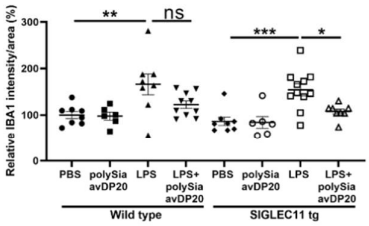
Relative IBA1 intensity/area (%)
**
ns
***
*
PBS
polySia avDP20
LPS
LPS+ polySia avDP20
Wild type
SIGLEC11 tg

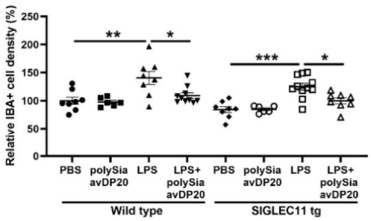
Relative IBA+ cell density (%)
**
*
***
*
PBS
polySia avDP20
LPS
LPS+ polySia avDP20
Wild type
SIGLEC11 tg

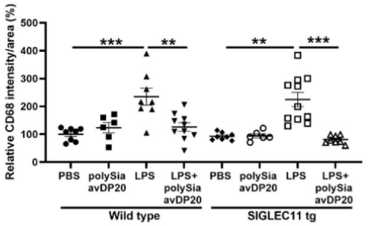
Relative CD68 intensity/area (%)
***
**
**
***
PBS
polySia avDP20
LPS
LPS+ polySia avDP20
Wild type
SIGLEC11 tg

Figure 3 - 6 PolySia avDP20 inhibited the microglia activation in both wild type and *SIGLEC11* transgenic mice brain upon repeated systemic challenge with LPS. Immunohistochemical staining of the SN*pr* area with antibodies against the microglial marker IBA1 and microglial activation marker CD68 were performed to determine the effects of polySia avDP20 on microglial protein levels in both wild type mice and *SIGLEC11* transgenic mice on day 19. (A). Representative images of immunohistochemical staining of SN*pr* area stained for IBA1 (green) and CD68 (red) in wild type and *SIGLEC11* transgenic mice injected with LPS or LPS + polySia avDP20 or polySia avDP20 or PBS as control for experiments on day 19. Scale bar: 50 µm. (B). Quantification of CD68 and IBA1 immunostaining in SN*pr* area on day 19. PolySia avDP20 attenuated LPS-induced CD68 and IBA1 immunoreactivity and IBA+ cell density in *SIGLEC11* transgenic mice on day 19. In addition, polySia avDP20 inhibited the LPS-induced CD68 immunoreactivity and IBA1+ cell density in wild type mice on day 19. Data are presented as mean ± SEM. n = 6-11, ns = not significant, *P < 0.05, **P < 0.01, ***P < 0.001, Welch's ANOVA followed by Dunnett's T3 post hoc test for unequal variances and one-way ANOVA followed by Bonferroni post hoc test for equal variances.

Overall, polySia avDP20 inhibited the elevated expression of IBA1 and CD68 upon LPS challenge in *SIGLEC11* transgenic mice on day 19 at both transcription and protein levels. Consistently, polySia avDP20 prevented the increase of IBA1+ cell density upon LPS challenge in *SIGLEC11* transgenic mice on day 19. Additionally, increased IBA1+ cell density and protein expression of CD68 upon LPS challenge in wild type mice was also attenuated by polySia avDP20 treatment on day 19. Furthermore, the transcription levels of *Iba1* were higher in the group treated with polySia avDP20 alone than those observed in PBS controls in wild type mice on day 5. In opposite, the transcription levels of *Cd68* were lower in the group treated with polySia avDP20 alone than those observed in PBS controls in *SIGLEC11* transgenic mice on day 5.

3.7 PolySia avDP20 restored the loss of dopaminergic neurons in the substantia nigra *pars compacta* induced by LPS challenge

To study the effect of polySia avDP20 on LPS-triggered loss of dopaminergic neurons on day 19, antibodies against dopaminergic marker tyrosine hydroxylase (TH) and neural nuclei marker NeuN were utilized for immunohistochemical staining of the SN*pc* area

(Figure 3-6A). Quantification of the immunohistochemistry data was carried out at three bregma levels (e.g. bregma −3.20, −3.40 and −3.80 mm). Then the average of the relative cell numbers obtained from the three levels were displayed. PolySia avDP20 restored the relative loss of TH positive neurons in the SN*pc* area in both wild type mice (mean ± SEM; 61.79 ± 2.30 % vs 88.24 ± 2.78 %; $p < 0.0001$; Figure 3-7B) and *SIGLEC11* transgenic mice (mean ± SEM; 72.20 ± 4.45 % vs 101.2 ± 4.34 %; $p = 0.0003$; Figure 3-7B). Moreover, the reduction of NeuN positive neurons induced by LPS was also rescued by polySia avDP20 treatment in wild type mice (mean ± SEM; 70.30 ± 4.06 % vs 93.68 ± 4.51 %; $p = 0.0062$; Figure 3-7B). Likewise, polySia avDP20 also showed a tendency to prevent the loss of NeuN positive neurons upon LPS injection in *SIGLEC11* transgenic mice (mean ± SEM; 88.75 ± 3.99 % vs 100.2 ± 2.80 %; $p = 0.1925$; Figure 3-7B).

In summary, polySia avDP20 restored the loss of dopaminergic neurons in the SN*pc* area induced by LPS challenge in both wild type mice and *SIGLEC11* transgenic mice.

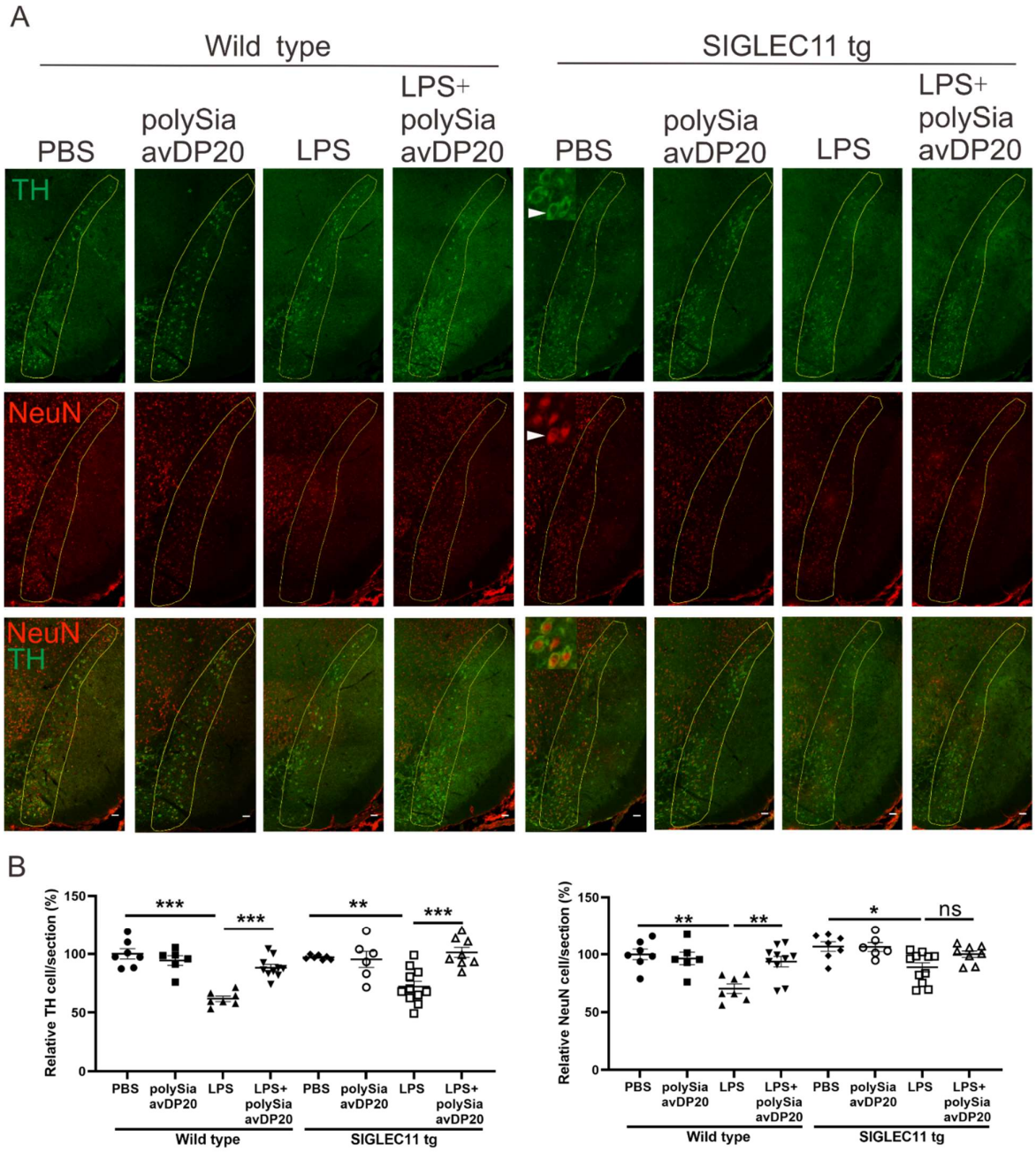

Figure 3 - 7 PolySia avDP20 restored the loss of dopaminergic neurons in the substantia nigra pars compacta (SN*pc*) area in both wild type and *SIGLEC11* transgenic mice brain upon repeated systemic challenge with LPS. Immunohistochemical staining of SN*pc* area stained for dopaminergic marker TH and neural nuclei marker NeuN were utilized to study the effects of polySia avDP20 on neurodegeneration in both wild type mice and *SIGLEC11* transgenic mice on day 19. (A). Representative images of immunohistochemical staining of SN*pc* area stained for TH (green) and NeuN (red) in wild type and *SIGLEC11* transgenic mice injected with LPS or LPS + polySia avDP20 or polySia avDP20 or PBS as control for experiments on day 19.

Scale bar: 50 µm. (B). Quantification of TH positive cells (B, left) and NeuN positive cells (B, right) in SN*pc* area on Day 19. PolySia avDP20 restored the loss of TH positive cells in SN*pc* area in both wild type and *SIGLEC11* transgenic mice. In addition, polySia avDP20 restored the reduction of NeuN positive cells in SN*pc* area in wild type mice. Data are presented as mean ± SEM. n = 6-11, ns = not significant, *P < 0.05, **P < 0.01, ***P < 0.001, one-way ANOVA followed by Bonferroni post hoc test.

4. Discussion

In this study, intraperitoneal application of low molecular weight polysialic acid (polySia avDP20) prevented dopaminergic neurodegeneration, induced by systemic repeated LPS-challenge, in humanized *SIGLEC11* transgenic and wild type mice. RT-PCR revealed that polySia avDP20 reduced the elevated gene transcripts of inflammation, phagocytosis, complement, radical production, lysosome, apoptosis and necroptosis pathways in the brains of humanized *SIGLEC11* transgenic mice after repeated systemic LPS challenge at day 19, without having a prominent anti-inflammatory activity at day 5. Furthermore, immunohistochemistry demonstrated that polySia avDP20 prevented microglia activation triggered by the systemic LPS challenge in humanized *SIGLEC11* transgenic, clearly visible at day 19. These findings are in line with previous studies, showing that interaction between polysialic acid and SIGLEC11 ameliorated inflammation and neurotoxicity *in vitro* (Shahraz *et al.*, 2015; Wang & Neumann, 2010) and prevented laser-induced inflammatory damage in the retina in humanized *SIGLEC11* transgenic mice (Karlstetter *et al.*, 2017). Thus, data in this thesis now provide further insights into the *in vivo* effects of polySia avDP20 on another inflammatory neurodegenerative process.

4.1 Confirmation of anti-inflammatory effects of polySia avDP20 *in vitro*

In this thesis, polySia avDP20 was produced by heat-mediated hydrolysis followed by anion-exchange chromatography for purification. After the determination of its concentration via a thiobarbituric acid-based assay, polySia avDP20 was applied to the LPS-challenged microglia cells ESdM to confirm the anti-inflammatory effects. It was observed that polySia avDP20 inhibited LPS-induced *Tnf-α* mRNA expression in the microglial cell line model ESdM. This is consistent with previous findings, in which it has been shown that this anti-inflammatory effects of polySia avDP20 was mediated by SIGLEC-E (Karlstetter *et al.*, 2017). In detail, lentiviral knockdown of *Siglec-E* prevented

the anti-inflammatory effects of polySia avDP20 on *Tnf-α* mRNA transcription of LPS-stimulated ESdM (Karlstetter *et al.*, 2017).

Interestingly, 1.5 µM polySia avDP20 reduced the LPS-induced increase of *Tnf-α* mRNA expression around 68 % in the previous study (Karlstetter *et al.*, 2017). However, 5 µM polySia avDP20 only decreased the LPS-induced increase of *Tnf-α* mRNA around 25 % in the current thesis. Several reasons could explain this difference in effect size and concentration. First, different batches of polySia avDP20 based on slightly distinct methods were employed, possibly leading to different qualities of polySia avDP20. Second, different assays were used to determine the concentration of polySia avDP20, thus possibly causing slightly different concentrations. Third, ESdM in the previous publication (Karlstetter *et al.*, 2017) showed a higher LPS response than what was observed in this thesis. This might due to different passages of ESdM and different batches of LPS that were used in the experiments.

Overall, the anti-inflammatory effects of polySia avDP20 were confirmed *in vitro*. Therefore, the polySia avDP20 was further applied in an LPS-induced mouse model of Parkinson's disease to check its effects *in vivo*.

4.2 Establishment of LPS-induced mouse model of PD

Multiple animal models have been established to improve our understanding of PD and substantially contributed to the development of neuroprotective agents. Animal models of PD broadly encompass four main types, including pharmacological models (such as reserpine model and haloperidol model), genetic based models (based on the genes associated with monogenic PD, such as α-synuclein (α-syn) and leucine rich repeat kinase 2 (LRRK2)), neurotoxin based models (based on treatment of 6-OHDA, or MPTP, or rotenone, or paraquat) and inflammatory models (based on treatment of polyinosinic

polycytidylic acid (poly (I:C)) and LPS) (Deng *et al*, 2020; Duty & Jenner, 2011). Each animal model of PD has specific advantages and disadvantages.

Accumulating evidence has strongly implicated the involvement of neuroinflammation in the pathogenesis of PD (Tan *et al*, 2020). To explore the anti-inflammatory effects of polySia avDP20, a LPS-induced inflammatory PD model was chosen for investigation in this thesis. There are different types of LPS-induced models of PD based on the routes of administration (e.g. systemic, stereotaxic and intranasal) and dosage regimens (Deng *et al.*, 2020). The model with repeated intraperitoneal injection of bacterial LPS over four consecutive days in male mice was selected, due to the following reasons. First, intraperitoneal injection in mice is easy to implement and mice do not suffer from a direct injection into the brain. Second, intraperitoneal injection of LPS could better mimic the exposure to toxic agents from environment, because this type of administration does not bypass the physical defence of the brain, the blood brain barrier (BBB). Thus, this model of PD might better represent environmental exposures of the clinical disease. Third, repeated systemic injection of LPS (Beier *et al*, 2017; Bodea *et al.*, 2014; Shahraz *et al.*, 2021) takes much less time to induce similar extent of dopaminergic neurodegeneration in the SN (approximately 19 days versus 7-10 months) than a single systemic injection (Liu *et al*, 2008; Qin *et al*, 2013; Qin *et al*, 2007). Fourth, the mouse model of PD with repeated systemic injection of LPS has been reproduced in different research groups (Beier *et al.*, 2017; Bodea *et al.*, 2014; Shahraz *et al.*, 2021). Finally, female mice showed more resistance to LPS than male mice (Liu *et al.*, 2008).

The passage of LPS from systemic injection into the brain is compromised by the BBB (Banks & Robinson, 2010). Thus, it has been proposed that systemic LPS most probably cause neuroinflammation indirectly (Qin *et al.*, 2007). For instance, intraperitoneal administration of LPS activates TLR4 receptors on peritoneal macrophages / dendritic cells, leading to local release of inflammatory cytokines such as IL-1, TNF-α and IL-6

(Block *et al.*, 2007; Konsman *et al*, 1999). Then, systemic inflammation could induce neuroinflammation through several mechanisms. Firstly, IL-1 binds to the IL-1 receptor on the abdominal vagal nerve, which terminates in the brainstem, thus stimulating the CNS (Block *et al.*, 2007; Konsman *et al.*, 1999; Lane, 2009; Vitkovic *et al*, 2000). Secondly, pathological conditions can compromise the integrity of BBB, thus peripheral immune cells such as CD4+ / CD8+ T-lymphocytes and inflammatory cytokines could enter the brain, resulting in neuroinflammation (Dantzer *et al*, 2008; Flores-Martinez *et al*, 2018; Hoban *et al*, 2013). Lastly, circumventricular organs (CVOs) are structures located around the third and fourth ventricles in the CNS, which lack the BBB. Inflammatory cytokines in the bloodstream can communicate with these organs and activate microglia and astrocytes in these regions (Perry, 2010; Vitkovic *et al.*, 2000). Thus, intraperitoneal injection of LPS causes neuroinflammation and degeneration of dopaminergic neurons (Beier *et al.*, 2017; Bodea *et al.*, 2014).

4.2.1 Confirmation of the mouse model in wild type mice

In line with literatures (Beier *et al.*, 2017; Bodea *et al.*, 2014; Shahraz *et al.*, 2021), repeated intraperitoneal injection of LPS in this thesis successfully induced inflammation at day 5 and caused dopaminergic neuronal loss at day 19. Since the LPS-induced inflammation was more prominent at day 5 than that at day 19, Shahraz and colleagues (Shahraz *et al.*, 2021) performed RNA sequencing to reveal the transcriptome changes induced by LPS challenge at day 5. They found increased activation of inflammation, phagocytosis, TLR4 signaling, complement, oxidative burst, lysosome, apoptosis and necroptosis pathways in wild type mice after LPS challenge (Shahraz *et al.*, 2021). These findings were further confirmed by sqRT-PCR (Shahraz *et al.*, 2021). Likewise, those data from day 5 were confirmed via sqRT-PCR in this thesis.

However, data from day 19 showed slight differences between the distinct studies (Beier *et al.*, 2017; Bodea *et al.*, 2014; Shahraz *et al.*, 2021). Shahraz et al. found about 27 % loss of TH positive cells at day 19 (Shahraz *et al.*, 2021), while Bodea et al. and Beier et al. demonstrated about 40 % (Bodea *et al.*, 2014) and 36% (Beier *et al.*, 2017) loss of TH positive cells at day 19, respectively. In comparison, this thesis observed 38 % loss of TH positive cells at day 19. In addition, Bodea et al. revealed insignificant increase of the gene expression of *Iba1*, *Tnf-α* and *Il-1β,* and immunoreactivity of IBA1 and CD68 after repeated LPS challenge at day 19, with the significant increase of *Cd68* gene expression (Bodea *et al.*, 2014). Shahraz et al confirmed their findings regarding the gene expression of *Tnf-α*, *Iba1* and immunoreactivity of IBA1, but found significant increase of the gene expression of *Il-1β* and immunoreactivity of CD68, with the insignificant increase of *Cd68* gene expression (Shahraz *et al.*, 2021). However, Beier et al. demonstrated significant increase of the gene expression of *Tnf-α*, *Il-1β*, *Iba1* and *Cd68* and immunoreactivity of IBA1 after LPS treatment at day 19, without checking the immunoreactivity of CD68 (Beier *et al.*, 2017). Similar to the findings from Beier et al., this thesis observed significant increase of the gene expression of *Tnf-α*, *Il-1β*, *Iba1* and *Cd68* and immunoreactivity of IBA1 and CD68 after LPS treatment at day 19. In line with the literature (Shahraz *et al.*, 2021), the genes with insignificant increase (*Myd88*, *Itgam*, *Nos2*, *Bad*, *Fadd*, *Erk1*, *Pik3cd*, *Ripk3* and *Tmem119*) and the genes with significant increase (*C3*, *Cybb* and *Cd14*) were also observed in this thesis. In contrast, this thesis found more genes with significant increase at day 19 after LPS challenge than that in the literature (Shahraz *et al.*, 2021), such as *Tlr4*, *Dap12*, *Fcer1g*, *Cyba*, *Casp8*, *Mlkl* and *Ripk1*. Regardless of the very mild differences of the data on day 19 from the distinct studies, there is obvious evidence for continues brain inflammation induced by repeated systemic injection of LPS at day 19.

The very mild differences between the distinct studies might due to the following reasons. First, although all the four studies used the LPS from the same manufacturer, different batches of LPS could lead to different response in mice. Second, different handling of

experiments from different researchers could also cause different results. Third, although the mice with the same age and gender were used in different studies, mice in different environment and mice from different generations might have different sensitivity to LPS. Finally, different sample size and different statistical analysis in different studies could lead to minor changes in the statistical interpretation.

4.2.2 Establishment of the mouse model in *SIGLEC11* transgenic mice

To investigate the effects of the interaction between polySia avDP20 and SIGLEC11, a PD mouse model with repeated systemic administration of LPS in *SIGLEC11* transgenic mice was established. In comparison with the findings in wild type mice, similar inflammatory changes were observed in the brains of *SIGLEC11* transgenic mice after repeated systemic challenge with LPS. Interestingly, *SIGLEC11* transgenic mice without application of polySia avDP20 showed a tendency to have less loss of TH positive cells and NeuN positive cells compared to wild type mice at day 19 after LPS challenge. This might due to decreased phagocytic capacity of microglia bearing SIGLEC11 receptors, because exacerbated phagocytosis might cause neurodegeneration (Tremblay *et al*, 2019). It is observed that LPS treated *SIGLEC11* transgenic mice showed a visible tendency to have less gene transcription of phagocytosis marker, *Cd68* than that in LPS treated wild type mice at day 19, although the same tendency was not detected at protein levels. Thus, this finding indicated a neuroprotective role of SIGLEC 11 in the presence of LPS stimulation.

Overall, repeated systemic administration of LPS caused reproducible brain inflammation and loss of dopaminergic neurons in both *SIGLEC11* transgenic and wild type mice. Therefore, we explored the immunomodulatory and neuroprotective roles of polySia avDP20 in the LPS-induced PD mouse model in wild type mice and humanized transgenic mice expressing SIGLEC11 on microglia and tissue macrophages.

4.3 Effects of polySia avDP20 in the mouse model

4.3.1 PolySia avDP20 prevented inflammation-related gene transcription in *SIGLEC11* transgenic mice

Multitude clinical and experimental evidence supports the notion that neuroinflammation is connected to the pathogenesis of PD. Increased levels of several inflammatory mediators (such as TNFα, IFNγ, IL1β, IL6, transforming growth factor-α) have been observed in the cerebrospinal fluid and/or in the postmortem samples of SN and striatum of PD patients (Blum-Degen *et al.*, 1995; Hunot *et al.*, 1999; Mogi *et al*, 1995; Mogi *et al*, 1996b; Mogi *et al.*, 1994b; Shimoji *et al.*, 2009). It is known that the release of cytokines contributes to the amplification of local inflammation in the brain, resulting in neuronal death (Tan *et al.*, 2020). Therefore, alleviation of neuroinflammation could be a potential target to slow down the progression of PD. In this thesis, polySia avDP20 reduced the increased mRNA levels of the proinflammatory mediator *Il-1β* after LPS challenge in *SIGLEC11* transgenic mice at day 19. This observation is consistent with the findings in another study, in which artificial stimulation of ectopically expressed SIGLEC11 by cross-linking antibodies suppressed the LPS-induced gene transcription of *Il-1β* in cultured murine microglial cells (Wang & Neumann, 2010). Thus, our finding supports the concept that the inhibitory ITIMs containing receptor SIGLEC11 negatively regulates activatory ITAM-domain receptor associated inflammation (Klaus *et al.*, 2020).

Furthermore, it was observed that polySia avDP20 inhibited the LPS-triggered augmented gene transcription of TLR4 signaling pathway related genes (*Cd14* and *Myd88*) in *SIGLEC11* transgenic mice at day 19. Recently, Allendorf and colleagues discovered that SIGLEC-E bound to TLR4 via sialic acid residues and prevented cytokine IL-6 release by the murine microglia cell line BV-2 (Allendorf *et al*, 2020). Allendorf and colleagues described that LPS caused the neuraminidase 1 to translocate to the microglia cell surface and to desialylate TLR4. Thus, inhibitory SIGLEC-E was removed from the TLR4 and

microglia was activated (Allendorf *et al.*, 2020). Since murine SIGLEC-E is a functionally related SIGLEC receptor to human SIGLEC11, we assume that polySia avDP20 might also help to re-sialylate TLR4 and thereby re-activate inhibitory SIGLEC 11 and reduce microglia activation. Interestingly, around a ten-fold higher concentration of polySia avDP20 was required to attenuate the pro-inflammatory reactivity of mouse microglia via SIGLEC-E receptors compared to human THP1 macrophages via SIGLEC-11 (Karlstetter *et al.*, 2017). This might explain the observed phenomenon that polySia avDP20 only showed a tendency to inhibit the LPS-triggered increase in mRNA levels of *Cd14* and *Myd88* in wild type mice.

4.3.2 PolySia avDP20 reduced phagocytosis-related gene transcription in *SIGLEC11* transgenic mice

Phagocytosis is one of the critical function of microglia. It is responsible for microglia to engulf synapses, infectious agents, apoptotic cells, and tissue debris to maintain the homeostasis of CNS. However, elevated CNS inflammation might exacerbate the phagocytic capacity of microglia, leading to enhanced, uncontrolled and potentially toxic phagocytosis. This pathological clearance capacity of microglia could contribute to synaptic degeneration and loss of viable neurons, which are all potentially relevant to PD pathogenesis (Barcia *et al*, 2013; Tremblay *et al.*, 2019). CD68 is a suggested marker of phagocytosis. It has been documented that CD68 increased early prior to neurodegeneration (Theodore *et al*, 2008). In addition, increased CD68 has been correlated with dopaminergic neuronal loss (Sanchez-Guajardo *et al*, 2010), a delicate regulation of the microglial phagocytosis might benefit PD patients (Janda *et al*, 2018).

PolySia avDP20 reduced the increased mRNA levels of the phagocytosis pathway related genes, *Fcer1g* and *Cd68*, after LPS challenge in *SIGLEC11* transgenic mice at day 19. As well, polySia avDP20 decreased the augmented immunoreactivity of CD68 in both

SIGLEC11 transgenic and wild type mice at day 19. In line with these findings, it has been reported that phagocytosis of apoptotic neuronal debris was compromised in SIGLEC11 expressing murine microglia compared to control microglia without SIGLEC11 (Wang & Neumann, 2010). In addition, polySia avDP20 neutralized the LPS-triggered increase in the inflammation associated phagocytosis of microbeads in human THP1 macrophages involving the SIGLEC11 receptor (Shahraz *et al.*, 2015). Similarly, polySia avDP20 also inhibited phagocytosis of mouse ESdM after incubation with drusen-like material derived from necrotic human retinal pigment epithelial cells (ARPE-19 cells) (Karlstetter *et al.*, 2017). Additionally, SIGLEC-E on microglia inhibited phagocytosis of neural debris (Claude *et al.*, 2013). Thus, our finding supports the concept that SIGLEC receptors bearing inhibitory ITIMs (e.g. SIGLEC11 and SIGLEC-E) negatively regulates activatory ITAM-domain receptor associated phagocytosis (Liao *et al.*, 2020).

4.3.3 PolySia avDP20 mitigated complement-related gene transcription in *SIGLEC11* transgenic mice

Complement activation has been associated with the pathogenesis of PD (Carpanini *et al*, 2019). C3 is a key component of complement system. One of its cleavage products interacts with CR3, an ITAM-signaling bearing receptor of microglia, to induce phagocytosis (Fu *et al*, 2012). It has been demonstrated that knockout of C3 restored the loss of dopaminergic neurons induced by repeated systemic LPS application (Bodea *et al.*, 2014). Similarly, another study discovered that CR3 deficient mice were protected from dopaminergic neuron loss and motor dysfunction in a toxin-induced PD model (Hou *et al*, 2018). Thus, targeting aberrant activation of the complement-phagosome pathway might be a potential therapeutic intervention for PD.

PolySia avDP20 reduced the elevated gene transcription of complement pathway related genes (*Itgam* and *C4*) after LPS challenge in a SIGLEC11-dependent fashion on day 19.

However, previous *in vivo* experiments revealed a SIGLEC11-independent effect of polySia avDP20 on complement-mediated membrane attack complex (MAC) formation in the retina (Karlstetter *et al.*, 2017). This might be caused by different dose effects of polySia avDP20 applied in the two different mouse models or by the different detection systems applied (transcription of complement genes versus protein-based MAC formation). Local intravitreal injection and systemic intraperitoneal injection might also lead to different local concentration of polySia avDP20 in the targeted organs. Thus, we assume that the dose of polySia avDP20 applied systemically in the current PD model is not high enough to inhibit the ITAM-signaling in the brain of wild type mice in the absence of SIGLEC11.

4.3.4 PolySia avDP20 attenuated oxidative burst-related gene transcription in *SIGLEC11* transgenic mice

Oxidative stress has been indicated to play a critical role in PD (Gaki & Papavassiliou, 2014). Considering the inconsistency between studies regarding the oxidative stress markers in PD patients, a recent study utilized meta-analytic technique to explore the changes of circulating oxidative stress markers in patients with PD (Wei *et al*, 2018). This study demonstrated higher levels of oxidative stress (injury) makers and lower levels of antioxidants in patients with PD compared with controls, thus providing strong clinical evidence that patients with PD have exacerbated oxidative stress. Hence, oxidative stress is a potential therapeutic target in PD.

PolySia avDP20 reduced elevated transcription levels of the oxidative burst gene *Cybb* after LPS challenge in *SIGLEC11* transgenic mice on day 19. In line with this finding, previous studies demonstrated that polySia avDP20 prevented the oxidative burst of human THP1 macrophages expressing SIGLEC11 triggered by neural debris (Shahraz *et al.*, 2015) or fibrillary amyloid-β1–42 (Shahraz *et al.*, 2015) or drusen-like material derived

from necrotic human ARPE-19 cells (Karlstetter *et al.*, 2017). Similarly, polySia avDP20 also inhibited reactive oxygen species (ROS) production of mouse ESdM after incubation with drusen-like material derived from necrotic human ARPE-19 cells (Karlstetter *et al.*, 2017). Likewise, mouse SIGLEC-E inhibited the production of superoxide of phagocytes *in vivo* (Schwarz *et al*, 2015) and *in vitro* (Claude *et al.*, 2013) by interaction with sialic acid residues on neurons in “trans”. Hence, the findings in this thesis support the observation that the ITIM-signaling receptors such as SIGLEC11 and SIGLEC-E negatively interfere with the phagocytosis associated oxidative burst. Interestingly, higher concentration of polySia avDP20 completely inhibited superoxide release as potently as the scavengers SOD1 or Trolox (Karlstetter *et al.*, 2017; Shahraz *et al.*, 2015). However, LPS-induced raise of Cybb mRNA was only partially attenuated by polySia avDP20 treatment in *SIGLEC11* transgenic mice on day 19 in the current study.

4.3.5 PolySia avDP20 prevented microglia activation in both *SIGLEC11* transgenic and wild type mice

According to *in vivo* analysis of microglia activation using positron emission tomography (PET) in PD patients, dopaminergic neuronal loss was preceded by microglia activation (Ferreira & Romero-Ramos, 2018). Consistently, multiple post-mortem studies revealed that microgliosis existed in all the regions where α-synuclein accumulation and neurodegeneration visible, no matter whether there was cell death or not (Croisier *et al*, 2005; Doorn *et al*, 2014; Halliday & Stevens, 2011; Hunot *et al*, 1996; Imamura *et al*, 2003; Knott *et al*, 2000). Activated microglia can have detrimental effects on dopaminergic neurons via multiple pathways, including direct degradation of neurons by phagocytosis, release of proinflammatory cytokines, activation of the complement cascade and oxidative damage (Tan *et al.*, 2020). In the current study, polySia avDP20 only showed a tendency to reduce the relative IBA1 intensity and IBA1 positive cell density induced by LPS challenge in *SIGLEC11* transgenic mice on day 5 after disease initiation. But, polySia

avDP20 prevented the increase of IBA1+ cell density upon LPS challenge in *SIGLEC11* transgenic mice on day 19. Moreover, polySia avDP20 attenuated LPS-triggered increased expression of IBA1 and CD68 in *SIGLEC11* transgenic mice on day 19 at both transcription and protein levels. Interestingly, augmented IBA1+ cell density and protein levels of CD68 after LPS challenge in wild type mice was only prevented by polySia avDP20 on day 19, but not at day 5. Therefore, polySia avDP20 showed potential benefits of preventing LPS-induced microgliosis at an earlier time point in the presence of SIGLEC11. These findings might explain, why polySia avDP20 completely restored the LPS-induced loss of TH+ dopaminergic neurons in the SNpc area in *SIGLEC11* transgenic mice, while only partially in wild type mice. Of note, polySia avDP20 also restored the LPS-triggered neurodegeneration, as determined by NeuN staining, in wild type mice. However, less neurodegeneration, as determined by NeuN staining, was induced in *SIGLEC11* transgenic mice by LPS. Accordingly, we failed to observe a significant restoration of the NeuN staining in *SIGLEC11* transgenic mice by polySia avDP20 treatment.

4.3.6 PolySia avDP20 restored dopaminergic neuronal loss in both *SIGLEC11* transgenic and wild type mice

Loss of dopaminergic neurons in the substantia nigra is one of the main hallmark pathological changes in PD (Tan *et al.*, 2020). Recently, RNA sequencing analysis showed that the loss of dopaminergic neurons, which was triggered by repeated LPS-challenge, was mainly associated with apoptosis- and necroptosis-related pathways (Shahraz *et al.*, 2021). In the current study, polySia avDP20 attenuated the elevated transcription levels of the apoptosis-related gene *Casp8* and the necroptosis-related genes *Ripk1* and *Ripk3* after LPS challenge in *SIGLEC11* transgenic mice on day 19.

The neuroprotective effects of polySia avDP20, as well as SIGLEC11 have been reported before. More neurites and neuronal cell bodies survived in coculture of microglia ectopically expressed SIGLEC11 and neurons. The neuroprotective function of SIGLEC11 was mainly activated by polySia on neurons in “trans,” but not on microglia in “cis” (Wang & Neumann, 2010). In addition, polySia avDP20 alleviated neurotoxicity of fibrillary amyloid-β1–42 in a human macrophage-neuron co-culture system (Shahraz *et al.*, 2015). Similarly, SIGLEC-E of microglia recognized sialic acid residues on neurons in “trans” and prevented the removal of neurites in a microglia–neuron coculture system (Claude *et al.*, 2013). The neuroprotective effect of polySia avDP20 in the co-culture system might attribute to prevention of the macrophages oxidative burst (Claude *et al.*, 2013; Shahraz *et al.*, 2015).

Furthermore, we observed 38 % of LPS-caused TH+ dopaminergic neuronal loss in SN*pc* in wild type mice without manifestation of motor signs, similarly to 27-40 % of dopaminergic neuronal loss observed in previous studies (Beier *et al.*, 2017; Bodea *et al.*, 2014; Shahraz *et al.*, 2021). Interestingly, first motor signs of PD only occur in the presence of approximately 50 % loss of SN dopamine neurons, although some estimation of up to 60 % to 70 % neuronal loss have also been proposed to see symptoms (Cheng *et al*, 2010). Since *SIGLEC11* transgenic mice showed even less LPS-triggered TH+ dopaminergic neuronal loss (28 %), we do not expect any behavioral changes. However, since polySia avDP20 completely restored the loss of TH+ dopaminergic neurons in the SN*pc* area induced by LPS challenge in *SIGLEC11* transgenic mice, polySia avDP20 should be a promising candidate at an early pre-symptomatic stage to prevent future occurrence of motor symptoms of PD.

4.4 PolySia avDP20 induced oversialylation in healthy controls in both *SIGLEC11* transgenic and wild type mice

Unexpectedly, polySia avDP20 treatment alone slightly elevated the mRNA expression of *Il-1β*, *Cd14*, *Fcer1g*, *Itgam*, *C4*, *Cybb*, *Pik3cd*, *Ripk1* and *Iba1* in wild type mice without LPS challenge on day 5. Interestingly, although polySia avDP20 treatment alone slightly reduced the mRNA levels of *Itgam*, *C4* and *Cd68* on day 5 in *SIGLEC11* transgenic mice without LPS challenge, it increased *Bad* and *Pik3cd* mRNA levels on day 19. Therefore, although polySia avDP20 showed neuroprotective effects via inhibiting LPS-triggered microglia activation by preventing inflammation, phagocytosis, complement activation and radical production, healthy individuals might fail to benefit from a treatment of polySia avDP20, potentially due to oversialylation as described in the literature before. Oversialylation could inhibit the maturation of lysosomes (Schmid *et al*, 1999) and phagosomes (Mukherjee *et al*, 2020), thus disturbing proper lysosomal digestion and reuse of lipids and proteins (Pan *et al*, 2017; Pshezhetsky & Ashmarina, 2018; Zhou *et al*, 1995), leading to micro- and astrogliosis, neuroinflammation, and accumulation of lipofuscin bodies in the mouse brain (Pan *et al.*, 2017).

Over all, data in this thesis now demonstrate that low molecular weight polySia avDP20 is a promising innate immunomodulatory biological compound. Thus, treatment with polySia avDP20 might be a plausible therapeutic strategy for inflammatory neurodegenerative diseases, particularly PD.

5. Abstract

Parkinson's disease is one of the most common neurodegenerative diseases in the elderly population, with a pathophysiology linked to neuroinflammation, complement activation and oxidative damage. Soluble polysialic acid with an average degree of polymerization 20 (polySia avDP20) prevents inflammation and oxidative burst in human macrophages via sialic acid-binding immunoglobulin like lectin-11 (SIGLEC11) receptor and interferes with alternative complement activation. Here, we confirmed the anti-inflammatory capacity of polySia avDP20 on cultured embryonic stem cell-derived microglia (ESdM) and analyzed the effect of polySia avDP20 in a lipopolysaccharide (LPS)- triggered animal model of PD. *In vitro*, 5 µM and 15 µM polySia avDP20 attenuated the tumor necrosis factor-α (*Tnf–α*) mRNA gene transcription of LPS treated ESdM. We also demonstrated a neuroprotective effect of polySia avDP20 in LPS-challenged humanized *SIGLEC11* transgenic mice. *In vivo*, intraperitoneal application of 10µg/g body weight polySia avDP20 attenuated the LPS-triggered increase in mRNA levels of immune-related genes (*Il-1β, Cd14*, *Myd88, Fcer1g, Itgam, C4, Cybb, Iba1* and *Cd68*) and cell death-related genes (*Casp8, Ripk1* and *Ripk3*) in the brains after repeated systemic LPS challenge in *SIGLEC11* transgenic mice on day 19, but not on day 5. Moreover, immunohistochemistry demonstrated that polySia avDP20 inhibited the LPS-induced increase in immunoreactivity of IBA1 and CD68 in the substantia nigra *pars reticulata* in *SIGLEC11* transgenic and wild type mice on day 19. Furthermore, treatment with polySia avDP20 restored the loss of dopaminergic neurons in the substantia nigra *pars compacta* induced by LPS challenge in, both, *SIGLEC11* transgenic and wild type mice on day 19. Thus, data demonstrates that polySia avDP20 ameliorates inflammatory dopaminergic neurodegeneration in *SIGLEC11* transgenic and partially in wild type mice and thus is a promising drug candidate to prevent PD-related inflammation and neurodegeneration.

6. Supplemental figures

Day 5

A

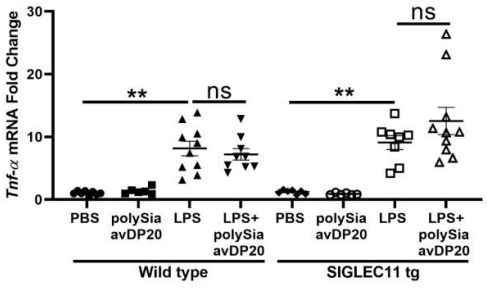

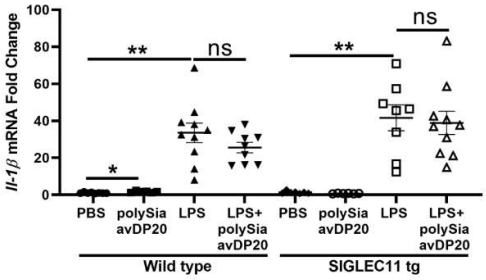

B

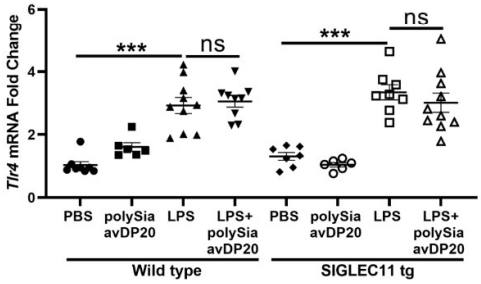

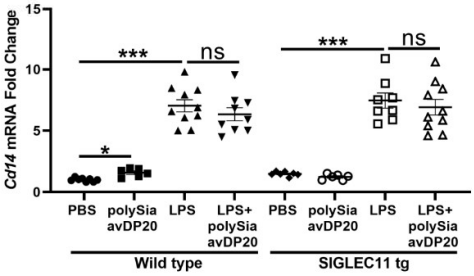

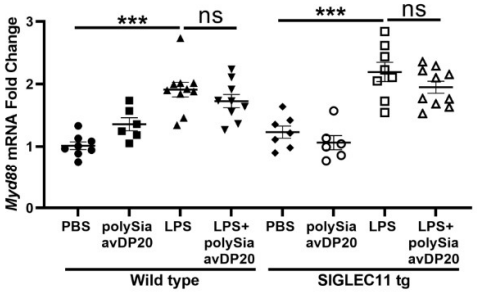

C

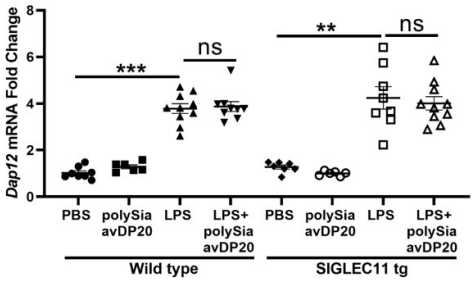

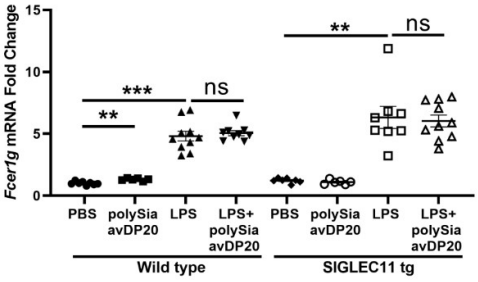

Supplementary figure S 1 PolySia avDP20 failed to inhibit elevated transcription levels of inflammatory pathway-, TLR4 signaling pathway-, and phagocytosis pathway-related genes in both wild type and *SIGLEC11* transgenic mice brains upon repeated systemic challenge with LPS on day 5. (A). *Tnf-α* and *Il-1β* transcription was analyzed to study the inflammatory pathway, in both wild type mice and *SIGLEC11* transgenic mice on day 5. PolySia avDP20 failed to inhibit the LPS-induced gene transcription of *Tnf-α* and *Il-1β* in both *SIGLEC11* transgenic and wild type mice on day 5. Unexpectedly, polySia avDP20 elevated *Il-1β* mRNA expression in wild type mice without LPS challenge on day 5. (B). Transcription of the TLR4 signaling pathway genes *Tlr4*, *Cd14*, and *Myd88* transcription were studied in both wild type mice and *SIGLEC11* transgenic mice on day 5. PolySia avDP20 failed to inhibit the LPS-induced gene transcription of *Tlr4*, *Cd14*, and *Myd88* in both *SIGLEC11* transgenic and wild type mice on day 5. Additionally, polySia avDP20 elevated *Cd14* mRNA expression in wild type mice without LPS challenge on day 5. (C). Transcription of the phagocytosis pathway genes *Dap12* and *Fcer1g* were analyzed in both wild type mice and *SIGLEC11* transgenic mice on day 5. PolySia avDP20 failed to inhibit the LPS-induced gene transcription of *Dap12* and *Fcer1g* in both *SIGLEC11* transgenic and wild type mice on day 5. In addition, the *Fcer1g* mRNA levels upon polySia avDP20 treatment alone was slightly higher than those observed in PBS control group in wild type mice on day 5. Data are presented as mean ± SEM. n = 6-10, ns = not significant, *P < 0.05, **P < 0.01, ***P < 0.001, Welch's ANOVA followed by Dunnett's T3 post hoc test for unequal variances and one-way ANOVA followed by Bonferroni post hoc test for equal variances.

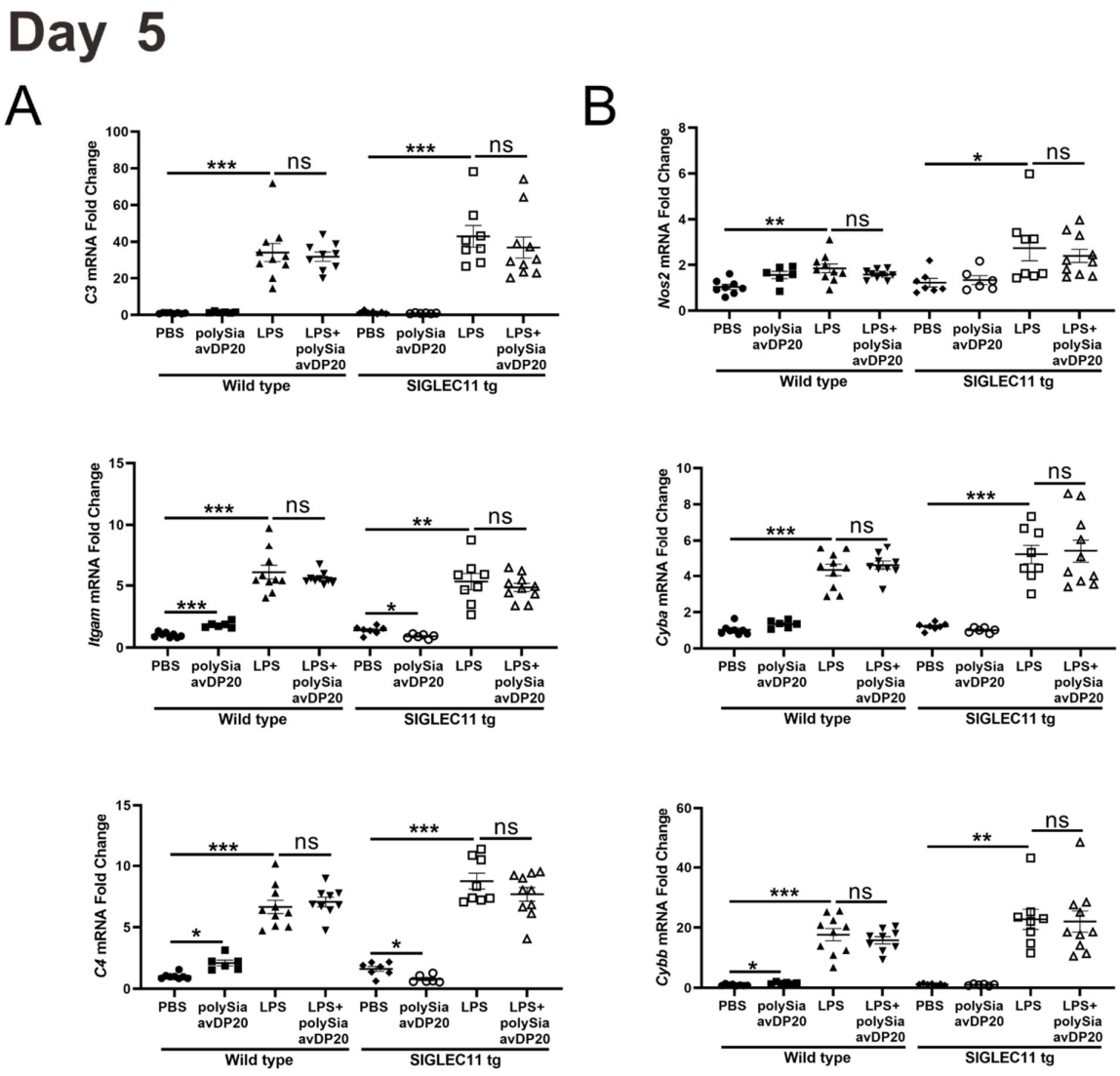

Supplementary figure S 2 PolySia avDP20 failed to inhibit elevated transcription levels of complement pathway- and radical production pathway-related genes in both wild type and *SIGLEC11* transgenic mice brains upon repeated systemic challenge with LPS on day 5. (A). Transcription of the complement pathway genes *C3*, *Itgam*, and *C4* were analyzed in both wild type mice and *SIGLEC11* transgenic mice on day 5. PolySia avDP20 failed to inhibit the LPS-induced gene transcription of *C3*, *Itgam*, and *C4* in both *SIGLEC11* transgenic and wild type mice on day 5. Interestingly, polySia avDP20 treatment alone elevated the mRNA levels of both *Itgam* and *C4* in wild type mice on day 5, while it decreased the mRNA levels of both *Itgam* and *C4* in *SIGLEC11* transgenic mice on day 5. (B). Transcription of the radical production pathway genes *Nos2*, *Cyba*, and *Cybb* transcription were studied in both wild type mice and *SIGLEC11* transgenic mice on day 5. PolySia avDP20 failed to inhibit the LPS-induced gene transcription of *Nos2*, *Cyba*, and *Cybb* in both *SIGLEC11* transgenic and wild type mice

on day 5. Interestingly, polySia avDP20 treatment alone elevated *Cybb* mRNA expression in wild type mice on day 5. Data are presented as mean ± SEM. n = 6-10, ns = not significant, *P < 0.05, **P < 0.01, ***P < 0.001, Welch's ANOVA followed by Dunnett's T3 post hoc test for unequal variances and one-way ANOVA followed by Bonferroni post hoc test for equal variances.

Day 5

A

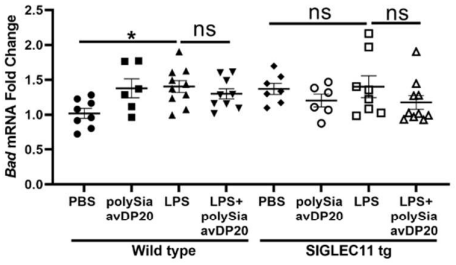
Bad mRNA Fold Change
2.5
2.0
1.5
1.0
0.5
0.0
*
ns
ns
ns
PBS
polySia avDP20
LPS
LPS+ polySia avDP20
PBS
polySia avDP20
LPS
LPS+ polySia avDP20
Wild type
SIGLEC11 tg

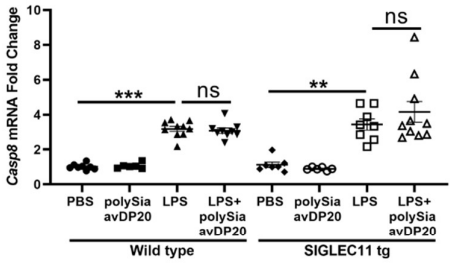
Casp8 mRNA Fold Change
10
8
6
4
2
0
***
ns
**
ns
PBS
polySia avDP20
LPS
LPS+ polySia avDP20
PBS
polySia avDP20
LPS
LPS+ polySia avDP20
Wild type
SIGLEC11 tg

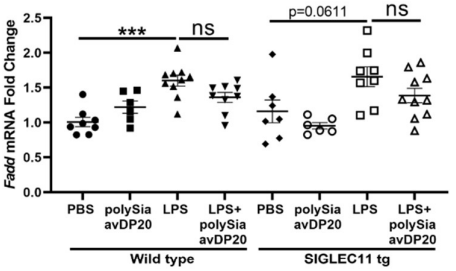
Fadd mRNA Fold Change
2.5
2.0
1.5
1.0
0.5
0.0
***
ns
p=0.0611
ns
PBS
polySia avDP20
LPS
LPS+ polySia avDP20
PBS
polySia avDP20
LPS
LPS+ polySia avDP20
Wild type
SIGLEC11 tg

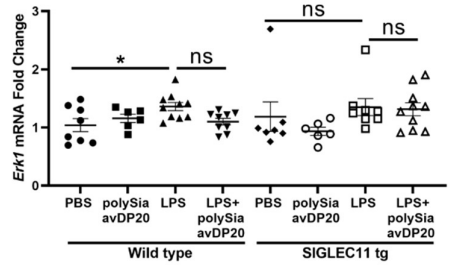
Erk1 mRNA Fold Change
3
2
1
0
*
ns
ns
ns
PBS
polySia avDP20
LPS
LPS+ polySia avDP20
PBS
polySia avDP20
LPS
LPS+ polySia avDP20
Wild type
SIGLEC11 tg

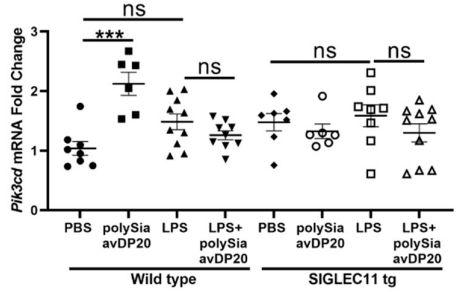
Pik3cd mRNA Fold Change
3
2
1
0
***
ns
ns
ns
ns
PBS
polySia avDP20
LPS
LPS+ polySia avDP20
PBS
polySia avDP20
LPS
LPS+ polySia avDP20
Wild type
SIGLEC11 tg

B

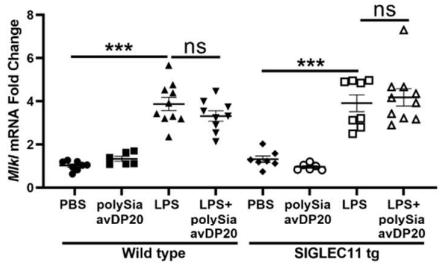
Mlkl mRNA Fold Change
8
6
4
2
0
***
ns
***
ns
PBS
polySia avDP20
LPS
LPS+ polySia avDP20
PBS
polySia avDP20
LPS
LPS+ polySia avDP20
Wild type
SIGLEC11 tg

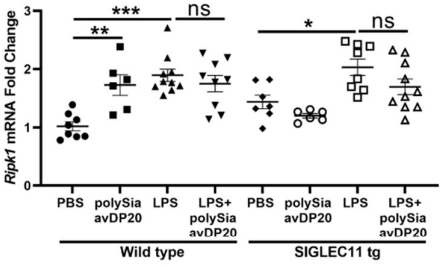
Ripk1 mRNA Fold Change
3
2
1
0
***
**
ns
*
ns
PBS
polySia avDP20
LPS
LPS+ polySia avDP20
PBS
polySia avDP20
LPS
LPS+ polySia avDP20
Wild type
SIGLEC11 tg

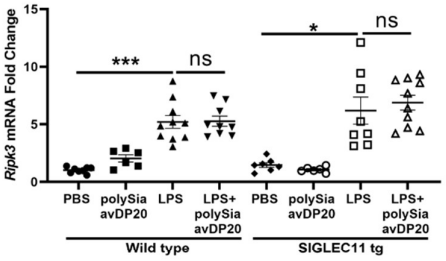
Ripk3 mRNA Fold Change
15
10
5
0
***
ns
*
ns
PBS
polySia avDP20
LPS
LPS+ polySia avDP20
PBS
polySia avDP20
LPS
LPS+ polySia avDP20
Wild type
SIGLEC11 tg

Supplementary figure S 3 PolySia avDP20 failed to inhibit elevated transcription levels of apoptosis pathway- and necroptosis pathway-related genes in both wild type and *SIGLEC11* transgenic mice brains upon repeated systemic challenge with LPS on day 5. (A). Transcription of the apoptosis pathway genes *Bad*, *Casp8*, *Fadd*, *Erk1*, and *Pik3cd* transcription were analyzed in both wild type mice and *SIGLEC11* transgenic mice on day 5. PolySia avDP20 failed to inhibit the LPS-induced gene transcription of *Bad*, *Casp8*, *Fadd*, *Erk1*, and *Pik3cd* in both *SIGLEC11* transgenic and wild type mice on day 5. Additionally, *Pik3cd* transcripts were slightly elevated in the group treated with polySia avDP20 alone compared to PBS controls in wild type mice on day 5. (B). Transcription of the necroptosis pathway genes *Mlkl*, *Ripk1*, and *Ripk3* transcription were studied in both wild type mice and *SIGLEC11* transgenic mice on day 5. PolySia avDP20 failed to inhibit the LPS-induced gene transcription of *Mlkl*, *Ripk1* and *Ripk3* in *SIGLEC11* transgenic mice on day 5. Unexpectedly, *Ripk1* mRNA levels was higher in the group treated with polySia avDP20 alone than those observed in PBS controls in wild type mice on day 5. Data are presented as mean ± SEM. n = 6-10, ns = not significant, *P < 0.05, **P < 0.01, ***P < 0.001, Welch's ANOVA followed by Dunnett's T3 post hoc test for unequal variances and one-way ANOVA followed by Bonferroni post hoc test for equal variances.

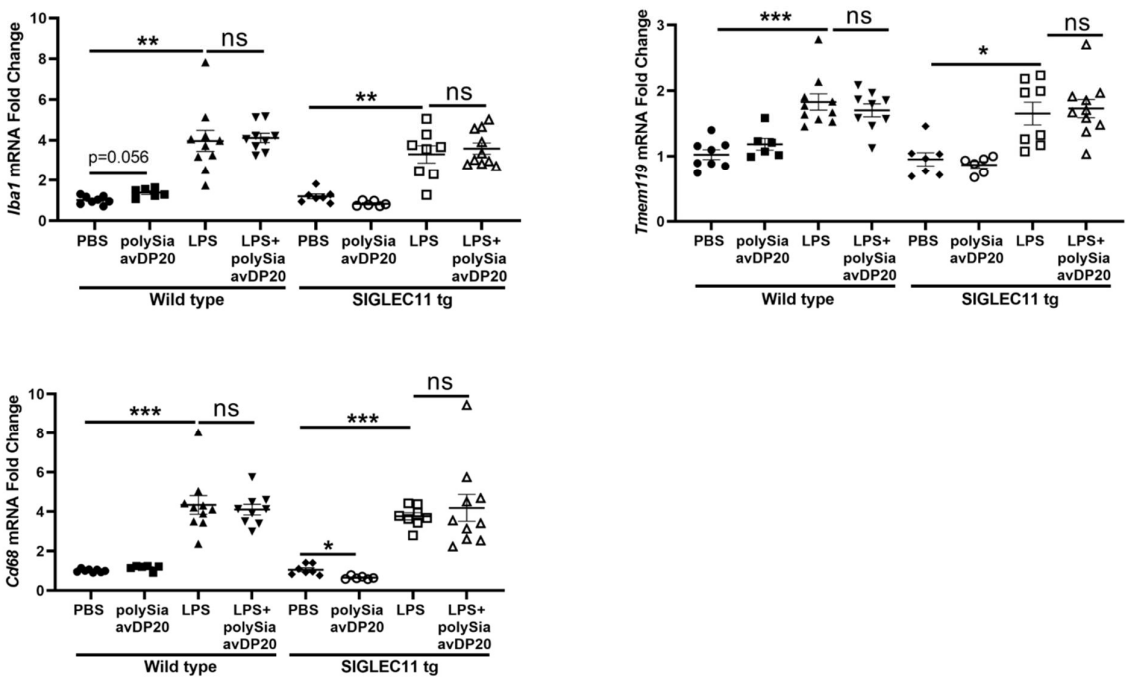

Supplementary figure S 4 PolySia avDP20 failed to attenuate the increased transcription levels of the microgial marker genes *Cd68 and Iba1* in both wild type and *SIGLEC11* transgenic mice brains upon repeated systemic challenge with LPS on day 5. *Cd68*, *Iba1*, and *Tmem119* gene transcription was analyzed in both wild type mice and *SIGLEC11* transgenic mice on day 5. PolySia avDP20 failed to inhibit the LPS-induced gene transcription of *Cd68*, *Iba1*, and *Tmem119* in both *SIGLEC11* transgenic and wild type mice on day 5. Furthermore, *Iba1* mRNA levels were higher in the group treated with polySia avDP20 alone than those observed in PBS controls in wild type mice on day 5. However, *Cd68* mRNA levels were lower in the group treated with polySia avDP20 alone than those treated with PBS control in *SIGLEC11* transgenic mice on day 5. Data are presented as mean ± SEM. n = 6-10, ns = not significant, *P < 0.05, **P < 0.01, ***P < 0.001, Welch's ANOVA followed by Dunnett's T3 post hoc test for unequal variances and one-way ANOVA followed by Bonferroni post hoc test for equal variances.

Day 5

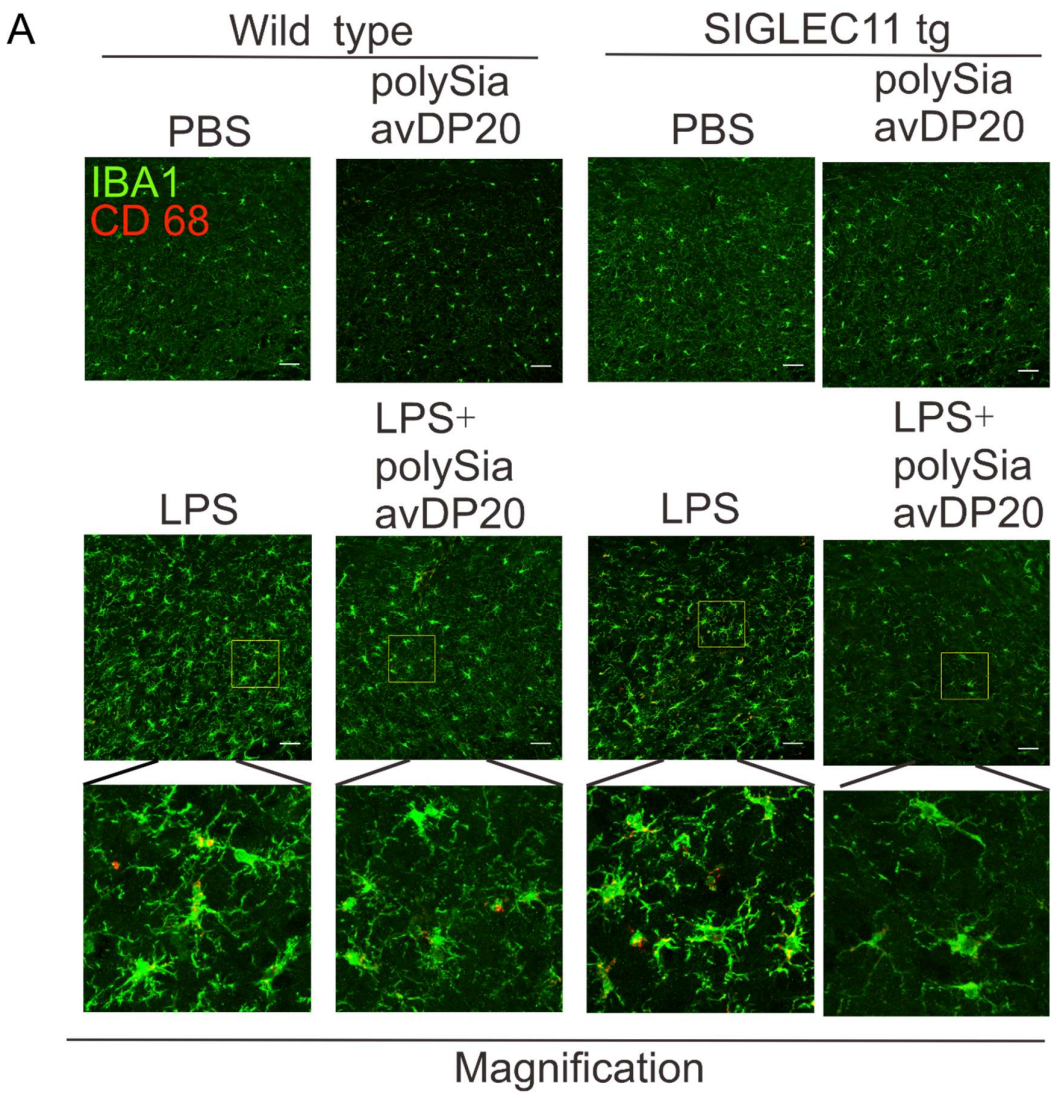
A
Wild type
SIGLEC11 tg
PBS
polySia avDP20
PBS
polySia avDP20
IBA1
CD 68
LPS
LPS+ polySia avDP20
LPS
LPS+ polySia avDP20
Magnification

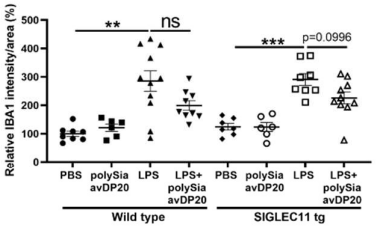
B
Relative IBA1 intensity/area (%)
**
ns
***
p=0.0996
PBS
polySia avDP20
LPS
LPS+ polySia avDP20
Wild type
SIGLEC11 tg

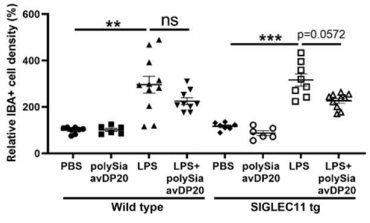
Relative IBA+ cell density (%)
**
ns
***
p=0.0572
PBS
polySia avDP20
LPS
LPS+ polySia avDP20
Wild type
SIGLEC11 tg

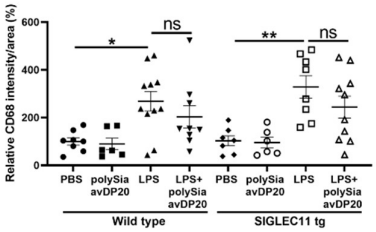
Relative CD68 intensity/area (%)
*
ns
**
ns
PBS
polySia avDP20
LPS
LPS+ polySia avDP20
Wild type
SIGLEC11 tg

Supplementary figure S 5 PolySia avDP20 showed a trend to attenuate LPS-induced IBA1 immunoreactivity and IBA1+ cell density in *SIGLEC11* transgenic mice on day 5. Immunohistochemical stainings of SN*pr* area for the microglial marker IBA1 and the microglial activation marker CD68 were performed in both wild type mice and *SIGLEC11* transgenic mice on day 5. (A). Representative images of immunohistochemical staining of SN*pr* area stained for IBA1 (green) and CD68 (red) in wild type and *SIGLEC11* transgenic mice injected with LPS or LPS + polySia avDP20 or polySia avDP20 or PBS as control on day 5. Scale bar: 50 µm. (B). Quantification of CD68 and IBA1 immunostaining in SN*pr* area on day 5. PolySia avDP20 showed a tendency to attenuate LPS-induced IBA1 immunoreactivity and IBA1+ cell density in *SIGLEC11* transgenic mice on day 5. Data are presented as mean ± SEM. n = 6-10, ns = not significant, *P < 0.05, **P < 0.01, ***P < 0.001, Welch's ANOVA followed by Dunnett's T3 post hoc test for unequal variances and one-way ANOVA followed by Bonferroni post hoc test for equal variances.

7. List of figures

8. List of tables

9. References

Abeln M, Albers I, Peters-Bernard U, Flachsig-Schulz K, Kats E, Kispert A, Tomlinson S, Gerardy-Schahn R, Munster-Kuhnel A, Weinhold B (2019) Sialic acid is a critical fetal defense against maternal complement attack. *J Clin Invest* 129: 422-436

Ajami B, Bennett JL, Krieger C, Tetzlaff W, Rossi FM (2007) Local self-renewal can sustain CNS microglia maintenance and function throughout adult life. *Nat Neurosci* 10: 1538-1543

Allendorf DH, Franssen EH, Brown GC (2020) Lipopolysaccharide activates microglia via neuraminidase 1 desialylation of Toll-like Receptor 4. *J Neurochem* 155: 403-416

Angata K, Long JM, Bukalo O, Lee W, Dityatev A, Wynshaw-Boris A, Schachner M, Fukuda M, Marth JD (2004) Sialyltransferase ST8Sia-II assembles a subset of polysialic acid that directs hippocampal axonal targeting and promotes fear behavior. *J Biol Chem* 279: 32603-32613

Angata T, Varki A (2002) Chemical diversity in the sialic acids and related alpha-keto acids: an evolutionary perspective. *Chem Rev* 102: 439-469

Banks WA, Robinson SM (2010) Minimal penetration of lipopolysaccharide across the murine blood-brain barrier. *Brain Behav Immun* 24: 102-109

Barcia C, Ros CM, Ros-Bernal F, Gomez A, Annese V, Carrillo-de Sauvage MA, Yuste JE, Campuzano CM, de Pablos V, Fernandez-Villalba E *et al* (2013) Persistent phagocytic characteristics of microglia in the substantia nigra of long-term Parkinsonian macaques. *J Neuroimmunol* 261: 60-66

Bardor M, Nguyen DH, Diaz S, Varki A (2005) Mechanism of uptake and incorporation of the non-human sialic acid N-glycolylneuraminic acid into human cells. *J Biol Chem* 280: 4228-4237

Beier EE, Neal M, Alam G, Edler M, Wu LJ, Richardson JR (2017) Alternative microglial activation is associated with cessation of progressive dopamine neuron loss in mice systemically administered lipopolysaccharide. *Neurobiol Dis* 108: 115-127

Beutner C, Linnartz-Gerlach B, Schmidt SV, Beyer M, Mallmann MR, Staratschek-Jox A, Schultze JL, Neumann H (2013) Unique transcriptome signature of mouse microglia. *Glia* 61: 1429-1442

Blaum BS, Hannan JP, Herbert AP, Kavanagh D, Uhrin D, Stehle T (2015) Structural basis for sialic acid-mediated self-recognition by complement factor H. *Nat Chem Biol* 11: 77-82

Block ML, Zecca L, Hong JS (2007) Microglia-mediated neurotoxicity: uncovering the molecular mechanisms. *Nat Rev Neurosci* 8: 57-69

Blum-Degen D, Muller T, Kuhn W, Gerlach M, Przuntek H, Riederer P (1995) Interleukin-1 beta and interleukin-6 are elevated in the cerebrospinal fluid of Alzheimer's and de novo Parkinson's disease patients. *Neurosci Lett* 202: 17-20

Bodea LG, Wang Y, Linnartz-Gerlach B, Kopatz J, Sinkkonen L, Musgrove R, Kaoma T, Muller A, Vallar L, Di Monte DA *et al* (2014) Neurodegeneration by activation of the microglial complement-phagosome pathway. *J Neurosci* 34: 8546-8556

Bolam JP, Pissadaki EK (2012) Living on the edge with too many mouths to feed: why dopamine neurons die. *Mov Disord* 27: 1478-1483

Braak H, Del Tredici K, Rub U, de Vos RA, Jansen Steur EN, Braak E (2003) Staging of brain pathology related to sporadic Parkinson's disease. *Neurobiol Aging* 24: 197-211

Brodacki B, Staszewski J, Toczylowska B, Kozlowska E, Drela N, Chalimoniuk M, Stepien A (2008) Serum interleukin (IL-2, IL-10, IL-6, IL-4), TNFalpha, and INFgamma concentrations are elevated in patients with atypical and idiopathic parkinsonism. *Neurosci Lett* 441: 158-162

Carpanini SM, Torvell M, Morgan BP (2019) Therapeutic Inhibition of the Complement System in Diseases of the Central Nervous System. *Front Immunol* 10: 362

Chang D, Nalls MA, Hallgrimsdottir IB, Hunkapiller J, van der Brug M, Cai F, International Parkinson's Disease Genomics C, andMe Research T, Kerchner GA, Ayalon G *et al* (2017) A meta-analysis of genome-wide association studies identifies 17 new Parkinson's disease risk loci. *Nat Genet* 49: 1511-1516

Cheng HC, Ulane CM, Burke RE (2010) Clinical progression in Parkinson disease and the neurobiology of axons. *Ann Neurol* 67: 715-725

Claude J, Linnartz-Gerlach B, Kudin AP, Kunz WS, Neumann H (2013) Microglial CD33-related Siglec-E inhibits neurotoxicity by preventing the phagocytosis-associated oxidative burst. *J Neurosci* 33: 18270-18276

Collaborators GBDPsD (2018) Global, regional, and national burden of Parkinson's disease, 1990-2016: a systematic analysis for the Global Burden of Disease Study 2016. *Lancet Neurol* 17: 939-953

Colley KJ, Kitajima K, Sato C (2014) Polysialic acid: biosynthesis, novel functions and applications. *Crit Rev Biochem Mol Biol* 49: 498-532

Colonna M, Butovsky O (2017) Microglia Function in the Central Nervous System During Health and Neurodegeneration. *Annu Rev Immunol* 35: 441-468

Cremer H, Lange R, Christoph A, Plomann M, Vopper G, Roes J, Brown R, Baldwin S, Kraemer P, Scheff S *et al* (1994) Inactivation of the N-CAM gene in mice results in size reduction of the olfactory bulb and deficits in spatial learning. *Nature* 367: 455-459

Crocker PR (2005) Siglecs in innate immunity. *Curr Opin Pharmacol* 5: 431-437
Crocker PR, Paulson JC, Varki A (2007) Siglecs and their roles in the immune system. *Nat Rev Immunol* 7: 255-266

Croisier E, Moran LB, Dexter DT, Pearce RK, Graeber MB (2005) Microglial inflammation in the parkinsonian substantia nigra: relationship to alpha-synuclein deposition. *J Neuroinflammation* 2: 14

Curreli S, Arany Z, Gerardy-Schahn R, Mann D, Stamatos NM (2007) Polysialylated neuropilin-2 is expressed on the surface of human dendritic cells and modulates dendritic cell-T lymphocyte interactions. *J Biol Chem* 282: 30346-30356

Czlonkowska A, Kohutnicka M, Kurkowska-Jastrzebska I, Czlonkowski A (1996) Microglial reaction in MPTP (1-methyl-4-phenyl-1,2,3,6-tetrahydropyridine) induced Parkinson's disease mice model. *Neurodegeneration* 5: 137-143

Damier P, Hirsch EC, Agid Y, Graybiel AM (1999) The substantia nigra of the human brain. II. Patterns of loss of dopamine-containing neurons in Parkinson's disease. *Brain* 122 (Pt 8): 1437-1448

Dantzer R, O'Connor JC, Freund GG, Johnson RW, Kelley KW (2008) From inflammation to sickness and depression: when the immune system subjugates the brain. *Nat Rev Neurosci* 9: 46-56

de Vries I, Busse C, Kopatz J, Neumann H, Beutel S, Scheper T (2017) Polysialic acid production using Escherichia coli K1 in a disposable bag reactor. *Eng Life Sci* 17: 723-731

Deng I, Corrigan F, Zhai G, Zhou X, Bobrovskaya L (2020) Lipopolysaccharide animal models of Parkinson’s disease: Recent progress and relevance to clinical disease. *Brain, Behavior, & Immunity - Health* 4

Doorn KJ, Moors T, Drukarch B, van de Berg W, Lucassen PJ, van Dam AM (2014) Microglial phenotypes and toll-like receptor 2 in the substantia nigra and hippocampus of incidental Lewy body disease cases and Parkinson's disease patients. *Acta Neuropathol Commun* 2: 90

Dorsey ER, Constantinescu R, Thompson JP, Biglan KM, Holloway RG, Kieburtz K, Marshall FJ, Ravina BM, Schifitto G, Siderowf A *et al* (2007) Projected number of people

with Parkinson disease in the most populous nations, 2005 through 2030. *Neurology* 68: 384-386

Duan S, Paulson JC (2020) Siglecs as Immune Cell Checkpoints in Disease. *Annu Rev Immunol* 38: 365-395

Duty S, Jenner P (2011) Animal models of Parkinson's disease: a source of novel treatments and clues to the cause of the disease. *Br J Pharmacol* 164: 1357-1391

Fearnley JM, Lees AJ (1991) Ageing and Parkinson's disease: substantia nigra regional selectivity. *Brain* 114 (Pt 5): 2283-2301

Ferreira SA, Romero-Ramos M (2018) Microglia Response During Parkinson's Disease: Alpha-Synuclein Intervention. *Front Cell Neurosci* 12: 247

Flores-Martinez YM, Fernandez-Parrilla MA, Ayala-Davila J, Reyes-Corona D, Blanco-Alvarez VM, Soto-Rojas LO, Luna-Herrera C, Gonzalez-Barrios JA, Leon-Chavez BA, Gutierrez-Castillo ME *et al* (2018) Acute Neuroinflammatory Response in the Substantia Nigra Pars Compacta of Rats after a Local Injection of Lipopolysaccharide. *J Immunol Res* 2018: 1838921

Fong JJ, Tsai CM, Saha S, Nizet V, Varki A, Bui JD (2018) Siglec-7 engagement by GBS beta-protein suppresses pyroptotic cell death of natural killer cells. *Proc Natl Acad Sci U S A* 115: 10410-10415

Fourgeaud L, Traves PG, Tufail Y, Leal-Bailey H, Lew ED, Burrola PG, Callaway P, Zagorska A, Rothlin CV, Nimmerjahn A *et al* (2016) TAM receptors regulate multiple features of microglial physiology. *Nature* 532: 240-244

Fu H, Liu B, Frost JL, Hong S, Jin M, Ostaszewski B, Shankar GM, Costantino IM, Carroll MC, Mayadas TN *et al* (2012) Complement component C3 and complement receptor type 3 contribute to the phagocytosis and clearance of fibrillar Abeta by microglia. *Glia* 60: 993-1003

Fujita T, Satomura A, Hidaka M, Ohsawa I, Endo M, Ohi H (1999) Inhibitory effect of free sialic acid on complement activation and its significance in hypocomplementemic glomerulonephritis. *J Clin Lab Anal* 13: 173-179

Gaki GS, Papavassiliou AG (2014) Oxidative stress-induced signaling pathways implicated in the pathogenesis of Parkinson's disease. *Neuromolecular Med* 16: 217-230

Galuska SP, Rollenhagen M, Kaup M, Eggers K, Oltmann-Norden I, Schiff M, Hartmann M, Weinhold B, Hildebrandt H, Geyer R *et al* (2010) Synaptic cell adhesion molecule SynCAM 1 is a target for polysialylation in postnatal mouse brain. *Proc Natl Acad Sci U S A* 107: 10250-10255

Gao HM, Jiang J, Wilson B, Zhang W, Hong JS, Liu B (2002) Microglial activation-mediated delayed and progressive degeneration of rat nigral dopaminergic neurons: relevance to Parkinson's disease. *J Neurochem* 81: 1285-1297

Gao HM, Kotzbauer PT, Uryu K, Leight S, Trojanowski JQ, Lee VM (2008) Neuroinflammation and oxidation/nitration of alpha-synuclein linked to dopaminergic neurodegeneration. *J Neurosci* 28: 7687-7698

Gerhard A, Pavese N, Hotton G, Turkheimer F, Es M, Hammers A, Eggert K, Oertel W, Banati RB, Brooks DJ (2006) In vivo imaging of microglial activation with [11C](R)-PK11195 PET in idiopathic Parkinson's disease. *Neurobiol Dis* 21: 404-412

Ginhoux F, Greter M, Leboeuf M, Nandi S, See P, Gokhan S, Mehler MF, Conway SJ, Ng LG, Stanley ER *et al* (2010) Fate mapping analysis reveals that adult microglia derive from primitive macrophages. *Science* 330: 841-845

Griciuc A, Serrano-Pozo A, Parrado AR, Lesinski AN, Asselin CN, Mullin K, Hooli B, Choi SH, Hyman BT, Tanzi RE (2013) Alzheimer's disease risk gene CD33 inhibits microglial uptake of amyloid beta. *Neuron* 78: 631-643

Guzman JN, Sanchez-Padilla J, Wokosin D, Kondapalli J, Ilijic E, Schumacker PT, Surmeier DJ (2010) Oxidant stress evoked by pacemaking in dopaminergic neurons is attenuated by DJ-1. *Nature* 468: 696-700

Halliday GM, Holton JL, Revesz T, Dickson DW (2011) Neuropathology underlying clinical variability in patients with synucleinopathies. *Acta Neuropathol* 122: 187-204

Halliday GM, Stevens CH (2011) Glia: initiators and progressors of pathology in Parkinson's disease. *Mov Disord* 26: 6-17

Hamza TH, Zabetian CP, Tenesa A, Laederach A, Montimurro J, Yearout D, Kay DM, Doheny KF, Paschall J, Pugh E *et al* (2010) Common genetic variation in the HLA region is associated with late-onset sporadic Parkinson's disease. *Nat Genet* 42: 781-785

Hara S, Takemori Y, Yamaguchi M, Nakamura M, Ohkura Y (1987) Fluorometric high-performance liquid chromatography of N-acetyl- and N-glycolylneuraminic acids and its

application to their microdetermination in human and animal sera, glycoproteins, and glycolipids. *Anal Biochem* 164: 138-145

Herrera AJ, Castano A, Venero JL, Cano J, Machado A (2000) The single intranigral injection of LPS as a new model for studying the selective effects of inflammatory reactions on dopaminergic system. *Neurobiol Dis* 7: 429-447

Hildebrandt H, Dityatev A (2015) Polysialic Acid in Brain Development and Synaptic Plasticity. *Top Curr Chem* 366: 55-96

Hirsch EC, Hunot S (2009) Neuroinflammation in Parkinson's disease: a target for neuroprotection? *Lancet Neurol* 8: 382-397

Hoban DB, Connaughton E, Connaughton C, Hogan G, Thornton C, Mulcahy P, Moloney TC, Dowd E (2013) Further characterisation of the LPS model of Parkinson's disease: a comparison of intra-nigral and intra-striatal lipopolysaccharide administration on motor function, microgliosis and nigrostriatal neurodegeneration in the rat. *Brain Behav Immun* 27: 91-100

Hoenen C, Gustin A, Birck C, Kirchmeyer M, Beaume N, Felten P, Grandbarbe L, Heuschling P, Heurtaux T (2016) Alpha-Synuclein Proteins Promote Pro-Inflammatory Cascades in Microglia: Stronger Effects of the A53T Mutant. *PLoS One* 11: e0162717

Hong S, Beja-Glasser VF, Nfonoyim BM, Frouin A, Li S, Ramakrishnan S, Merry KM, Shi Q, Rosenthal A, Barres BA *et al* (2016) Complement and microglia mediate early synapse loss in Alzheimer mouse models. *Science* 352: 712-716

Hou L, Wang K, Zhang C, Sun F, Che Y, Zhao X, Zhang D, Li H, Wang Q (2018) Complement receptor 3 mediates NADPH oxidase activation and dopaminergic neurodegeneration through a Src-Erk-dependent pathway. *Redox Biol* 14: 250-260

Hunot S, Boissiere F, Faucheux B, Brugg B, Mouatt-Prigent A, Agid Y, Hirsch EC (1996) Nitric oxide synthase and neuronal vulnerability in Parkinson's disease. *Neuroscience* 72: 355-363

Hunot S, Dugas N, Faucheux B, Hartmann A, Tardieu M, Debre P, Agid Y, Dugas B, Hirsch EC (1999) FcepsilonRII/CD23 is expressed in Parkinson's disease and induces, in vitro, production of nitric oxide and tumor necrosis factor-alpha in glial cells. *J Neurosci* 19: 3440-3447

Hyvarinen S, Meri S, Jokiranta TS (2016) Disturbed sialic acid recognition on endothelial cells and platelets in complement attack causes atypical hemolytic uremic syndrome. *Blood* 127: 2701-2710

Imamura K, Hishikawa N, Sawada M, Nagatsu T, Yoshida M, Hashizume Y (2003) Distribution of major histocompatibility complex class II-positive microglia and cytokine profile of Parkinson's disease brains. *Acta Neuropathol* 106: 518-526

Inoue S, Kitajima K, Inoue Y (1996) Identification of 2-keto-3-deoxy-D-glycero--galactononononic acid (KDN, deaminoneuraminic acid) residues in mammalian tissues and human lung carcinoma cells. Chemical evidence of the occurrence of KDN glycoconjugates in mammals. *J Biol Chem* 271: 24341-24344

Janda E, Boi L, Carta AR (2018) Microglial Phagocytosis and Its Regulation: A Therapeutic Target in Parkinson's Disease? *Front Mol Neurosci* 11: 144

Joers V, Tansey MG, Mulas G, Carta AR (2017) Microglial phenotypes in Parkinson's disease and animal models of the disease. *Prog Neurobiol* 155: 57-75

Kannarkat GT, Boss JM, Tansey MG (2013) The role of innate and adaptive immunity in Parkinson's disease. *J Parkinsons Dis* 3: 493-514

Karlstetter M, Kopatz J, Aslanidis A, Shahraz A, Caramoy A, Linnartz-Gerlach B, Lin Y, Luckoff A, Fauser S, Duker K *et al* (2017) Polysialic acid blocks mononuclear phagocyte reactivity, inhibits complement activation, and protects from vascular damage in the retina. *EMBO Mol Med* 9: 154-166

Klaus C, Liao H, Allendorf DH, Brown GC, Neumann H (2020) Sialylation acts as a checkpoint for innate immune responses in the central nervous system. *Glia*

Knott C, Stern G, Wilkin GP (2000) Inflammatory regulators in Parkinson's disease: iNOS, lipocortin-1, and cyclooxygenases-1 and -2. *Mol Cell Neurosci* 16: 724-739

Konsman JP, Kelley K, Dantzer R (1999) Temporal and spatial relationships between lipopolysaccharide-induced expression of Fos, interleukin-1beta and inducible nitric oxide synthase in rat brain. *Neuroscience* 89: 535-548

Labzin LI, Heneka MT, Latz E (2018) Innate Immunity and Neurodegeneration. *Annu Rev Med* 69: 437-449

Lane AP (2009) The role of innate immunity in the pathogenesis of chronic rhinosinusitis. *Curr Allergy Asthma Rep* 9: 205-212

Lawson LJ, Perry VH, Dri P, Gordon S (1990) Heterogeneity in the distribution and morphology of microglia in the normal adult mouse brain. *Neuroscience* 39: 151-170

Li YI, Wong G, Humphrey J, Raj T (2019) Prioritizing Parkinson's disease genes using population-scale transcriptomic data. *Nat Commun* 10: 994

Liao H, Klaus C, Neumann H (2020) Control of Innate Immunity by Sialic Acids in the Nervous Tissue. *Int J Mol Sci* 21

Linnartz-Gerlach B, Schuy C, Shahraz A, Tenner AJ, Neumann H (2016) Sialylation of neurites inhibits complement-mediated macrophage removal in a human macrophage-neuron Co-Culture System. *Glia* 64: 35-47

Linnartz B, Kopatz J, Tenner AJ, Neumann H (2012) Sialic acid on the neuronal glycocalyx prevents complement C1 binding and complement receptor-3-mediated removal by microglia. *J Neurosci* 32: 946-952

Linnartz B, Neumann H (2013) Microglial activatory (immunoreceptor tyrosine-based activation motif)- and inhibitory (immunoreceptor tyrosine-based inhibition motif)-signaling receptors for recognition of the neuronal glycocalyx. *Glia* 61: 37-46

Linnartz B, Wang Y, Neumann H (2010) Microglial immunoreceptor tyrosine-based activation and inhibition motif signaling in neuroinflammation. *Int J Alzheimers Dis* 2010

Liu Y, Qin L, Wilson B, Wu X, Qian L, Granholm AC, Crews FT, Hong JS (2008) Endotoxin induces a delayed loss of TH-IR neurons in substantia nigra and motor behavioral deficits. *Neurotoxicology* 29: 864-870

Lotharius J, Brundin P (2002) Pathogenesis of Parkinson's disease: dopamine, vesicles and alpha-synuclein. *Nat Rev Neurosci* 3: 932-942

Manocha GD, Floden AM, Puig KL, Nagamoto-Combs K, Scherzer CR, Combs CK (2017) Defining the contribution of neuroinflammation to Parkinson's disease in humanized immune system mice. *Mol Neurodegener* 12: 17

Marinova-Mutafchieva L, Sadeghian M, Broom L, Davis JB, Medhurst AD, Dexter DT (2009) Relationship between microglial activation and dopaminergic neuronal loss in the substantia nigra: a time course study in a 6-hydroxydopamine model of Parkinson's disease. *J Neurochem* 110: 966-975

McGuire SO, Ling ZD, Lipton JW, Sortwell CE, Collier TJ, Carvey PM (2001) Tumor necrosis factor alpha is toxic to embryonic mesencephalic dopamine neurons. *Exp Neurol* 169: 219-230

Mogi M, Harada M, Kondo T, Narabayashi H, Riederer P, Nagatsu T (1995) Transforming growth factor-beta 1 levels are elevated in the striatum and in ventricular cerebrospinal fluid in Parkinson's disease. *Neurosci Lett* 193: 129-132

Mogi M, Harada M, Kondo T, Riederer P, Inagaki H, Minami M, Nagatsu T (1994a) Interleukin-1 beta, interleukin-6, epidermal growth factor and transforming growth factor-alpha are elevated in the brain from parkinsonian patients. *Neurosci Lett* 180: 147-150

Mogi M, Harada M, Kondo T, Riederer P, Nagatsu T (1996a) Interleukin-2 but not basic fibroblast growth factor is elevated in parkinsonian brain. Short communication. *J Neural Transm (Vienna)* 103: 1077-1081

Mogi M, Harada M, Narabayashi H, Inagaki H, Minami M, Nagatsu T (1996b) Interleukin (IL)-1 beta, IL-2, IL-4, IL-6 and transforming growth factor-alpha levels are elevated in ventricular cerebrospinal fluid in juvenile parkinsonism and Parkinson's disease. *Neurosci Lett* 211: 13-16

Mogi M, Harada M, Riederer P, Narabayashi H, Fujita K, Nagatsu T (1994b) Tumor necrosis factor-alpha (TNF-alpha) increases both in the brain and in the cerebrospinal fluid from parkinsonian patients. *Neurosci Lett* 165: 208-210

Monnier PP, Beck SG, Bolz J, Henke-Fahle S (2001) The polysialic acid moiety of the neural cell adhesion molecule is involved in intraretinal guidance of retinal ganglion cell axons. *Dev Biol* 229: 1-14

Mosharov EV, Larsen KE, Kanter E, Phillips KA, Wilson K, Schmitz Y, Krantz DE, Kobayashi K, Edwards RH, Sulzer D (2009) Interplay between cytosolic dopamine, calcium, and alpha-synuclein causes selective death of substantia nigra neurons. *Neuron* 62: 218-229

Mount MP, Lira A, Grimes D, Smith PD, Faucher S, Slack R, Anisman H, Hayley S, Park DS (2007) Involvement of interferon-gamma in microglial-mediated loss of dopaminergic neurons. *J Neurosci* 27: 3328-3337

Mukherjee K, Khatua B, Mandal C (2020) Sialic Acid-Siglec-E Interactions During Pseudomonas aeruginosa Infection of Macrophages Interferes With Phagosome Maturation by Altering Intracellular Calcium Concentrations. *Front Immunol* 11: 332

Nalls MA, Blauwendraat C, Vallerga CL, Heilbron K, Bandres-Ciga S, Chang D, Tan M, Kia DA, Noyce AJ, Xue A *et al* (2019) Identification of novel risk loci, causal insights, and

heritable risk for Parkinson's disease: a meta-analysis of genome-wide association studies. *Lancet Neurol* 18: 1091-1102

Nalls MA, Pankratz N, Lill CM, Do CB, Hernandez DG, Saad M, DeStefano AL, Kara E, Bras J, Sharma M *et al* (2014) Large-scale meta-analysis of genome-wide association data identifies six new risk loci for Parkinson's disease. *Nat Genet* 46: 989-993

Nash Y, Schmukler E, Trudler D, Pinkas-Kramarski R, Frenkel D (2017) DJ-1 deficiency impairs autophagy and reduces alpha-synuclein phagocytosis by microglia. *J Neurochem* 143: 584-594

Nimmerjahn A, Kirchhoff F, Helmchen F (2005) Resting microglial cells are highly dynamic surveillants of brain parenchyma in vivo. *Science* 308: 1314-1318

Ojha S, Javed H, Azimullah S, Haque ME (2016) beta-Caryophyllene, a phytocannabinoid attenuates oxidative stress, neuroinflammation, glial activation, and salvages dopaminergic neurons in a rat model of Parkinson disease. *Mol Cell Biochem* 418: 59-70

Pan X, De Aragao CBP, Velasco-Martin JP, Priestman DA, Wu HY, Takahashi K, Yamaguchi K, Sturiale L, Garozzo D, Platt FM *et al* (2017) Neuraminidases 3 and 4 regulate neuronal function by catabolizing brain gangliosides. *FASEB J* 31: 3467-3483

Paolicelli RC, Bolasco G, Pagani F, Maggi L, Scianni M, Panzanelli P, Giustetto M, Ferreira TA, Guiducci E, Dumas L *et al* (2011) Synaptic pruning by microglia is necessary for normal brain development. *Science* 333: 1456-1458

Parente R, Clark SJ, Inforzato A, Day AJ (2017) Complement factor H in host defense and immune evasion. *Cell Mol Life Sci* 74: 1605-1624

Parkhurst CN, Yang G, Ninan I, Savas JN, Yates JR, 3rd, Lafaille JJ, Hempstead BL, Littman DR, Gan WB (2013) Microglia promote learning-dependent synapse formation through brain-derived neurotrophic factor. *Cell* 155: 1596-1609

Pei Z, Pang H, Qian L, Yang S, Wang T, Zhang W, Wu X, Dallas S, Wilson B, Reece JM *et al* (2007) MAC1 mediates LPS-induced production of superoxide by microglia: the role of pattern recognition receptors in dopaminergic neurotoxicity. *Glia* 55: 1362-1373

Pereira JR, Santos LVD, Santos RMS, Campos ALF, Pimenta AL, de Oliveira MS, Bacheti GG, Rocha NP, Teixeira AL, Christo PP *et al* (2016) IL-6 serum levels are elevated in Parkinson's disease patients with fatigue compared to patients without fatigue. *J Neurol Sci* 370: 153-156

Perry VH (2010) Contribution of systemic inflammation to chronic neurodegeneration. *Acta Neuropathol* 120: 277-286

Pisanu A, Lecca D, Mulas G, Wardas J, Simbula G, Spiga S, Carta AR (2014) Dynamic changes in pro- and anti-inflammatory cytokines in microglia after PPAR-gamma agonist neuroprotective treatment in the MPTPp mouse model of progressive Parkinson's disease. *Neurobiol Dis* 71: 280-291

Pissadaki EK, Bolam JP (2013) The energy cost of action potential propagation in dopamine neurons: clues to susceptibility in Parkinson's disease. *Front Comput Neurosci* 7: 13

Pluvinage JV, Haney MS, Smith BAH, Sun J, Iram T, Bonanno L, Li L, Lee DP, Morgens DW, Yang AC *et al* (2019) CD22 blockade restores homeostatic microglial phagocytosis in ageing brains. *Nature* 568: 187-192

Poewe W, Seppi K, Tanner CM, Halliday GM, Brundin P, Volkmann J, Schrag AE, Lang AE (2017) Parkinson disease. *Nat Rev Dis Primers* 3: 17013

Pringsheim T, Jette N, Frolkis A, Steeves TD (2014) The prevalence of Parkinson's disease: a systematic review and meta-analysis. *Mov Disord* 29: 1583-1590

Pshezhetsky AV, Ashmarina M (2018) Keeping it trim: roles of neuraminidases in CNS function. *Glycoconj J* 35: 375-386

Qin L, Liu Y, Hong JS, Crews FT (2013) NADPH oxidase and aging drive microglial activation, oxidative stress, and dopaminergic neurodegeneration following systemic LPS administration. *Glia* 61: 855-868

Qin L, Wu X, Block ML, Liu Y, Breese GR, Hong JS, Knapp DJ, Crews FT (2007) Systemic LPS causes chronic neuroinflammation and progressive neurodegeneration. *Glia* 55: 453-462

Ramaglia V, Hughes TR, Donev RM, Ruseva MM, Wu X, Huitinga I, Baas F, Neal JW, Morgan BP (2012) C3-dependent mechanism of microglial priming relevant to multiple sclerosis. *Proc Natl Acad Sci U S A* 109: 965-970

Ransohoff RM (2016) How neuroinflammation contributes to neurodegeneration. *Science* 353: 777-783

Rapoport EM, Sapot'ko YB, Pazynina GV, Bojenko VK, Bovin NV (2005) Sialoside-binding macrophage lectins in phagocytosis of apoptotic bodies. *Biochemistry (Mosc)* 70: 330-338

Rayaprolu S, Mullen B, Baker M, Lynch T, Finger E, Seeley WW, Hatanpaa KJ, Lomen-Hoerth C, Kertesz A, Bigio EH *et al* (2013) TREM2 in neurodegeneration: evidence for association of the p.R47H variant with frontotemporal dementia and Parkinson's disease. *Mol Neurodegener* 8: 19

Rode B, Endres C, Ran C, Stahl F, Beutel S, Kasper C, Galuska S, Geyer R, Muhlenhoff M, Gerardy-Schahn R *et al* (2008) Large-scale production and homogenous purification of long chain polysialic acids from E. coli K1. *J Biotechnol* 135: 202-209

Sanchez-Guajardo V, Febbraro F, Kirik D, Romero-Ramos M (2010) Microglia acquire distinct activation profiles depending on the degree of alpha-synuclein neuropathology in a rAAV based model of Parkinson's disease. *PLoS One* 5: e8784

Sato C, Kitajima K (2013) Disialic, oligosialic and polysialic acids: distribution, functions and related disease. *J Biochem* 154: 115-136

Sato C, Kitajima K (2019) Sialic Acids in Neurology. *Adv Carbohydr Chem Biochem* 76: 1-64

Schafer DP, Lehrman EK, Kautzman AG, Koyama R, Mardinly AR, Yamasaki R, Ransohoff RM, Greenberg ME, Barres BA, Stevens B (2012) Microglia sculpt postnatal neural circuits in an activity and complement-dependent manner. *Neuron* 74: 691-705

Schmid JA, Mach L, Paschke E, Glossl J (1999) Accumulation of sialic acid in endocytic compartments interferes with the formation of mature lysosomes. Impaired proteolytic

processing of cathepsin B in fibroblasts of patients with lysosomal sialic acid storage disease. *J Biol Chem* 274: 19063-19071

Schnaar RL, Gerardy-Schahn R, Hildebrandt H (2014) Sialic acids in the brain: gangliosides and polysialic acid in nervous system development, stability, disease, and regeneration. *Physiol Rev* 94: 461-518

Schwarz F, Pearce OM, Wang X, Samraj AN, Laubli H, Garcia JO, Lin H, Fu X, Garcia-Bingman A, Secrest P *et al* (2015) Siglec receptors impact mammalian lifespan by modulating oxidative stress. *Elife* 4

Shahraz A, Kopatz J, Mathy R, Kappler J, Winter D, Kapoor S, Schutza V, Scheper T, Gieselmann V, Neumann H (2015) Anti-inflammatory activity of low molecular weight polysialic acid on human macrophages. *Sci Rep* 5: 16800

Shahraz A, Wissfeld J, Ginolhac A, Mathews M, Sinkkonen L, Neumann H (2021) Phagocytosis-related NADPH oxidase 2 subunit gp91phox contributes to neurodegeneration after repeated systemic challenge with lipopolysaccharides. *Glia* 69: 137-150

Shimoji M, Pagan F, Healton EB, Mocchetti I (2009) CXCR4 and CXCL12 expression is increased in the nigro-striatal system of Parkinson's disease. *Neurotox Res* 16: 318-328

Smeyne RJ, Breckenridge CB, Beck M, Jiao Y, Butt MT, Wolf JC, Zadory D, Minnema DJ, Sturgess NC, Travis KZ *et al* (2016) Assessment of the Effects of MPTP and Paraquat on Dopaminergic Neurons and Microglia in the Substantia Nigra Pars Compacta of C57BL/6 Mice. *PLoS One* 11: e0164094

Stevens B, Allen NJ, Vazquez LE, Howell GR, Christopherson KS, Nouri N, Micheva KD, Mehalow AK, Huberman AD, Stafford B *et al* (2007) The classical complement cascade mediates CNS synapse elimination. *Cell* 131: 1164-1178

Su X, Maguire-Zeiss KA, Giuliano R, Prifti L, Venkatesh K, Federoff HJ (2008) Synuclein activates microglia in a model of Parkinson's disease. *Neurobiol Aging* 29: 1690-1701

Sumida M, Hane M, Yabe U, Shimoda Y, Pearce OM, Kiso M, Miyagi T, Sawada M, Varki A, Kitajima K *et al* (2015) Rapid Trimming of Cell Surface Polysialic Acid (PolySia) by Exovesicular Sialidase Triggers Release of Preexisting Surface Neurotrophin. *J Biol Chem* 290: 13202-13214

Surmeier DJ, Guzman JN, Sanchez-Padilla J, Schumacker PT (2011) The role of calcium and mitochondrial oxidant stress in the loss of substantia nigra pars compacta dopaminergic neurons in Parkinson's disease. *Neuroscience* 198: 221-231

Surmeier DJ, Obeso JA, Halliday GM (2017) Selective neuronal vulnerability in Parkinson disease. *Nat Rev Neurosci* 18: 101-113

Tan EK, Chao YX, West A, Chan LL, Poewe W, Jankovic J (2020) Parkinson disease and the immune system - associations, mechanisms and therapeutics. *Nat Rev Neurol* 16: 303-318

Tangvoranuntakul P, Gagneux P, Diaz S, Bardor M, Varki N, Varki A, Muchmore E (2003) Human uptake and incorporation of an immunogenic nonhuman dietary sialic acid. *Proc Natl Acad Sci U S A* 100: 12045-12050

Terada T, Yokokura M, Yoshikawa E, Futatsubashi M, Kono S, Konishi T, Miyajima H, Hashizume T, Ouchi Y (2016) Extrastriatal spreading of microglial activation in Parkinson's disease: a positron emission tomography study. *Ann Nucl Med* 30: 579-587

Theodore S, Cao S, McLean PJ, Standaert DG (2008) Targeted overexpression of human alpha-synuclein triggers microglial activation and an adaptive immune response in a mouse model of Parkinson disease. *J Neuropathol Exp Neurol* 67: 1149-1158

Thiesler H, Beimdiek J, Hildebrandt H (2021) Polysialic acid and Siglec-E orchestrate negative feedback regulation of microglia activation. *Cell Mol Life Sci* 78: 1637-1653

Tremblay ME, Cookson MR, Civiero L (2019) Glial phagocytic clearance in Parkinson's disease. *Mol Neurodegener* 14: 16

Tsai CM, Riestra AM, Ali SR, Fong JJ, Liu JZ, Hughes G, Varki A, Nizet V (2020) Siglec-14 Enhances NLRP3-Inflammasome Activation in Macrophages. *J Innate Immun* 12: 333-343

Varki A (2017) Are humans prone to autoimmunity? Implications from evolutionary changes in hominin sialic acid biology. *J Autoimmun* 83: 134-142

Varki A, Gagneux P (2012) Multifarious roles of sialic acids in immunity. *Ann N Y Acad Sci* 1253: 16-36

Vitkovic L, Konsman JP, Bockaert J, Dantzer R, Homburger V, Jacque C (2000) Cytokine signals propagate through the brain. *Mol Psychiatry* 5: 604-615

Waisman A, Ginhoux F, Greter M, Bruttger J (2015) Homeostasis of Microglia in the Adult Brain: Review of Novel Microglia Depletion Systems. *Trends Immunol* 36: 625-636

Wang Y, Neumann H (2010) Alleviation of neurotoxicity by microglial human Siglec-11. *J Neurosci* 30: 3482-3488

Wei Z, Li X, Li X, Liu Q, Cheng Y (2018) Oxidative Stress in Parkinson's Disease: A Systematic Review and Meta-Analysis. *Front Mol Neurosci* 11: 236

Werneburg S, Buettner FF, Erben L, Mathews M, Neumann H, Muhlenhoff M, Hildebrandt H (2016) Polysialylation and lipopolysaccharide-induced shedding of E-selectin ligand-1 and neuropilin-2 by microglia and THP-1 macrophages. *Glia* 64: 1314-1330

Wu DC, Jackson-Lewis V, Vila M, Tieu K, Teismann P, Vadseth C, Choi DK, Ischiropoulos H, Przedborski S (2002) Blockade of microglial activation is neuroprotective in the 1-methyl-4-phenyl-1,2,3,6-tetrahydropyridine mouse model of Parkinson disease. *J Neurosci* 22: 1763-1771

Wyss-Coray T, Mucke L (2002) Inflammation in neurodegenerative disease--a double-edged sword. *Neuron* 35: 419-432

Zhou XY, Morreau H, Rottier R, Davis D, Bonten E, Gillemans N, Wenger D, Grosveld FG, Doherty P, Suzuki K *et al* (1995) Mouse model for the lysosomal disorder galactosialidosis and correction of the phenotype with overexpressing erythroid precursor cells. *Genes Dev* 9: 2623-2634

10. Acknowledgements

First of all, I would like to express my deepest gratitude to Prof. Dr. Harald Neumann for providing me the awesome opportunity to work in his group. I feel extremely lucky to have Harald as my direct project supervisor during my Ph.D. life. I must have done a lot of good things in my last decades to be lucky enough to meet him in Germany. He is always very generous to offer full support for my research. We had hundreds of discussions on my research in the past years. He is approachable, knowledgeable, professional and full of wisdom, thus I benefited a lot from his constructive guidance during each fruitful discussion. Moreover, his optimistic attitude towards work and life also inspired me a lot. Whenever I felt upset with failures during research, he always encouraged me to cheer up. Therefore, I had a very happy Ph.D. life because of him. Thank you, Harald!

I would also like to thank Prof. Wolfram Kunz, Prof. Jochen Walter and Prof. Thomas Langmann to be my thesis committee members. Their valuable comments and suggestions during annual progress report meeting contributed a lot to improve the quality of the project.

Many thanks to Jonas Winkler for his excellent help in purification of polySia avDP20. Additionally, I thank Jannis Wißfeld, Jonas Winkler, Marta Williams, Dr. Bettina Linnartz-Gerlach, Dr. Anahita Shahraz, Dr. Christine Klaus, Negin Afrang, Tawfik Abou Assale, Rita Jietou, and Annemarie Bungartz for excellent technical support for this project. Also, I thank Prof. Thomas Scheper and his lab for providing long chain polySia. Moreover, I would like to thank the Microscopy Core Facility of the Medical Faculty at the University of Bonn for providing help, services, and devices.

Furthermore, I thank all my colleagues in AG Neumann's lab: Ani, Christine, Amy, Jonas, Jannis, Tawfik, Negin, Rita, German, Carmen, Marius, Eshita, Ahmed, Denis, Bettina,

Katja, Marta, Lukas, Jasper, Katlynn, Michelle, Meng-chun, Tamara, Felix, Philippe, Vibha, Dhyani, Maria, Joshua, Miri, Latika. I also would like to thank other colleagues in the Institute of Reconstructive Neurobiology. Thank you for creating such a wonderful research environment and thank you all for your generous help and support all the time. Without you, I would not have such a great time in Germany.

Last but not least, I would like to thank my lovely and wonderful family, father Qiuyuan, mother Dongyou, sister Chun, brother-in-law Ronghua who always care about me and give me countless support. I would not have reached this stage without them. It's also important for me to thank my girlfriend's parents, Jinying and Junhua, for their full understanding and unlimited support. Finally, I would like to say a special 'thank you' to my girlfriend Lisa, who wisely supports me to pursue my Ph.D. degree in Germany. Although she is far away in China, I feel that we have always been together. Because of her, I seized the great opportunity to see a bigger world and understand what life is. I planned to end the self-funded 6-year project titled "How to deal with long-distance relationships" after my graduation and start a new self-funded project titled "How to grow old together in a happy marriage" with her.